SPECTROSCOPIC STUDIES OF ATOMIC OXYGEN

USING GAS LASER TECHNIQUES

by

MICHAEL STEPHEN FELD

S. B., Massachusetts Institute of Technology
1963

S. M., Massachusetts Institute of Technology
1963

SUBMITTED IN PARTIAL FULFILLMENT OF THE

REQUIREMENTS FOR THE DEGREE OF

DOCTOR OF PHILOSOPHY

at the

MASSACHUSETTS INSTITUTE OF TECHNOLOGY

Signature of Author _
Department of Physics, June 19, 1967

Certified by _
Thesis Supervisor

Accepted by _
Chairman, Departmental Committee on Graduate Students

SPECTROSCOPIC STUDIES OF ATOMIC OXYGEN

USING GAS LASER TECHNIQUES

by

MICHAEL STEPHEN FELD

S. B., Massachusetts Institute of Technology
1963

S. M., Massachusetts Institute of Technology
1963

SUBMITTED IN PARTIAL FULFILLMENT OF THE

REQUIREMENTS FOR THE DEGREE OF

DOCTOR OF PHILOSOPHY

at the

MASSACHUSETTS INSTITUTE OF TECHNOLOGY

SPECTROSCOPIC STUDIES OF ATOMIC OXYGEN

USING GAS LASER TECHNIQUES

by

Michael Stephen Feld

Submitted to the Department of Physics on June 19, 1967

in partial fulfillment of the requirement for the

degree of Doctor of Philosophy

ABSTRACT

Laser action on the $3p\,^3P_{0,2,1}$ - $3s\,^3S_1^o$ atomic oxygen triplet (0-1, 2-1, 1-1) at 8446Å cannot occur at its fluorescence peaks. The laser levels, populated by molecular dissociation, have much broader velocity distributions than ground state atoms, which are at room temperature. Strong selective reabsorption of U.V. resonance radiation from the $^3S^o$ level leads to increased population of those $^3S^o$ atoms with room temperature velocities. Thus, over a sizeable central portion of each 8446Å component the population inversion is reversed, excluding the possibility of laser oscillation there. The previously observed anomalous behavior, (2) in which laser action occurs on the high-frequency side of the 2-1 fluorescence peak, follows from this effect and the fact that the 2-1 and 0-1 fine-structure components partially overlap. Estimates of the size of the effect are given, and applicability to other systems is discussed.

At low pressures and favorable gain conditions a second, concurrent oscillation is observed on the 1-1 transition. Selective reabsorption prevents oscillation near line center. Despite the lack of overlap, laser action again occurs above the center frequency. This asymmetrical behavior arises because the 1-1 gain profile is influenced by the presence of the 2-1 laser line. In a detailed analysis the 1-1 small signal gain is calculated in the presence of a strongly-saturating, standing-wave optical field interacting with the 2-1 transition of the inhomogeneously-broadened 8446Å fine structure system. Different portions of the resulting 1-1 gain profile are influenced by population saturation and Raman-type coupling effects, and optimum conditions for simultaneous laser action on both fine-structure components occur when the laser frequency separation is very

close to the J = 2, J = 1 fine-structure splitting. Details of the lineshapes, polarization effects, and the possibility of accurately measuring the fine-structure splitting are discussed. Further fine-structure oscillations are also reported and explained.

The analysis is extended to a novel class of high-resolution, non-linear spectroscopic techniques[28] ideally suited to the strong, monochromatic multimode fields generated by lasers. In the simplest arrangement a multimoding laser is incident upon an inhomogeneously-broadened system with closely-spaced structure. The laser should resonate with the absorption (or emission) lines of the sample. The mode separation is assumed large compared to the system's natural (homogeneous) widths. It is also assumed that the level separation may be tuned by applying a DC magnetic or electric field. The intensity of the attenuated laser beam is studied as a function of the level separation. Each time the splitting of two levels, optically coupled to a common level, approaches the separation between a pair of modes of the laser field, the attenuation sharply increases. The widths of the observed resonances are determined by the natural widths of the two levels. This effect is referred to as mode-crossing. As the levels approach each other within their natural widths a further sharp increase in attenuation occurs. We refer to this effect as non-linear level crossing. The saturation aspects of the crossing techniques distinguish them from previous techniques, utilizing conventional light sources, which they superficially resemble.

By applying non-linear crossing techniques to the laser medium itself some of the g-values and linewidth parameters in a series of new C.W. oxygen laser transitions, as well as in the 8446Å transition, have been measured. The new laser lines are: 2.894μ ($4p^3P$--$4s^3S^O$), 4.563μ ($4p^3P$--$3d^3D^O$), 5.981μ ($7d^3D^O$--$6p^3P$), 6.858μ ($5p^3P$--$5s^3S^O$), and 10.400μ ($5p^3P$--$4d^3D^O$). Output powers in the range 0.1-1 mw are observed for a 3 m discharge, using DC or RF excitation in mixtures of approximately 80μ O_2 and 1/2-1 mm He or Ne. For the upper levels of the 8446Å, 2.89μ and 4.56μ lines we have obtained g-values of $1.51 + .01$, $1.51 + .05$, and $1.51 + .05$, respectively, which agree well with L-S coupling. The linewidths of these levels appear considerably power-broadened, indicating the extent of saturation of the laser media. Extension of these techniques to other systems may lead to resonant Raman lasers.

Thesis Supervisor: Ali Javan
Title: Professor of Physics

This thesis is dedicated to my wife, Mary Haskell Feld, and to my mother, Lillian Rosenberg Feld.

- 5 -

ACKNOWLEDGEMENTS

My warmest and deepest thanks go to Professor Ali Javan for his continual help and interest in the preparation of this study. Not only has he shared physics insights and offered much encouragement, he has also taught, by example, the fun of physics.

I wish to express particular thanks to Barry Feldman for close collaboration on the experimental work.

I am grateful to many of the members of the Optical Maser Group for illuminating discussions and laboratory assistance. For suggestions and assistance relating specifically to my thesis I thank Prof. Abraham Szöke, Prof. D. Ramachandra Rao, Dr. Paul Bonczyk, Prof. George Flynn, Leo Geoffrion, Larry Aronberg, and Jerry Adler.

For their patience and technical assistance, I am indebted to Richard Solomon, William Ryan, and Eugene Leonard. Dr. Daniel Murnick's instruction in the use of computers was most useful.

Mary E. Phipps and Ellen Desmond were very helpful with the typing.

Special gratitude and respect is reserved for Professor Koichi Shimoda because his teaching and writings have deeply influenced me.

TABLE OF CONTENTS

TABLE OF CONTENTS Cont.

TABLE OF FIGURES

TABLE OF FIGURES Cont.

TABLES

INTRODUCTION

The extraordinary behavior of the 8446 $\overset{o}{A}$ atomic oxygen laser involves several interesting radiative processes: one suggests a new mechanism for obtaining laser action in gas discharges; another provides a method for accurately determining the $3p\,^3P_2 - 3p\,^3P_1$ fine-structure splitting, as well as g-values and linewidth parameters of the levels involved. The present study examines these radiative processes; describes how, in combination, they lead to the observed laser behavior; and investigates in detail several of their consequences.

It will be convenient, hereafter, to refer to the $3p\,^3P_J - 3s\,^3S_1^o$ 8446 $\overset{o}{A}$ oxygen transition as the J-1 transition. The corresponding emission lines, in order of decreasing energy, are 0-1, 2-1, and 1-1 separated by 0.159 cm^{-1} and 0.557 cm^{-1}, respectively.[1] The spontaneous emission ratio of approximately 5:1:3 observed at various laser operating pressures indicates that the $3p\,^3P$ populations are distributed according to their statistical weights. The large Doppler widths, in excess of 0.1 cm^{-1}, are due to the energetic products of O_2 dissociation. Thus the 2-1 and 0-1 profiles overlap, as shown in Figure 1.

Laser action on this triplet was first obtained by Bennett, Faust, McFarlane and Patel,[2][3][4] who noted a single laser line that did not occur at the peak of the spontaneous emission profile but was shifted about 0.07 cm^{-1} above the 2-1 center frequency, almost midway between the 2-1
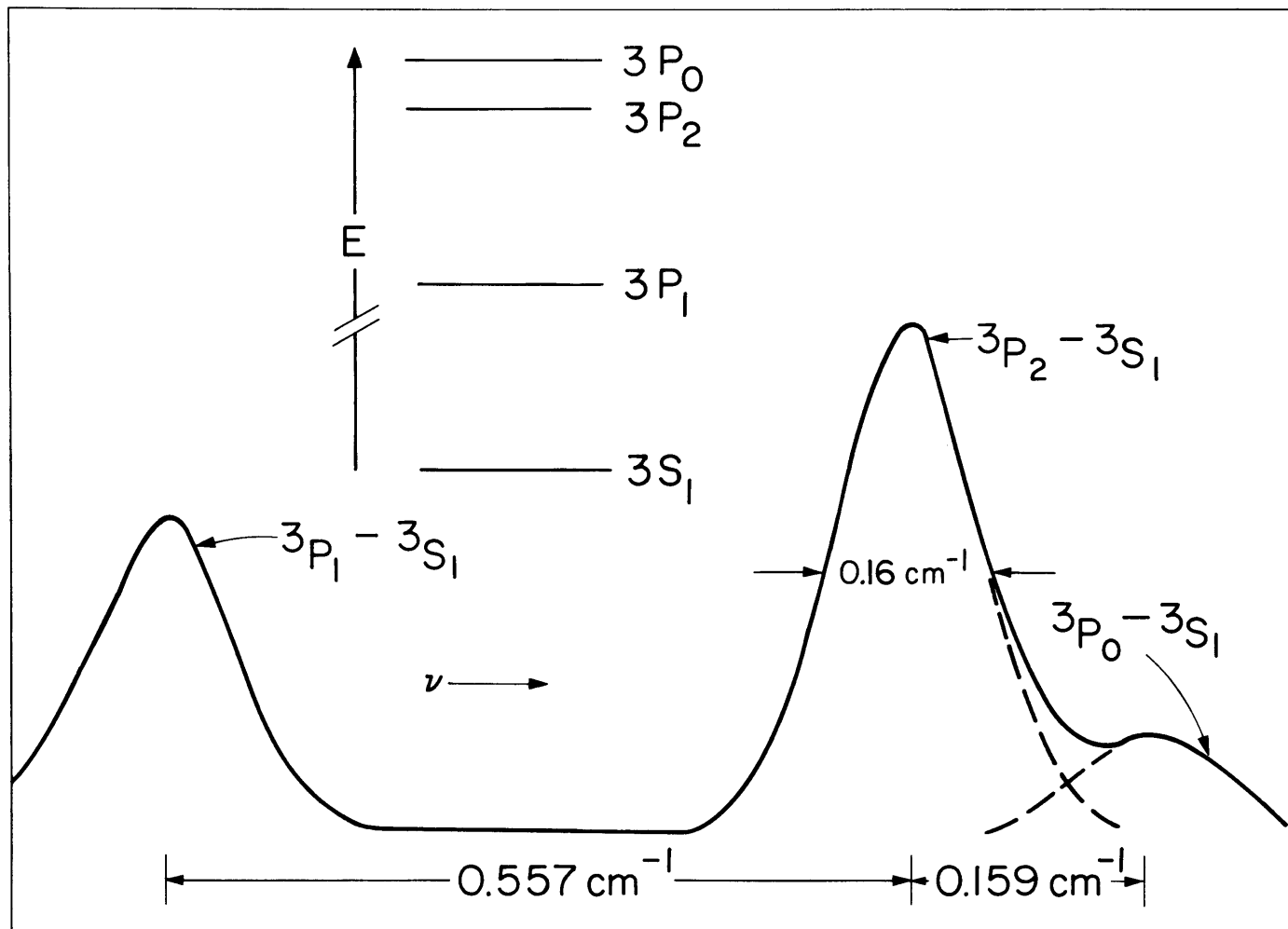
Figure 1   8446 Å Gain Profile (Fine Structure Separations are from Ref. 1)
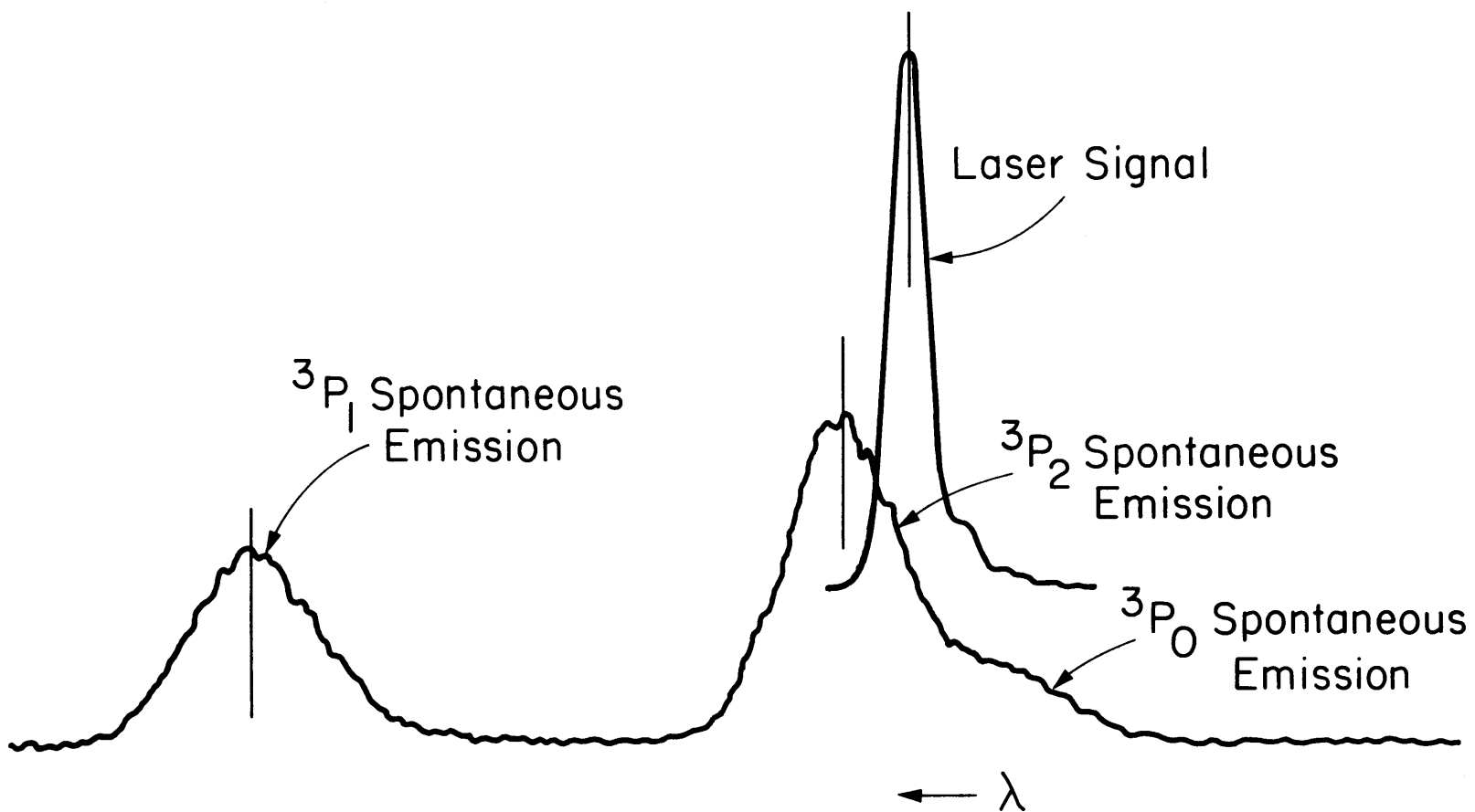
Figure 2   8446 Å Spontaneous Emission Profile, Showing Initially Observed Laser Line (After Bennett[3])

and 0-1 fluorescence peaks. (See Figure 2.) They further noted that although no laser action occured on the 1-1 line, its single-pass gain appeared to exceed oscillation threshold. [5]

Recently[6] we have confirmed the above behavior. In addition, at low pressures and under high gain conditions we have observed a second, concurrent oscillation shifted above the 1-1 center frequency by an amount about equal to the 2-1 frequency shift. The latter observation suggests the interesting possibility that the separation between the two laser lines is determined by the $J = 2$, $J = 1$ fine-structure splitting. Under optimum gain conditions two additional laser lines have been observed not quite symmetrically located below the 2-1 and 1-1 center frequencies, as shown in Figure 3. Tunitsky and Cherkasov[7] have also reported the observation of four laser lines. Under no circumstances has laser action been observed at any of the fluorescence peaks.

Parts I-III of the present study are devoted to the explanation of this striking behavior. In Part I the experimental observations and techniques are presented. Part II accounts for the frequency shift of the 2-1 laser line and the inability of the laser to oscillate close to the spontaneous emission peaks on the basis of a newly understood radiative effect which we call selective reabsorption. In Part III it is shown that the gain at the 1-1 transition is greatly influenced by the presence of laser action on the 2-1 gain profile via Raman-type processes which strongly couple the $J = 2$ and $J = 1$ levels. Conditions for oscillation on the 1-1 profile are most favorable when

Figure 3   Experimentally Observed Spontaneous Emission
Profile and Laser Lines.

the frequency separation between the two oscillations is very close to the

J = 2, J = 1 fine-structure splitting, leading to the observed laser behavior.

In Part IV the theory of Raman-type processes is extended to describe
a novel class of spectroscopic techniques particularly well-suited to studies
of closely spaced level structure in inhomogeneously-broadened systems.
Using these techniques, g-values and linewidth parameters of levels involved
in a new series of atomic oxygen laser lines are measured. [30]

Finally, in the concluding remarks some further applications of
selective reabsorption and Raman-type processes are discussed.

PART I: EXPERIMENTAL OBSERVATIONS AND TECHNIQUES

The 8446 Å spontaneous emission and laser behavior were studied photographically over a wide range of conditions using a Fabry-Perot interferometer. The near-confocal laser cavity was approximately 3 meters long with 99.6% reflecting dielectric-coated mirrors. The quartz laser tube had an 11 mm i.d. The laser could be made to oscillate CW over a factor of 10 range of pressures and a factor of 100 range of power levels. Mixtures of neon or argon with small amounts of oxygen were used.[2]

The free spectral range of the Fabry-Perot was 0.787 cm^{-1}. Freshly silvered mirrors of about 80% reflectivity were employed throughout. Negatives were made using Kodak type 1-N glass plates. Thirty-three plates were taken in all.

Typical Fabry-Perot photographs are shown in Figures 4-7. In Figure 4, which corresponds to moderate-gain conditions, the laser is oscillating on a single line. In Figure 5, taken at lower pressures and higher-gain conditions, two lines are oscillating. In Figure 6, also at low pressures but with discharge conditions adjusted for maximum gain, four lines can be discerned. To ascertain the positions of various lines on the spontaneous emission profile, Fabry-Perot photographs of the fluorescence were taken as in Figure 7, using filters to reduce the emission at unwanted wavelengths. As a check, photographs superimposing laser oscillations on the 8446 Å spontaneous emission background were also taken. A rather small free
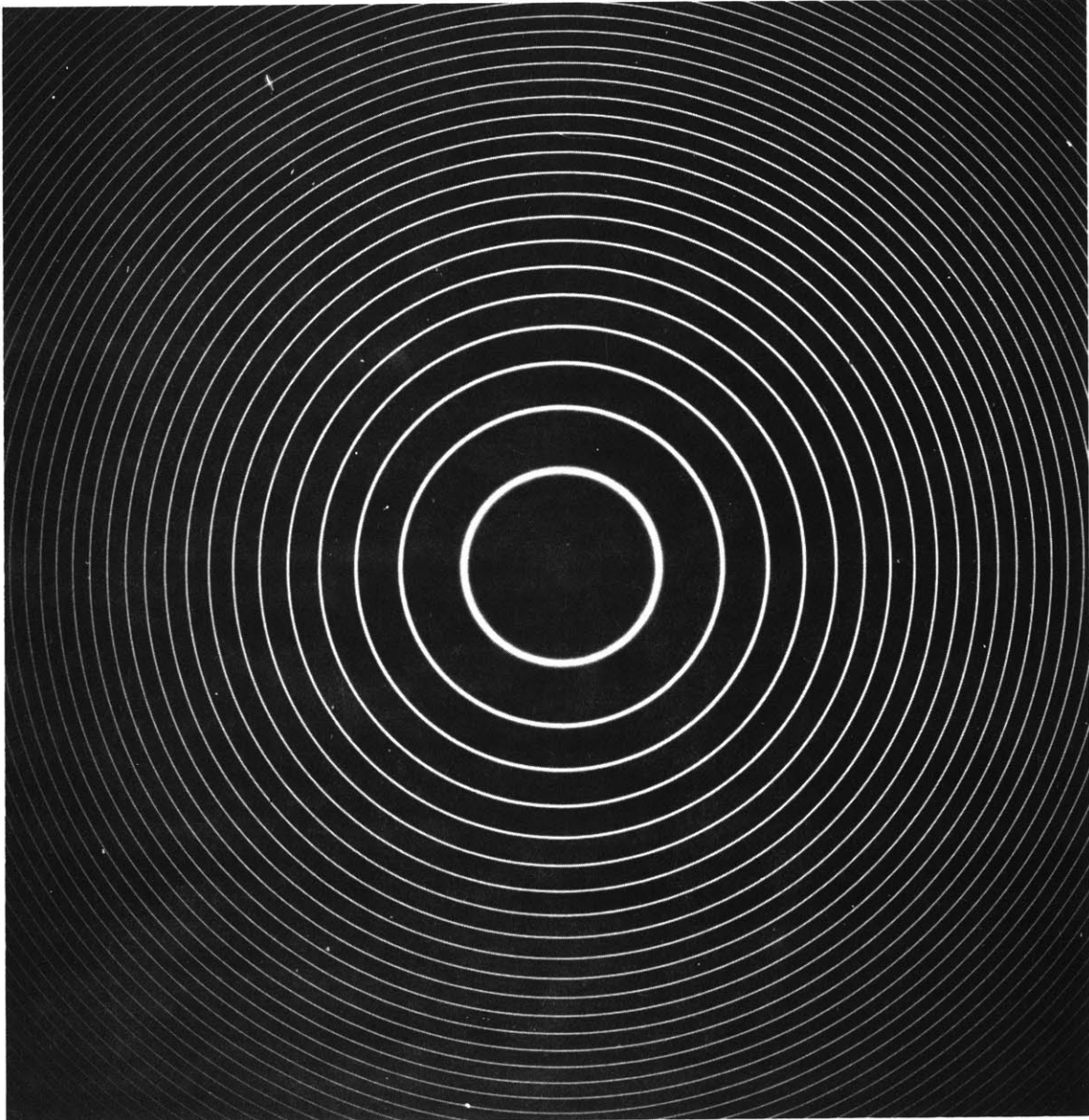
Figure 4   Fabry — Perot   Plate   No. 9
Single   Laser   Line
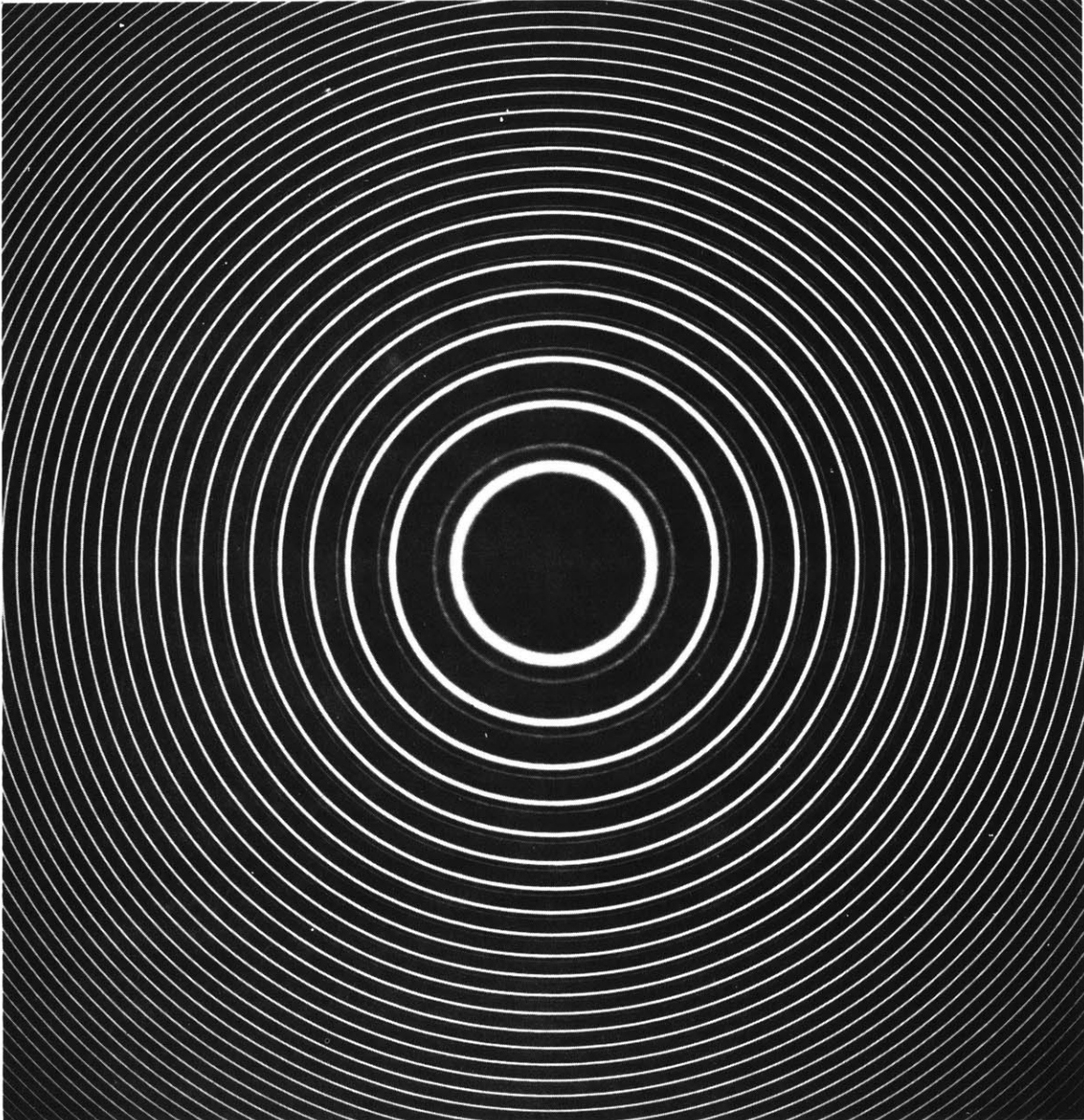
Figure 5   Fabry – Perot   No. 13
Two   Laser   Lines

Figure 6   Fabry – Perot Plate No. 33
Four Laser Lines
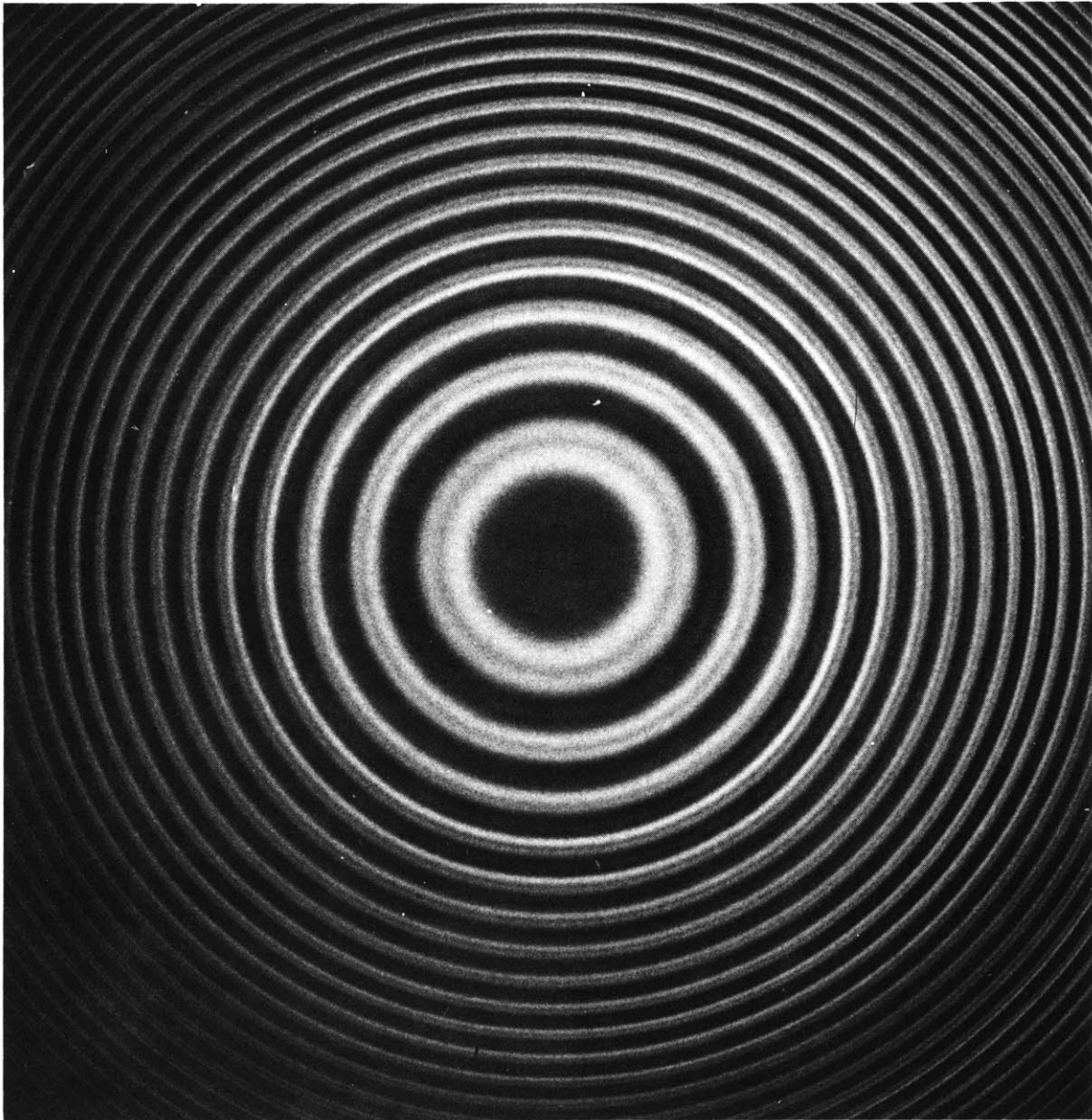
Figure 7 Fabry–Perot Plate No. 20
8446 Å Spontaneous
Emission Profile

spectral range was necessary to enable full resolution of the various laser lines. As a result, the wings of the spontaneous emission components slightly overlapped, as seen in Figure 7. However, this overlap did not cause any ambiguity in the analysis. The faint additional rings of Figure 7 are probably due to fluorescence of the nearby $3p^5P$ multiplet, which was not entirely filtered out.

Densities were obtained from the Fabry-Perot plates by means of a high-resolution microdensitometer.[8] For each plate the ring diameters were recorded on punch cards and analyzed at the M.I.T. computation center. A program (F.P.A.) was written to statistically analyze the 9 lowest orders of each plate. The program performed several functions: it checked the consistency of the data on each plate, obtained the frequency separations of the various spectral components of each plate, and compared the frequencies of particular lines from plate to plate. The final output tabulated relative frequencies, their standard deviations and the standard errors of the standard deviations.

Plates of particular interest were analyzed in greater detail. In these cases the three lowest orders of each plate were converted into densitometer tracings about five feet long. Each tracing was divided into approximately 700 parts and the corresponding densities recorded on punch cards. In a series of computer programs (H.R.F.P.A.) the diameters were converted into relative frequencies and the densities converted into relative intensities, and the results were plotted by the Calcomp plotter. The resulting lineshapes

could be well-fitted to Gaussians,[9] as indicated in Figure 16.

Three stages (A, B, C) of the analysis are illustrated in Figures 8-10 for a spontaneous emission exposure and in Figures 11-13 for a single laser line superimposed on the spontaneous emission background. Stage A is the unprocessed densitometer tracing; in stage B the ring center has been located and the density plotted as a function of the square of the radius (which is proportional to the frequency); finally, in stage C background corrections have been made and, using the 1-N characteristic (D log E) curve, the ordinate has been converted into units of relative intensity. The resulting fits are graphed in Figures 14 and 15, respectively.

The final results are presented in Figures 3 and 16. For multiple frequencies on a single plate the relative accuracy is estimated to be somewhat better than .01 cm^{-1}. However, the Fabry-Perot (with ball-bearing spacers) was found to drift considerably between exposures; accordingly, the errors in frequency measurements from plate to plate are somewhat greater. It was judged, nevertheless, that the laser frequencies were stable within .01 cm^{-1} over a wide range of pressures and intensities, and independent of the number of lines oscillating.
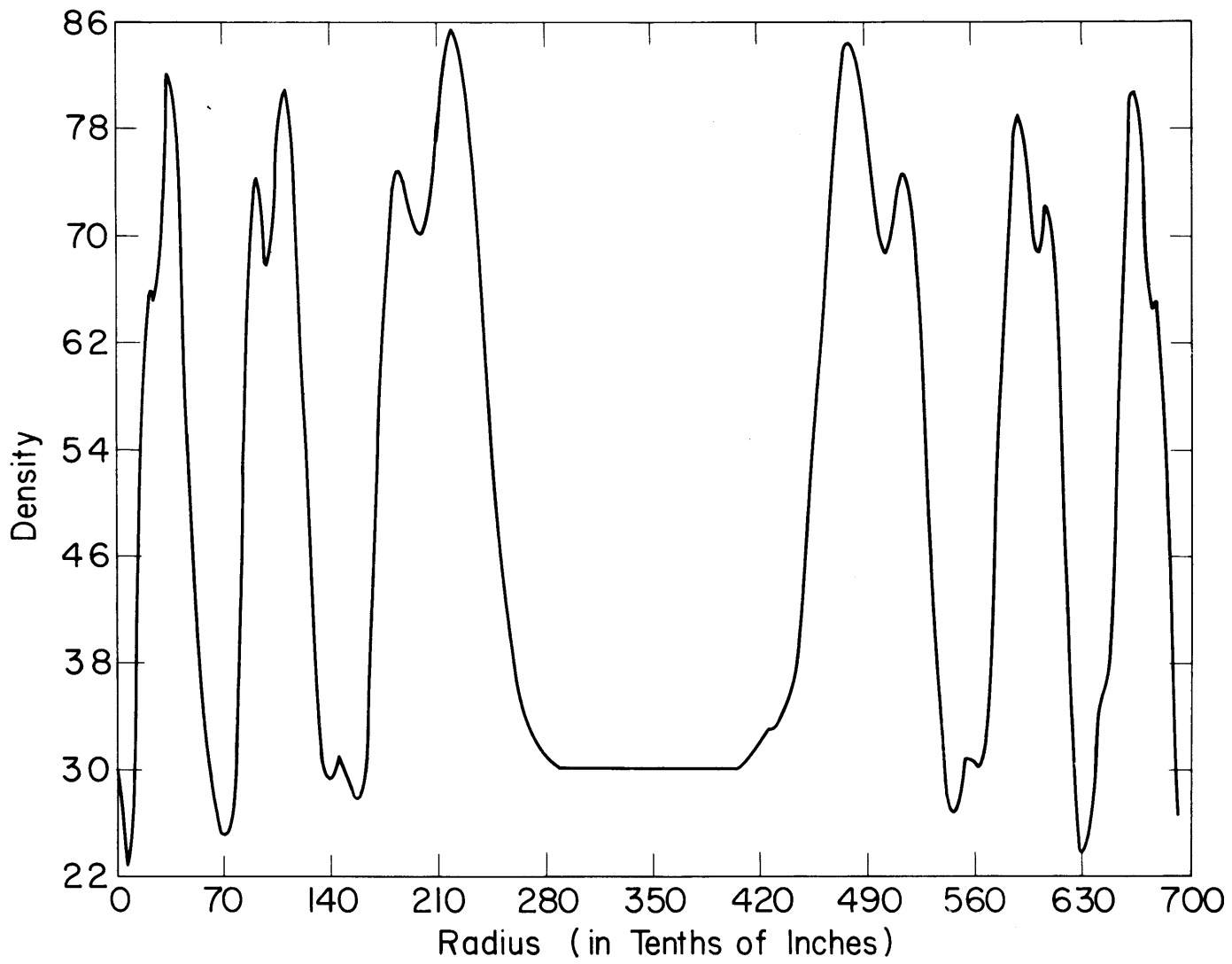
Figure 8   Computer   Analysis   of   Plate   No. 20: A
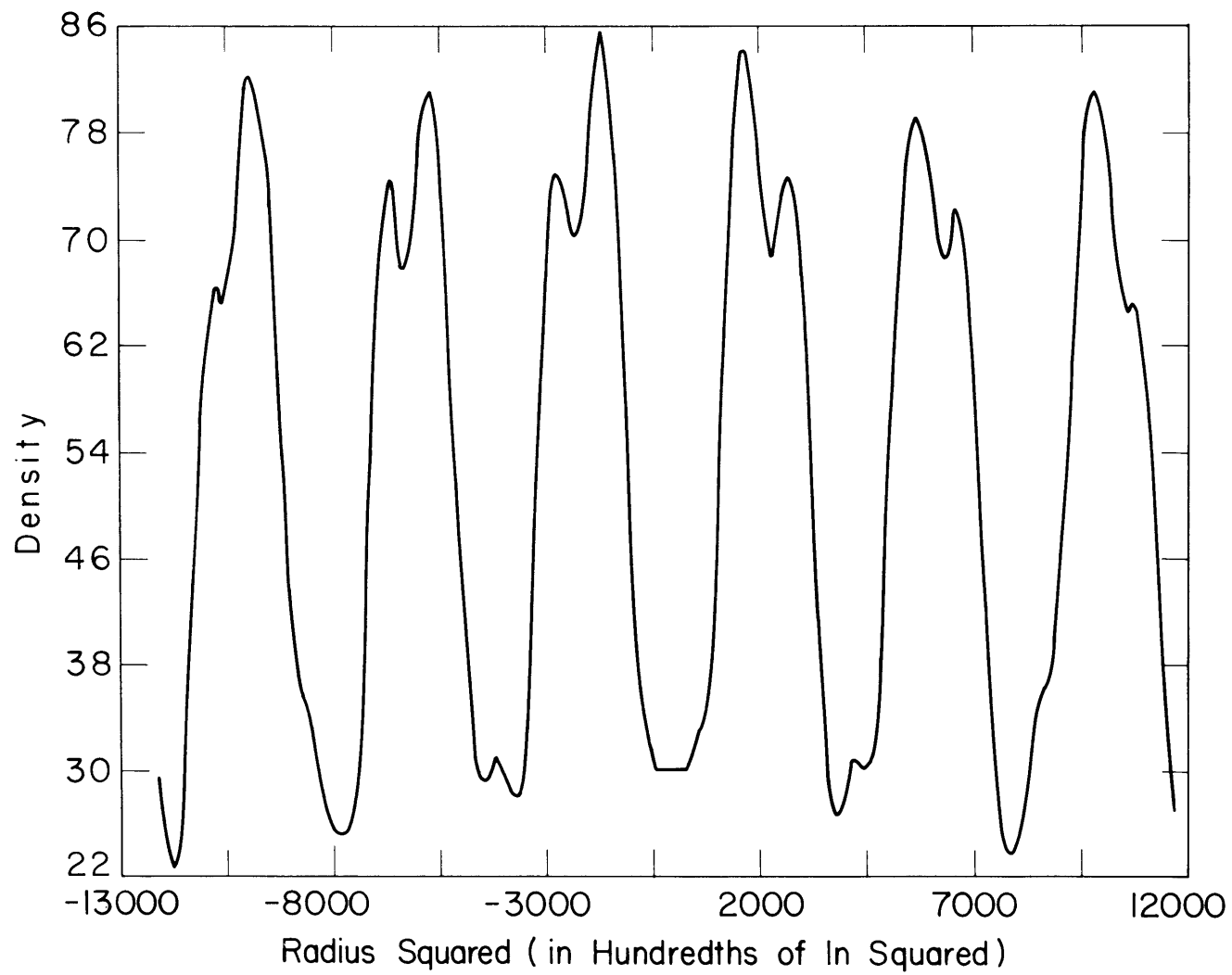
Figure 9 Computer Analysis of Plate No. 20:B
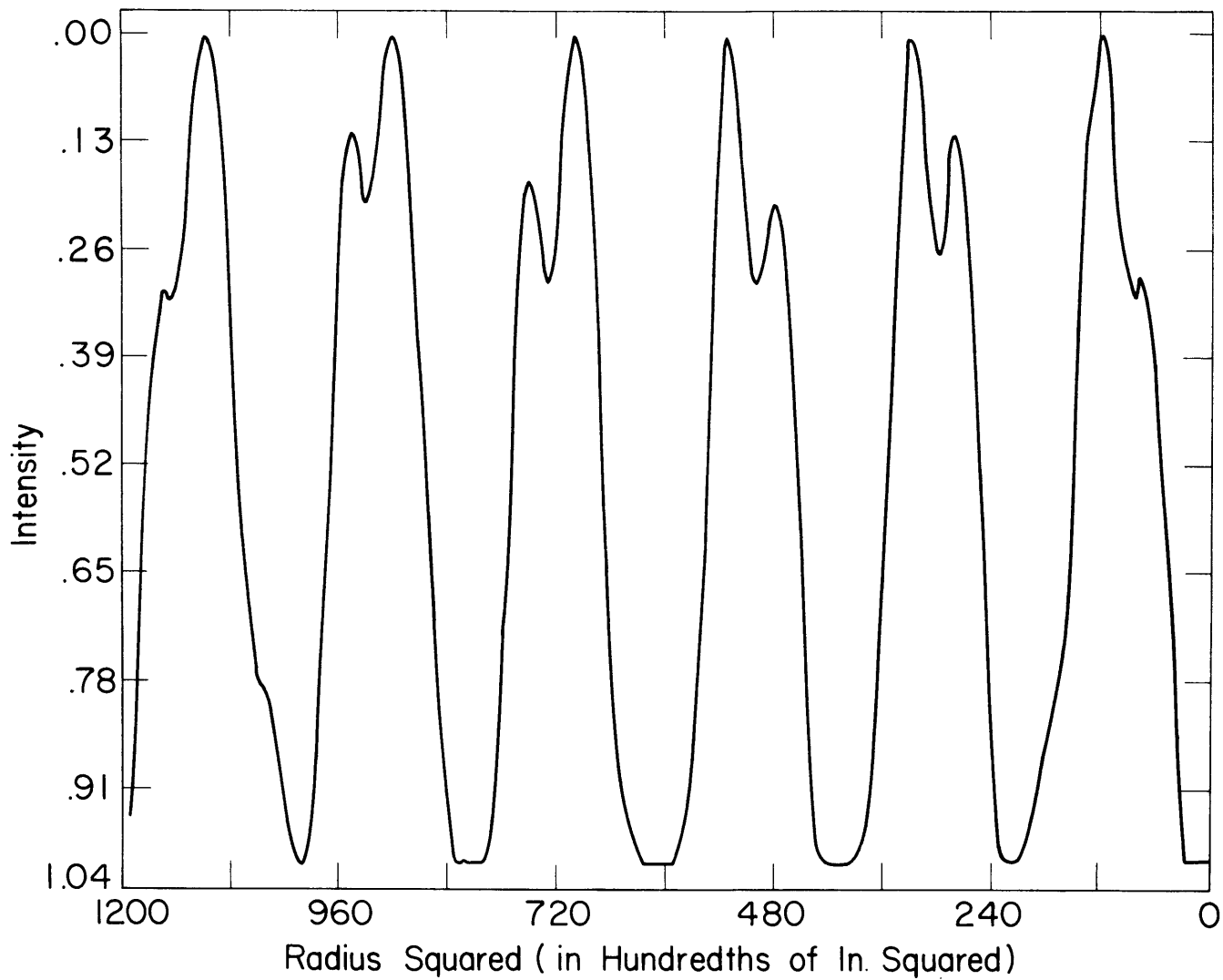
Figure 10 Computer Analysis of Plate No. 20:C
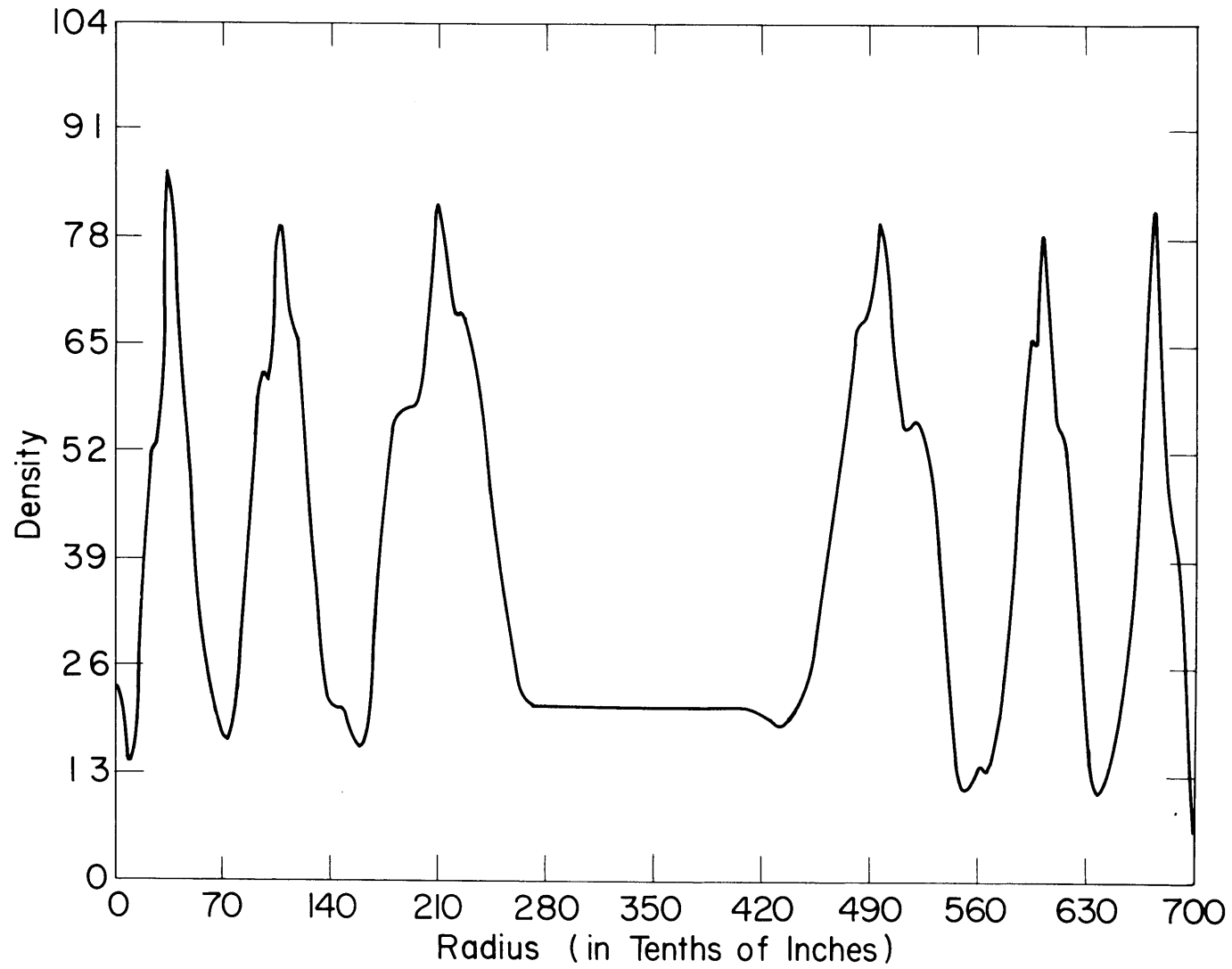
Figure II Computer Analysis of Plate No. 18:A
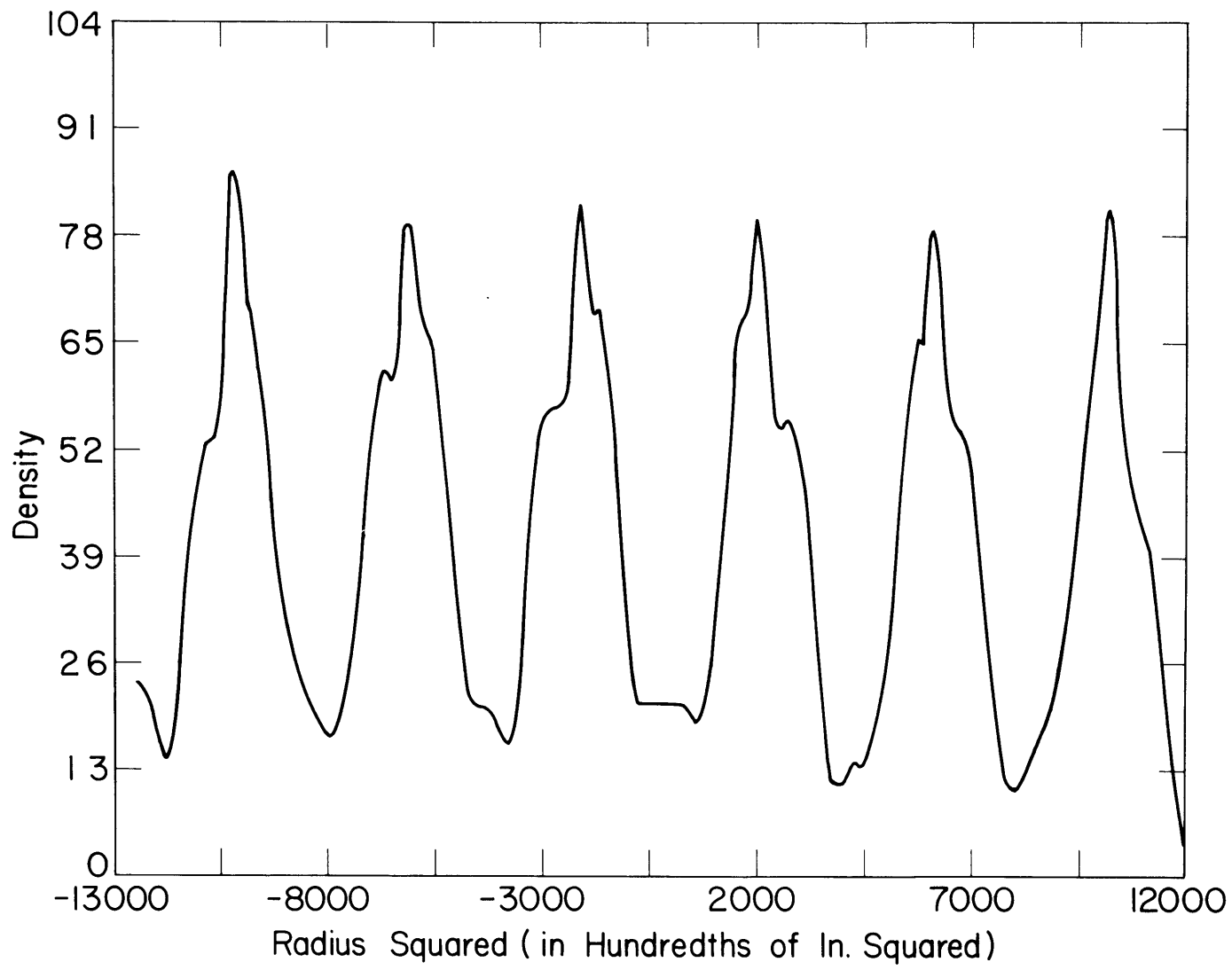
Figure 12   Computer   Analysis   of   Plate   No.   18 : B
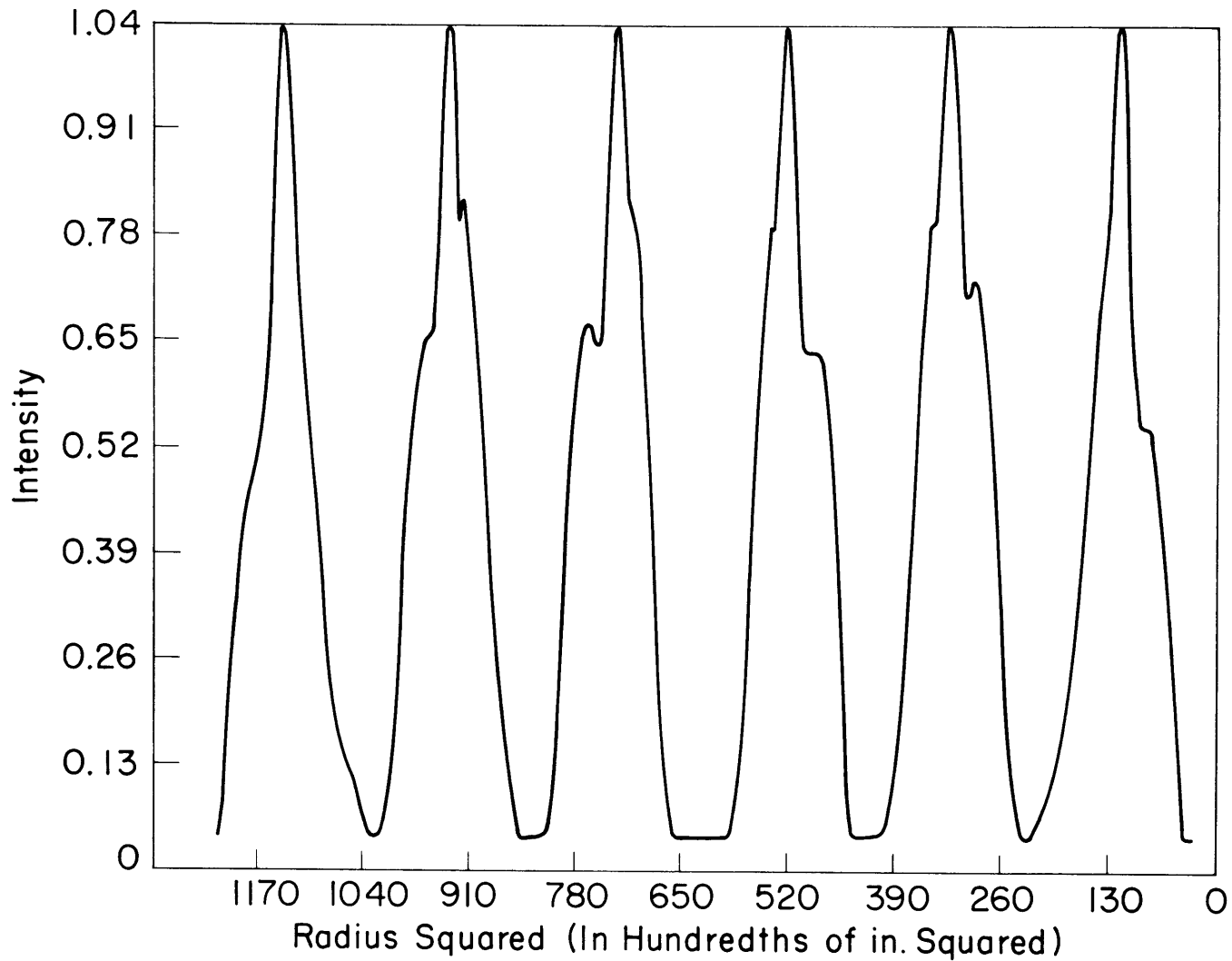
Figure 13   Computer Analysis of Plate No. 18 : C
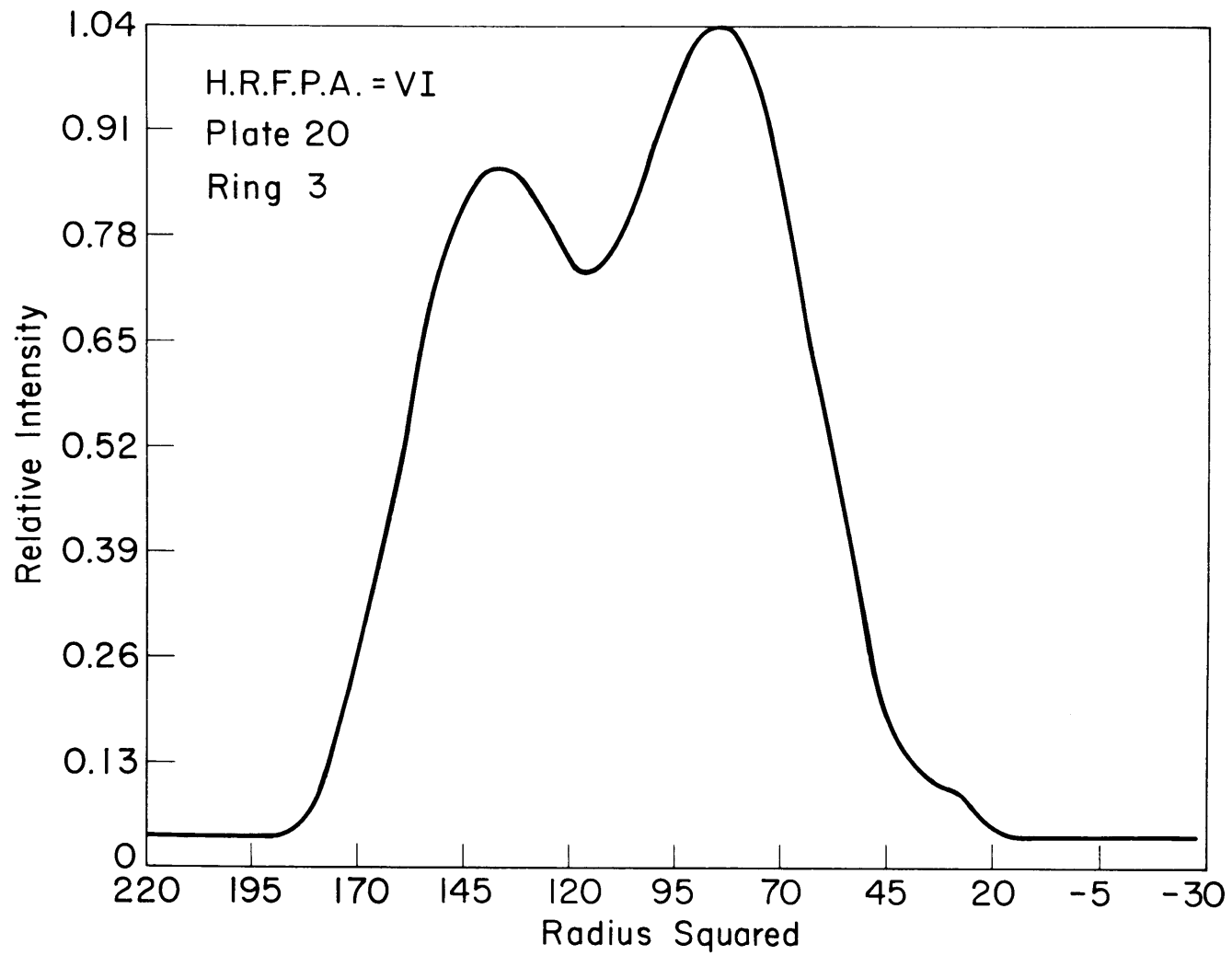
Figure 14   8446A Spontaneous Emission
Computer Analyzed Fabry- Perot Trace
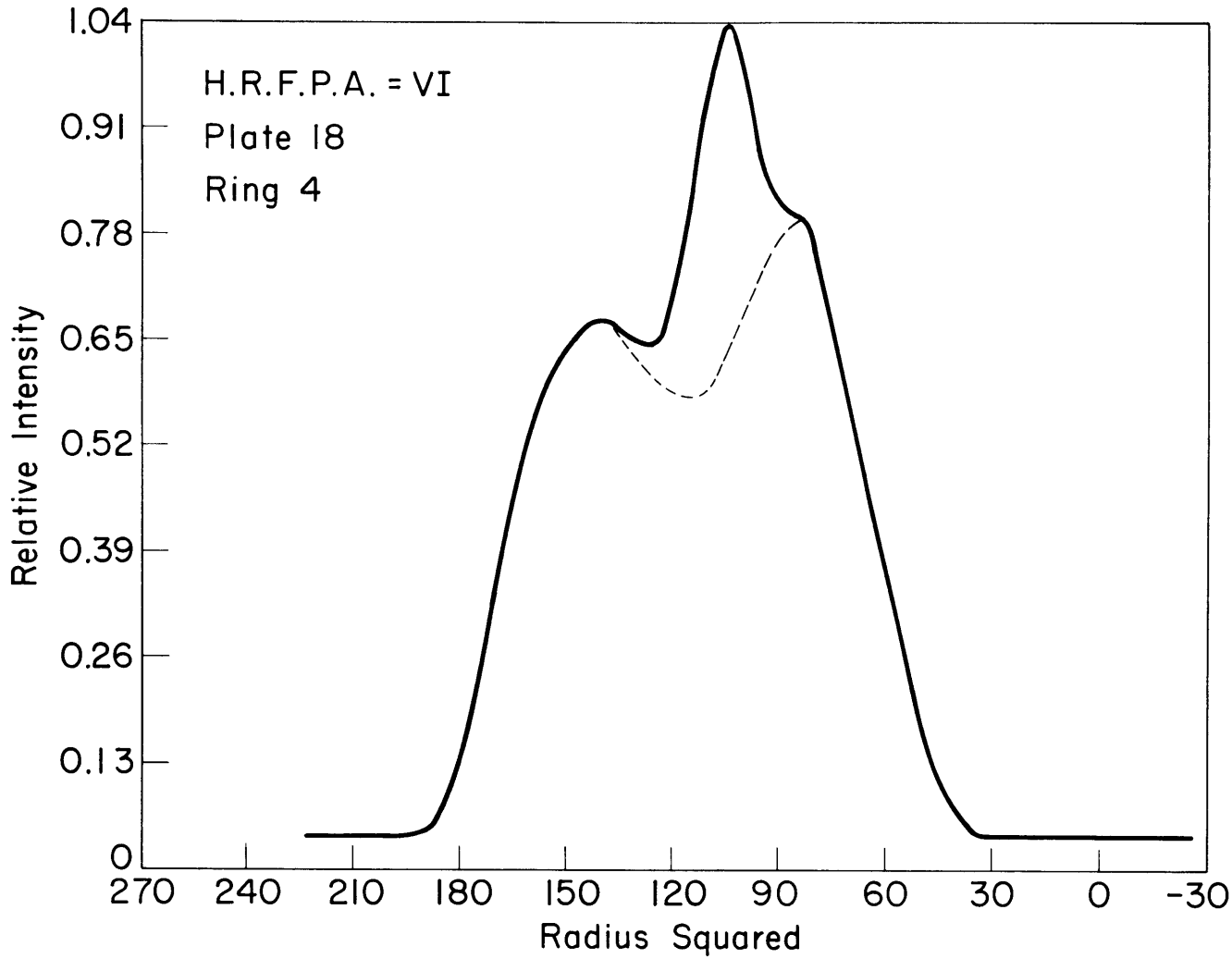
Figure 15   8446 Å Spontaneous Emission with Laser Superimposed
Computer Analyzed Fabry – Perot Trace
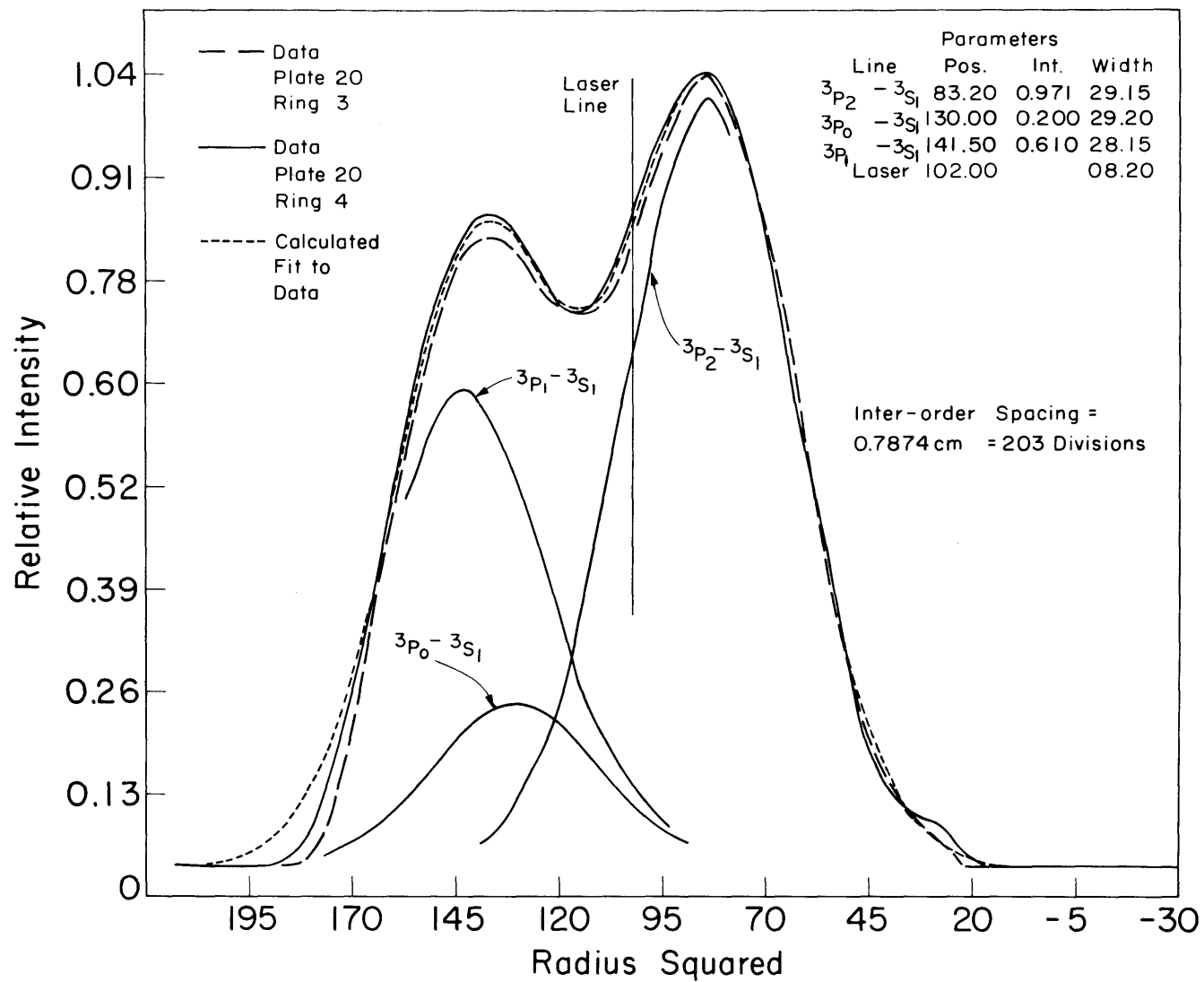
Figure 16   8446 A Intensities: Best Fit to Data of Fig's 14 and 15

PART II: LASER ACTION ON THE $^3P_{2,0}$-$^3S_1$ FINE STRUCTURE COMPONENTS

1. General Remarks

Radiative trapping of the lower level of a transition is generally regarded as a process which tends to inhibit laser action there.[10] This is not necessarily the case, however, when the velocity distributions of the laser levels are much broader than that of the level which reabsorbs the trapped photons. The latter situation leads to an effect which we shall call selective reabsorption to emphasize its inherent velocity dependence. Selective reabsorption plays an important role in laser action at 8446 Å.

2. Description of Laser Action Near the 2-1 Gain Peak

The upper levels (^3P) of the 8446 Å transitions are populated by the dissociation of oxygen molecules.[2] This leads to considerable broadening of the velocity distributions of both upper and lower laser levels, as schematically illustrated in Figure 17. Measurements of the ^3P fluorescence indicate breadths of about 0.17 cm^{-1}, 5 1/2 times those of the ground states, whose thermal distributions are determined by the walls of the discharge tube. The lower laser level ($^3S_1$) is strongly connected to the ground states via three ultraviolet transitions at about 1300 Å. This implies a large absorption cross-section, and for ground state densities as low as $10^{13}/cm^3$ the resonance radiation is sizably reabsorbed within one cm. Consequently, the population of the $^3S_1$ level is selectively increased over the central

portion of its broad velocity distribution. This strongly influences the 8446 $\overset{o}{A}$ gain profile: over the central portion of each fine-structure component the population inversion is considerably reduced and may well be reversed, and symmetrical gain peaks occur above and below line center, where there is little reabsorption. (See Figure 17.) A quantitative discussion of the selective reabsorption process described above is deferred to the following section.

The broad laser gain profile contains a very large number of axial modes, spaced 50 Mhz. apart in the present case. If the individual gain profiles did not overlap, laser action would most readily occur at the two peaks of each fine-structure component. Those of the 2-1 component, having the largest gain, would most easily exceed the threshold for oscillation. In actual fact, however, the weaker 0-1 gain profile partially overlaps the 2-1 line, and the additional gain leads to an overall population inversion peak close to the 2-1 high-frequency maximum. This results in the observed shift of the laser frequency to a point about 0.07 cm^{-1} above line center. Under typical operating conditions this laser "line" consists of a number of axial modes, and beatnotes up to 300 Mhz. have been observed.

The second highest gain maximum of the multiplet also occurs on the 2-1 line, of course, at the low-frequency peak. However, the presence of strong standing-wave optical fields on the opposite side of line center tends to suppress laser action there, as will be discussed in Part III.

$\Delta n = n_P - n_S$

$+$

$\Delta n(v)$

$-$

$-$ v $+$

C) Inverted Population

R_P

$|P)$ $\begin{matrix}0\\2\\1\end{matrix}$ $3_p\,{}^3P$

8446 Å
Fluoresence

R_S $|S)$ —————— 1 $3_s\,{}^3S^0$

Fast
u.v. Transitions,

~ 1300 Å

Selective
resonance
reabsorption

Ground $|G)$ $\begin{matrix}0\\1\\2\end{matrix}$ $2_p^4\,{}^3P$
state

Dissociation
broadened
width   3p levels

$n_P(v)$

$-$ v $+$

Bump due to
selective
reabsorption 3_s level

$n_S(v)$

$-$ v $+$

Room temp.
width   Ground State

$n_G(v)$

$-$ v $+$

a) Levels involved in
laser action

b)   Velocity   Distributions
     (units of $\sqrt{k\,T_{ROOM}\,/\,M_{ox.}}$)

Figure 17   Selective Reabsorption Effects at 8446 Å

Under optimum gain conditions a second laser line does, in fact, appear on the low-frequency side of the 2-1 gain curve. In agreement with the foregoing assertion it is not quite symmetrically positioned about line center. The above considerations similarly account for the two laser lines which occur on opposite sides of the 1-1 gain profile under the highest gain conditions. The relative positions of the four laser lines are shown in Figure 3.

3.   Effects of Selective Reabsorption at 8446 Å

In this section quantitative aspects of the influence of selective reabsorption on laser action at 8446 Å are discussed. There are a number of other cases in which selective reabsorption may lead to laser action. One promising possibility will be described in the concluding remarks.

Consider the idealized system with levels $|P\rangle$, $|S\rangle$ and $|G\rangle$, which represent the $3p\,{}^3P$, $3s\,{}^3S$ and $2p^4\,{}^3P$ multiplets and are 9-, 3- and 9-fold degenerate, respectively. (See Figure 17a). The $|P\rangle - |S\rangle$ transitions are those involved in laser action, and fast U.V. transitions connect $|S\rangle$ to the ground state, $|G\rangle$. In the absence of laser action the rate equations for the densities of $|P\rangle$ and $|S\rangle$, n_P and n_S, may be written

$$\dot{n}_S = R_S + n_P \gamma_P - n_S \gamma_S \quad ,$$

$$\dot{n}_P = R_P - n_P \gamma_P \quad , \tag{1}$$

where γ_j is the decay rate of one particular sublevel of $|j\rangle$ and R_j is the net rate of excitation to $|j\rangle$ involving all other processes. In the case of the 8446 $\overset{o}{A}$ laser R_P is primarily determined by the dissociation rate of molecular oxygen into atoms in $|P\rangle$. A number of processes contribute to R_S including electron excitation, dissociation and radiative cascade, all of which tend to inhibit laser action. In the steady state (1) yields

$$\frac{n_P}{n_S} = \frac{\gamma_S/\gamma_P}{1+R_S/R_P} , \tag{2}$$

which shows that the maximum population inversion ratio, occurring when $R_S \ll R_P$, is proportional to the ratio of the respective lifetimes of the levels involved.

At pressures of interest γ_P is approximately equal to A_P, the Einstein spontaneous emission coefficient. However, the observed decay rate of an atom in $|S\rangle$ may differ considerably from its corresponding Einstein co-efficient, A_S, depending on its velocity. At low velocities the ground state density is high and γ_S may significantly exceed A_S, since resonance photons may be absorbed and emitted many times before escaping the enclosure. Then the radiation is effectively imprisoned or "trapped" within the gas. Away from the center of the velocity distribution radiative trapping is negligible and γ_S approaches A_S. Referring to (2), the population inversion ratio is velocity dependent through $\gamma_S(v)$ and it may be diminished or

reversed over the central portion of the gain profile, depending upon the temperature and density of ground state atoms.

Our present understanding of radiation trapping stems largely from the work of T. Holstein[11][12]. For a Doppler broadened line in the limit of strong reabsorption by the ground state, Holstein calculates the effective lifetime $\tau_S = \gamma_S^{-1}$ for an infinitely long cylindrical enclosure of radius R to be[12]

$$\tau_S = A_S^{-1} \frac{n_G \sigma R \, (\pi LN \, n_G \sigma R)^{1/2}}{1.60} \quad , \quad n_G \sigma R \gg 1 \quad , \tag{3}$$

where n_G is the ground state density and σ is the absorption cross-section for the resonance radiation,

$$\sigma = \frac{g_S}{g_G} \, \pi \lambdabar_0^2 \left\{ \frac{A_S}{k_o u_G / \sqrt{\pi}} \right\} . \tag{4}$$

In equation 4 $k_o = \lambdabar_o^{-1}$ is the propagation constant of the radiation at line center, $k_o u_G$ is the Doppler width of ground state atoms with mass M and most probable speed $u_G = (2kT_G/M)^{1/2}$ at temperature T_G (approximately room temperature) and g_j is the statistical weight of $|j>$. A detailed theory of selective reabsorption would calculate the velocity-dependent lifetime $\tau_S(v)$. In Holstein's treatment the velocity dependence, which enters through $n_G(v)$, has been averaged over in the initial stages , and equation 3 is a velocity-averaged lifetime. Nevertheless, τ_S is useful in emphasizing the importance of selective reabsorption in the 8446 $\overset{o}{A}$ laser.

The principle features of a particular fine-structure gain profile can be estimated from equations 2, 3 and 4. At line center $\tau_S(v)$ will be somewhat larger than the average value, given by (3), and will slowly decrease to A_S^{-1} at the wings of the line. Under typical operating conditions the experimental parameters are: R = 0.55 cm, $u_G = 5 \times 10^4$ cm/sec and $\lambda_0 = 1300$ Å; the radiative decay rates[13] are approximately $A_S = 126 \times 10^6$/sec and $A_P = 3.1 \times 10^6$/sec. Thus $\sigma = 4 \times 10^{-14}$ cm^2. The density of ground state atomic oxygen is largely governed by its diffusion to the walls of the discharge tube, where O_2 formation occurs; it is at least a few per cent of the total oxygen content (≈ 35 μHg for Ar-O_2 mixtures[2]) and possibly considerably larger. Representative values of $n_G = 10^{14}$/cm^3 and $n_G = 5 \times 10^{14}$/cm^3 lead to average decay rates of $\gamma_S = 57 \times 10^6$/sec and $\gamma_S = 6.8 \times 10^6$/sec, respectively. Referring to equation 2, the broad central region of the gain profile of each fine-structure component will be sizeably depleted and may actually be in an absorbing phase. Regions of maximum gain will occur somewhat further away on both sides of line center. The general features are illustrated in Figure 17.

PART III: LASER ACTION ON THE $^3P_1 - {}^3S_1$ FINE STRUCTURE COMPONENTS

1. General Remarks

The fact that laser action on the 1-1 line occurs most readily above the center frequency is a direct consequence of the presence of the 2-1, 0-1 oscillation, which breaks the symmetry between the two peaks of the 1-1 gain profile, leading to maximum linear gain at the high-frequency peak.[14] The build-up of stimulated emission is most rapid over this region. This build-up tends to suppress a similar build-up at the opposite side of line center. As a result it is considerably easier to obtain oscillation at the high-frequency peak than at the low-frequency peak. It will be noted that the asymmetrical behavior is determined by the linear gain of the 1-1 profile. This quantity will be presently calculated.

2. Laser Polarization

The modes of a Fabry-Perot laser cavity are standing waves. Thus in analyzing this situation it is necessary to calculate the polarization of a medium interacting with standing-wave fields. This was first achieved by Willis Lamb for a two-level laser,[15] and has recently been extended to three-level systems by Schlossberg and Javan.[16] To take account of the inhomogeneous broadening due to the Doppler effect, these treatments utilize a perturbation theory involving the integral form of the density matrix. The formulations are rather complex and results

have only been obtained for weakly-saturating fields. Although this is adequate in many cases, a more general approach is certainly of interest. Furthermore, in the case at hand strong saturation of the 2-1 transition plays an essential role in bringing about the unusual behavior in question. In the following an alternate approach is developed, with assumptions equivalent to those of Lamb. In many cases, however, this new approach enables results to be obtained in closed form, valid for fully saturated transitions.

In a laser cavity atoms may traverse many wavelengths of the standing-wave fields before decaying. To understand how this motion influences the polarization of the laser medium consider a particular group of atoms moving with axial velocity component v_p. Within this group the atoms are assumed to be excited into particular states at various times, when they begin interacting with the laser fields. The simplest model of atomic motion considers the atoms in a particular state to travel undeflected with constant velocity v_p from their creation until their decay. Thus, at a given position and time the group of atoms in a particular state is comprised of ensembles of atoms which began interacting with the field at various past times. The equations of motion of a particular velocity ensemble may be expressed in terms of its density matrix. Considering the collection of atoms as a whole, the question arises as to whether or not the ensemble-averaged equations of motion may be dealt with directly.[17] This can be done if it is permissable

to neglect the dependence of the interaction Hamiltonian upon initial conditions of constituent velocity ensembles. Otherwise it becomes necessary to solve the equations of motion for a particular ensemble, and then perform the average over all possible initial conditions.

In this regard it is important to point out that the present situation does not substantially differ from the case of atoms at rest. To see this consider the laser field $\mathcal{E}$ (z, t) composed of standing waves $\mathcal{E}_j(z, t)$, $j = 1, M$, propagating along the z-axis:

$$\mathcal{E}(z, t) = \sum_{j=1}^{M} \mathcal{E}_j(z, t) = \sum_{j=1}^{M} \mathcal{E}_j^0 \, U_j(z) \cos(\Omega_j t + \phi_j) , \tag{8}$$

in which $U_j(z)$ is the jth normal mode of the laser cavity, given by

$$U_j(z) = \cos k_j z, \qquad k_j = j\pi/L, \tag{9}$$

with cavity length L. Each $\mathcal{E}_j$ may be resolved into two travelling waves of equal amplitude propagating in opposite directions,

$$\mathcal{E}_j(z, t) = \mathcal{E}_j^+(z, t) + \mathcal{E}_j^-(z, t), \tag{10a}$$

in which the superscripts denote propagation along the $\pm z$ directions. Specifically,

$$\mathcal{E}_j^{\pm}(z,t) = \text{Re}\{ \mathbf{a}_j^{\pm}(z)\, e^{i\Omega_j t} \} \qquad , \qquad (10b)$$

$$\mathbf{a}_j^{\pm}(z) = \frac{1}{2}\, \mathcal{E}_j^{\,o}\, e^{i\phi_j}\, e^{\pm ik_j z} \qquad . \qquad (10c)$$

In the frame in which the group of atoms with v_p is at rest $\mathcal{E}_j(z,t)$ transforms into two oppositely propagating travelling components with coordinates $\{z',t'\}$:

$$E_j(z,t) \rightarrow E_j^+(z',t') + E_j^-(z',t') \quad , \qquad (11a)$$

where

$$E_j^{\pm}(z',t') = \text{Re}\{ A_j^{\pm}(z')\, e^{i\Omega_j^{\pm} t'} \} \qquad , \qquad (11b)$$

$$A_j^{\pm}(z') = \frac{1}{2}\, \mathcal{E}_j^{\,o}\, e^{i\phi_j}\, e^{\mp ik_j z'} \qquad . \qquad (11c)$$

The frequencies and propagation constants in the moving frame are related to those in the rest frame by

$$\Omega_j^{\pm} \cong \Omega_j(1 \mp v_p/c) \quad , \quad k_j^{\pm} = \Omega_j^{\pm}/c. \qquad (12)$$

In this reference frame the situation reduces to travelling-wave radiation fields interacting with stationary ensembles of atoms. The question of whether or not the ensemble average may be taken before solving the

equations of motion must still be resolved. But it is clear that in the moving coordinate system atomic motion does not influence the state of affairs.

Regardless of how the averaging is carried out, the ensemble-averaged polarization in the moving frame is obtained:

$$P'(z',t';v_p) = Re \sum_{j=1}^{M} \{ \chi_j^+ A_j^+ e^{i\Omega_j^+ t'} + \chi_j^- A_j^- e^{i\Omega_j^- t'} \} , \tag{13}$$

in which the $\chi_j^{\pm}$ are travelling-wave susceptibilities in the moving system. Equation 13 can then be transformed back into the laser rest frame to yield the ensemble-averaged polarizability, $P(z,t;v_p)$, at coordinates $\{z,t\}$:

$$P(x,t;v_p) = Re \sum_{j=1}^{M} \{ \chi_j^+ a_j^+ + \chi_j^- a_j^- \} e^{i\Omega_j^- t} . \tag{14}$$

The $\chi_j^{\pm}$ are unaffected by the transformation as long as they do not contain the moving-frame coordinates. This is generally the case.

This purely formal manipulation shows that the effects of motion of the group of atoms moving with v_p can generally be taken into account by first computing the travelling-wave susceptibilities neglecting atomic motion, then simply replacing the Ω_j by their Doppler shifted values $\Omega_j^{\pm}$, given by (12),

wherever they appear. Once this is done $P(z, t; v)$ may be averaged over the velocity distribution in a straightforward manner. Indicating the velocity averages by brackets, the net polarization $P(z, t)$ is given by

$$P(z, t) = \text{Re} \sum_{j=1}^{M} \{ <x_j^+> \alpha_j^+ + <x_j^-> \alpha_j^- \} \, e^{i\Omega_j t} . \tag{15}$$

The velocity distribution is, of course, symmetrical about the z-axis, and the $x_j^{\pm}$ contribute identically to the velocity averages. Thus

$$<x_j^+> = <x_j^-> \equiv X_j , \tag{16}$$

and (15) becomes

$$P(z, t) = \text{Re} \sum_{j=1}^{M} X_j U_j (z) \, \mathcal{E}_j^o \, e^{i(\Omega_j t + \phi_j)} . \tag{17}$$

Equation 17 gives the complete velocity-averaged standing-wave polarization. It is emphasized that the above technique is general and may be applied to a number of other cases of interest.

3. Quantum-Mechanical System

The 2-1, 0-1 oscillation influences the 1-1 gain profile through the coupling of the ${}^3P_1$ level with the rest of the multiplet. The presence of this strongly interacting field, taken to be polarized linearly along the axis of
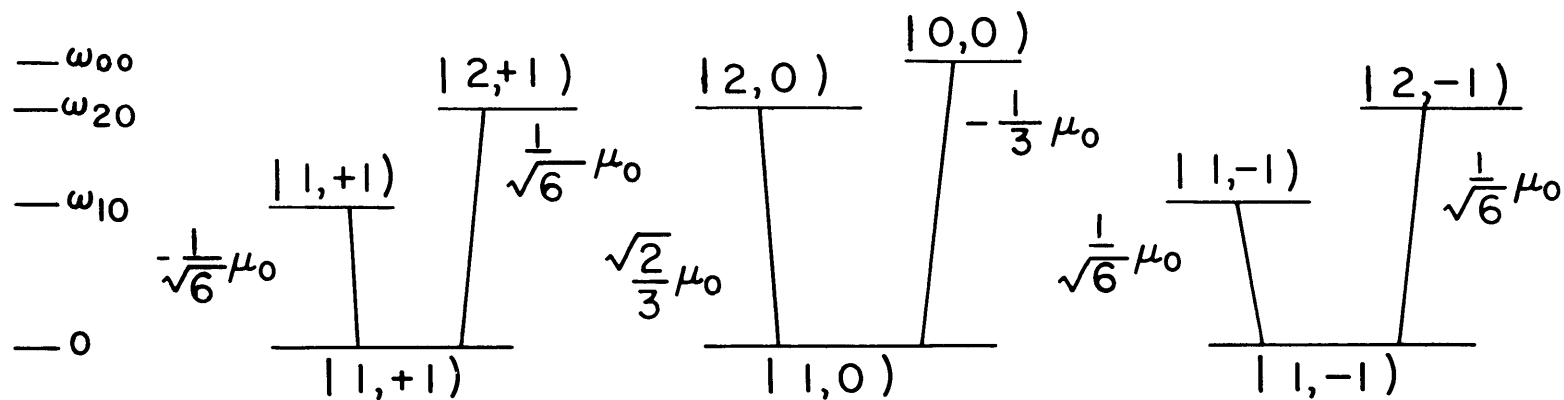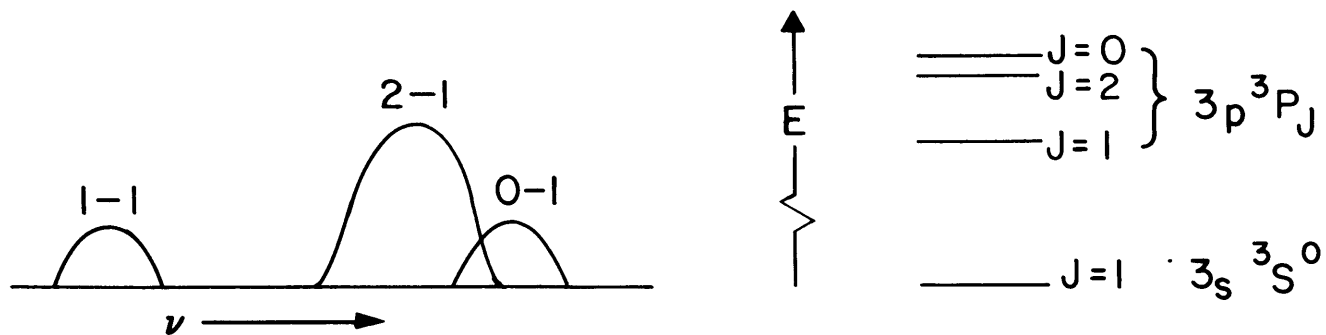
Figure 18 8446 Å Energy Levels and Matrix Elements, $\vec{\varepsilon_1} \parallel \vec{\varepsilon_2} \parallel \hat{Z}$

quantization,[18] destroys the rotational invariance of the atomic system. Accordingly, the 1-1 gain depends upon the relative direction of polarization of its associated field, also taken as linearly polarized. It is sufficient to consider the two possibilities of mutually parallel fields and mutually perpendicular fields, since any relative orientation may be resolved into these components. The former possibility is straightforward and will be dealt with shortly. The latter possibility involves a rather complex coupling scheme which may be considerably simplified, however, by a linear transformation of the coupled equations of motion. The transformed level scheme does not greatly differ from the case of mutually parallel fields and leads to a very similar gain profile. The details are somewhat lengthy and are deferred to Appendix B.

The case of mutually parallel fields is now considered. The coupling can be considered to precede entirely through the $\Delta M = 0$ transitions. This choice considerably simplifies matters, separating the 8446 $\overset{o}{A}$ multiplet into three isolated 3-level systems, shown in Figure 18 with R-S matrix elements indicated. The only coupling to the $^3P_1$ component occurs equally through the $M = +1$ and $M = -1$ states. Thus for our purposes the entire multiplet reduces to a lower state equally connected to two upper states separated by $J = 2$, $J = 1$, fine-structure splitting. In the following discussion the upper states, associated with the $J = 1$ and $J = 2$ components, are designated as $|1\rangle$ and $|2\rangle$, respectively, and the lower state, associated with the $^3S_1$ level, by $|0\rangle$. Equal electric dipole matrix elements μ_{10} and μ_{20} connect the lower state with $|1\rangle$ and $|2\rangle$, respectively. The energy of $|j\rangle$ is written as $E_j = \hbar\omega_j$ and $E_j - E_k = \hbar\omega_{jk}$. (See Figure 19.) Since there is no ambiguity we will continue to refer to the "1-1" and "2-1" fine-structure transitions.
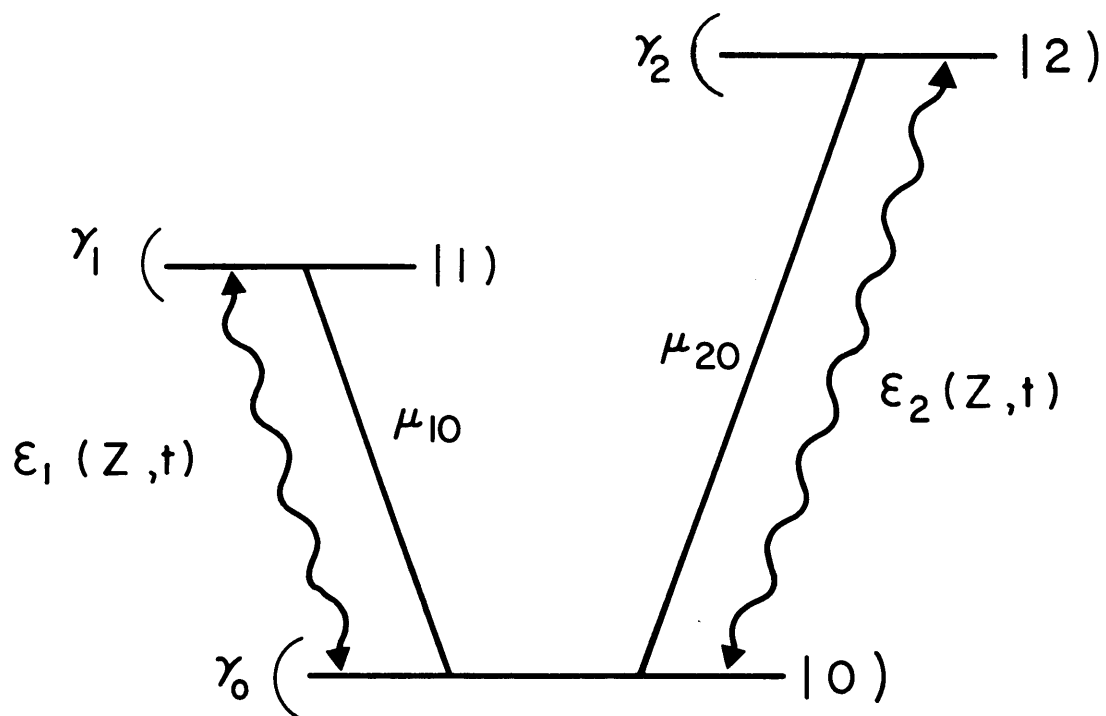
Figure 19 Coupling Scheme

4. Interaction of Laser Fields With Quantum-Mechanical System

This three-level system interacts with a strongly saturating field $\mathcal{E}_2(z,t)$, at Ω_2, a frequency slightly higher than ω_{20}. The 1-1 resonance is probed by the weak field $\mathcal{E}_1(z,t)$ of variable frequency Ω_1. Both fields are taken to be linearly polarized and propagate in the z direction, along the laser tube axis. Each standing-wave field may be resolved into its travelling-wave components. To a group of atoms moving with given axial velocity the right and left travelling components appear Doppler-shifted by different amounts. In the optical-infrared region these frequency shifts greatly exceed the homogeneously-broadened linewidth for all but the slowest atoms. Therefore, in general a particular laser oscillation couples most strongly to the two groups of atoms symmetrically located about the center of the velocity distribution which Doppler-shift one or the other travelling components into resonance. This leads to sharp changes in laser polarization whenever an atomic velocity group interacts simultaneously with two travelling-wave components. The extent over which these changes occur is characterized by the homogeneous widths of the system.

In the general case of two fields interacting with three coupled levels numerous situations arise in which two oppositely propagating components, at least one of which is capable of saturating the atomic transitions, interact with the same velocity group. In the present case the situation is somewhat simpler. First of all we need only consider a weak field at Ω_1. In this limit the oppositely travelling components of $\mathcal{E}_1$ do not interact with each other. Furthermore, Ω_2 is considerably displaced from the 2-1 center frequency. Thus, oppositely propagating components of $\mathcal{E}_2$ do not interact. These simplifications considerably reduce the complexity of the calculations.

To inspect the effects of $\mathcal{E}_2$ on the 1-1 gain profile consider its travelling-wave components $\mathcal{E}_2^+$ and $\mathcal{E}_2^-$, propagating along the +z and -z directions, respectively. Since $\Omega_2 > \omega_{20}$ the $\mathcal{E}_2^+$ component interacts resonantly with the set of atoms with velocity component $\pm v_r$ given by the Doppler resonance condition: $\Omega_2 \, (1 \mp \dfrac{v_r}{c}) = \omega_{20}$. (See Figure 20.) When $\mathcal{E}_1$ is near either of the 1-1 gain peaks it resonates with the same sets of atoms strongly interacting with $\mathcal{E}_2$. Resolving $\mathcal{E}_1$ into its travelling components $\mathcal{E}_1^+$ and $\mathcal{E}_1^-$, one sees that $\mathcal{E}_1^+$ interacts at the 1-1 high-frequency peak with the $\pm v_r$ set and at the low-frequency peak with the $\mp v_r$ set (See Figure 20.) In other words, stimulated emission at the 1-1 high-frequency peak couples together the field component pairs $\mathcal{E}_1^+, \mathcal{E}_2^+$ and $\mathcal{E}_1^-, \mathcal{E}_2^-$; at the low-frequency peak it couples together the field pairs $\mathcal{E}_1^+, \mathcal{E}_2^-$ and $\mathcal{E}_1^-, \mathcal{E}_2^+$. At other portions of the 1-1 gain profile coupling effects between field components are negligible. As explained in Section 2, the symmetry of the velocity distribution implies that at each of the 1-1 gain peaks both pairs of coupled fields contribute identically to the velocity-averaged gain. Thus the complete 1-1 gain profile can be obtained from two contributions: one arises from the interaction of two oppositely propagating travelling waves, and leads to resonant behavior at the low-frequency peak; the other arises from two interacting travelling waves propagating in the same direction, and leads to a resonance at the high-frequency peak. These will be referred to as the "anti-parallel" and "parallel" contributions, respectively. The characteristics of the two
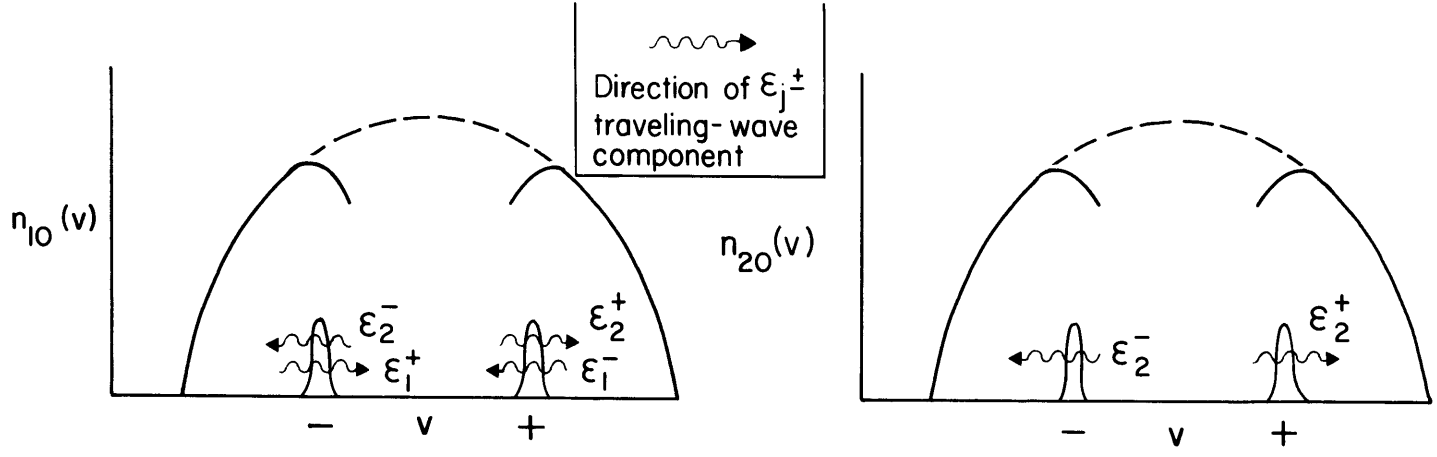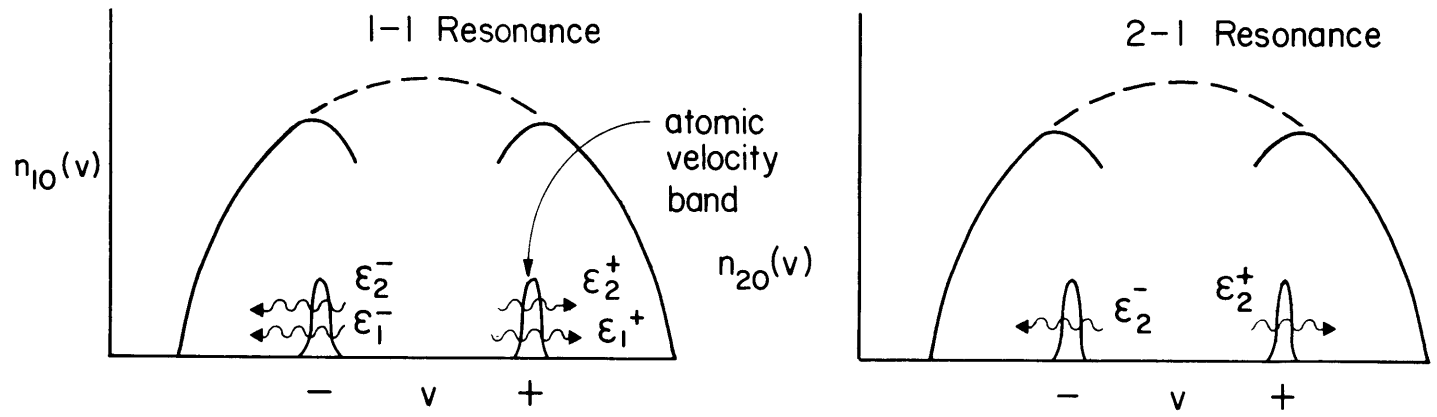
Figure 20 Interaction of Laser Fields with Atomic Velocity Distributions

resonances are quite different, resulting in an asymmetric gain profile.

5.   Ensemble-Averaged Polarization

In the following the ensemble-averaged polarization, (14), is obtained

for a group of atoms with axial velocity component v interacting with two

laser fields. It was pointed out in Section 2 that the method of calcula-

tion depends upon the applicability of the ensemble-averaged density matrix

equations of motion. It is certainly plausable that the approximations

involved are permissable in the present case. However, one is always on

firmer ground first calculating the induced dipole moment for arbitrary initial

conditions and subsequently taking the average over ensembles. For the

case at hand it has been directly verified that the two methods do indeed

lead to the same results. Because of its algebraic simplicity the following

presentation utilizes the ensemble-averaged density matrix. The alternate

approach, carried out using wave functions, is deferred to Appendix A .

Incidentally, the latter, although algebraically involved, is conceptually

simpler, and the interpretation of various contributions to the polariza-

tion is often more transparent in this treatment.

The quantum-mechanical state of a collection of ensembles at position

$\vec{r}$, at time t, and moving with axial velocity v may be described in terms of

its ensemble-averaged density matrix ρ $(\vec{r}, t; v)$[19] The Hamiltonian for this

collection is

$$H = H_0 + V \ (\vec{r}, t; v), \tag{18}$$

in which H_0, with eigenvalues E_0, E_1, E_2, describes an isolated atom and V is the interaction Hamiltonian. Inasmuch as the net interaction may be closely approximated by the coupling of individual travelling-wave components of $\mathcal{E}_1$ to those of $\mathcal{E}_2$, it is sufficient to deal with the field components two at a time. In other words, a particular contribution to the polarization results from the interaction Hamiltonian

$$V \ (\delta, \tau) = - \mu \mathcal{E}(\delta, \tau) = - \mu \ [\ \mathcal{E}_1^{\ \delta}(z, t) + \mathcal{E}_2^{\tau} \ (z, t) \ ], \tag{19}$$

where μ is the electric dipole operator and the $\mathcal{E}_j^{\alpha}$, $\alpha = +, -,$ are the travelling-wave components defined in (10). The ensemble-averaged polarization due to a particular pair of fields (19) is given by

$$P(\delta, \tau) = tr(\mu \rho) = 2 \ \text{Re} \ \{\mu_{10} \rho_{01} + \mu_{20} \rho_{02}\}$$

$$= \{ \chi_1(\delta, \tau) \mathcal{Q}_1^{\delta} \ e^{\ i \Omega_1 t} + \chi_2(\delta, \tau) \mathcal{Q}_2^{\tau} \ e^{\ i \Omega_2 t} \} \ . \tag{20}$$

The latter expression defines the general susceptibility components $\chi_1(\delta, \tau)$ and $\chi_2(\delta, \tau)$. After they have been obtained the substitutions

$$\Omega_1 \rightarrow \Omega_1 - \delta k_1 v,$$

$$\Omega_2 \rightarrow \Omega_2 - \tau k_2 v, \tag{21}$$

should be made, as discussed in Section 2 . For $\delta = \tau$, the $\chi_j (\delta, \tau)$ then yield the parallel contributions to the susceptibilities (c.f. equation 14):

$$\chi_j (\delta, \delta) = \chi_j^{\delta} \; ; \tag{22}$$

for $\delta = -\tau$, they yield the anti-parallel contributions:

$$\chi_1 (\delta, -\delta) = \chi_1^{\delta} ,$$

$$\chi_2 (-\delta, \delta) = \chi_2^{\delta} . \tag{23}$$

Inserting equations 22 and 23 into (14) (for M = 2 standing-wave fields) yields the parallel and anti-parallel contributions to the ensemble averaged polarization, respectively.

The general susceptibility components $\chi_1 (\delta, \tau)$ and $\chi_2(\delta, \tau)$ are now calculated. The ensemble-averaged equations of motion of the density matrix $[\rho_{ij} (\vec{r}, t; v)]$ may be written as follows:

$$\dot{\rho}_{00} = \gamma_0 (\rho_{00}^0 - \rho_{00}) - \frac{i\mathcal{E}}{\hbar} [(\mu_{10} \rho_{01} - \mu_{02}\rho_{20}) - c.c.] ,$$

$$\dot{\rho}_{11} = \gamma_1 (\rho_{11}^0 - \rho_{11}) + \frac{i\mathcal{E}}{\hbar} (\mu_{10}\rho_{01} - c.c.) \; ; \tag{24a}$$

$$\dot{\rho}_{22} = \gamma_2 (\rho_{22}^0 - \rho_{22}) - \frac{i\mathcal{E}}{\hbar} (\mu_{02}\rho_{20} - c.c.) \; ;$$

$$\dot{\rho}_{01} = - (\gamma_{01} + i\omega_{01}) \, \rho_{01} + \frac{i\mathcal{E}}{\hbar} \, [\mu_{01}(\rho_{11} - \rho_{00}) + \mu_{02}\rho_{21}] \, ,$$

$$\dot{\rho}_{20} = - (\gamma_{20} + i\omega_{20}) \, \rho_{20} - \frac{i\mathcal{E}}{\hbar} \, [\mu_{20} \, (\rho_{22} - \rho_{00}) + \mu_{10}\rho_{21}] \, , \qquad (24b)$$

$$\dot{\rho}_{21} = - (\gamma_{21} + i\omega_{21}) \, \rho_{21} + \frac{i\mathcal{E}}{\hbar} \, [\mu_{20} \, \rho_{01} \qquad - \mu_{01}\rho_{20}] \, .$$

In these equations ρ_{ii}^0 is the steady-state density of $|i>$ in the absence of impressed fields. The γ_{ij} are the decay rates of the corresponding ρ_{ij} and have been introduced phenomenologically in the following manner. The density matrix elements are bilinear combinations of the probability amplitudes of the various states. When relaxation occurs through spontaneous emission or, more generally, by hard collisions, the decay of $|i>$ can be assumed to be assumed to be exponential with decay constant γ_{ii}. (This point is amplified in Appendix A1.) Then each γ_{ij} is the sum of the decay constants of its constituent amplitudes:

$$\gamma_{ij} = \frac{1}{2} \, (\gamma_i + \gamma_j) \, , \qquad (25)$$

with $\gamma_{ii} = \gamma_i$ as the homogeneously broadened width of $|i>$.

In the steady state the $\dot{\rho}_{ii} = 0$ except for population fluctuations which are entirely negligible when the $\hbar\Omega_j >> <\mu\mathcal{E}>$. Under these conditions the density matrix equations may be compactly rewritten in the following form:

$$r_{10} = r^0_{10} + \frac{i\mathcal{E}}{\hbar} \left[\left\{ \frac{-\mu_{02}\rho_{20}}{\gamma_0} + \left(\frac{1}{\gamma_1} + \frac{1}{\gamma_0}\right) \mu_{10}\rho_{01} \right\} - \text{c. c.} \right]$$

$$r_{20} = r^0_{20} - \frac{i\mathcal{E}}{\hbar} \left[\left\{ -\frac{\mu_{10}\rho_{01}}{\gamma_0} + \left(\frac{1}{\gamma_2} + \frac{1}{\gamma_0}\right) \mu_{02}\rho_{20} \right\} - \text{c. c.} \right] \qquad (26a)$$

$$\gamma_0 \left(\rho_{00} - \rho^0_{00}\right) + \gamma_1 \left(\rho_{11} - \rho^0_{11}\right) + \gamma_2 \left(\rho_{22} - \rho^0_{22}\right) = 0;$$

$$\mathcal{L}_{01}\rho_{01} = -\frac{\mathcal{E}}{\hbar} \left(\mu_{01} r_{10} + \mu_{02}\rho_{21}\right),$$

$$\mathcal{L}_{20}\rho_{20} = +\frac{\mathcal{E}}{\hbar} \left(\mu_{20} r_{20} + \mu_{10}\rho_{21}\right), \qquad (26b)$$

$$\mathcal{L}_{21}\rho_{21} = -\frac{\mathcal{E}}{\hbar} \left(\mu_{20}\rho_{01} - \mu_{01}\rho_{20}\right).$$

In the latter equations we have introduced the operator

$$\mathcal{L}_{ij} = i\frac{d}{dt} - \omega_{ij} + i\gamma_{ij}, \qquad (27)$$

and have also written $r_{ij} = \rho_{ii} - \rho_{jj}$ and $r^0_{ij} = \rho^0_{ii} - \rho^0_{jj}$.

This set of equations may be solved by inserting $\mathcal{E}(\delta, \tau)$ in complex form. The various Fourier components of $\mathcal{E}$ drive the off-diagonal elements ρ_{ij}. Of special importance are the coefficients of the ρ_{ij} on the left-hand side of equations 26b. These are associated with the resonant behavior of the induced polarization. The only important frequency components of the ρ_{ij} are those which can reduce the magnitudes of their coefficients to the γ_{ij} for particular values of Ω_1 and Ω_2.

In other words, a nearly exact solution of equation 26 can be obtained by assuming the following form for the off-diagonal density-matrix components:

$$\rho_{20} \cong \lambda \, e^{-i\Omega_2 t},$$

$$\rho_{01} \cong \Lambda \, e^{+i\Omega_1 t}, \tag{28}$$

$$\rho_{21} \cong D \, e^{-i\Omega_{21} t}.$$

Inserting (28) into equations 26, one obtains a set of five simultaneous linear equations:

$$- i \, (r_{10} - r_{10}^0) = \left[-\frac{\beta}{\gamma_0} \lambda + (\frac{1}{\gamma_0} + \frac{1}{\gamma_1}) \, \alpha^* \Lambda \right] - c.c. \, ,$$

$$\tag{29a}$$

$$+ i \, (r_{20} - r_{20}^0) = \left[-\frac{\alpha^*}{\gamma_0} \Lambda + (\frac{1}{\gamma_0} + \frac{1}{\gamma_2}) \, \beta^* \lambda \right] - c.c. \, ,$$

$$L_{10}(-\Omega_1)^* \, \Lambda = \alpha \, r_{10} + \beta \, D,$$

$$L_{20}(-\Omega_2) \, \lambda = \beta^* \, r_{20} + \alpha^* \, D, \tag{29b}$$

$$L_{21}(-\Omega_{21}) \, D = \alpha \, \lambda - \beta^* \, \Lambda \, .$$

In equations 29 $\alpha = \mu_{01} \, \mathcal{Q}_1^\delta / 2\hbar$, $\beta = \mu_{02} \, \mathcal{Q}_2^\tau / 2\hbar$, $\Omega_{21} = \Omega_2 - \Omega_1$, and we have introduced the eigenvalues

$$L_{ij} \, (\Omega) = - (\Omega + \omega_{ij}) + i\gamma_{ij} \tag{30}$$

which correspond to the operators $\mathcal{L}_{ij}$ of equation 27.

A solution to this set of equations for all values of $\mathcal{E}_2^T$ and for weak $\mathcal{E}_1^\delta$ (i. e. $\alpha \ll 1$) can be obtained by means of a simple perturbation technique. In the absence of coupling through α the system reduces to a simple two-level system, and the off-diagonal matrix elements ρ_{01} and ρ_{21} vanish. Setting $\alpha = 0$, (29) simplifies to

$$\Lambda^u = D^u = 0 \; ;$$

$$i \, (r_{10}^u - r_{10}^0) = \frac{\beta}{\gamma_0} \, \lambda^u - \text{c. c.} \; ,$$

$$i \, (r_{20}^u - r_{20}^0) = (\frac{1}{\gamma_0} + \frac{1}{\gamma_2}) \, \beta \lambda^u - \text{c. c.} \; , \tag{31}$$

$$L_{20} \, \lambda^u = \beta^* \, r_{20}^u \; ,$$

in which the superscript u has been introduced to designate the parameters of the uncoupled system and the frequency dependence of the L_{ij} has been suppressed. Equations 31 yield the unperturbed solutions:

$$\lambda^u = \frac{r_{20}^0 \beta^* L_{20}^*}{\Delta} \; ,$$

$$r_{10}^u = r_{10}^0 - 2 \, \frac{\gamma_{20}}{\gamma_0} \, \frac{|\beta|^2 r_{20}^0}{\Delta} \; , \tag{32}$$

$$r_{20}^u = \frac{r_{20}^0 \, |L_{20}|^2}{\Delta} \; .$$

where

$$\Delta = |L_{20}|^2 + \frac{4\gamma_{02}^2}{\gamma_0 \gamma_2} \, |\beta|^2 \; . \tag{33}$$

The presence of coupling through $\mathcal{E}_1^\delta$ does not affect the unperturbed parameters λ^u, r_{10}^u, r_{20}^u to lowest order in α. Thus the first order coefficients Λ^1 and D^1 are determined by the first and third off-diagonal equations (29b):

$$L_{10}^* \Lambda^1 = \alpha r_{10}^u + \beta D^1 \ ,$$

$$L_{21} D^1 = \alpha \lambda^u - \beta^* \Lambda^1 \ . \tag{34}$$

These immediately yield

$$\Lambda^1 = \alpha \frac{r_{10}^u L_{21} + \beta \lambda^u}{L_{21} L_{10}^* + |\beta|^2} \ . \tag{35}$$

Further iteration of (29) may be performed if desired.

The general susceptibilities, defined in equation 20, may be obtained from (32) and (35) complete to first order in α:

$$\chi_1 (\delta, \tau) = \frac{2\mu_{10} \Lambda}{\alpha_1} \cong r_{10}^0 \frac{|\mu_{10}|^2 L_{21}}{\hbar \Gamma}$$

$$- r_{20}^0 \frac{|\mu_{20}|^2}{\hbar} \left| \frac{\mu_{10} E_2}{2\hbar} \right|^2 \left(\frac{2 \frac{\gamma_{20}}{\gamma_0} L_{21} - L_{20}^*}{\Delta \Gamma} \right), \tag{36}$$

$$\chi_2 (\delta, \tau) = \frac{2\mu_{20} \lambda^*}{\alpha_2} \cong r_{20}^0 \frac{|\mu_{20}|^2 L_{20}}{\hbar \Delta} \ , \tag{37}$$

in which

$$\Gamma = L_{21} L_{10}^{*} + |\beta|^{2}. \tag{38}$$

Equation 37 will be recognized as the homogeneously-broadened susceptibility of a two-level system. Setting all the relaxation rates equal, the imaginary part of (36) becomes equivalent to expressions first obtained by A. Javan using wave functions.[20] After summing over the velocity distribution many features of the rather interesting lineshape will average out. The reader is referred to the papers of Javan[20] and Yajima[21] for complete discussions of those features.

6. Velocity Averages

A. Discussion

To obtain the laser polarization, (17), it is necessary to calculate the velocity-averaged susceptibilities X_j, $j = 1$, 2, defined in equation 16, from (36) and (37). In subsequent discussion it is convenient to set $\tau = +$, since only the relative propagation direction between field components is of signifigance in the averages. Then $\delta = +$ (-) represents the parallel (anti-parallel) contribution to $P(z, t)$. Extending the notation of (16), let the parallel and anti-parallel contributions to X_j be denoted by X_j^p and X_j^a, respectively. Referring to (22) and (23),

$$X_j^p = < \chi_j \, (+,+) > \quad , \tag{39a}$$

$$X_j^a = < \chi_j \, (-,+) > \quad . \tag{39b}$$

At the high-frequency peaks $X_j = X_j^p$ and at the low-frequency peaks $X_j = X_j^a$; at other regions of interest field components do not couple and $X_j = X_j^p = X_j^a$.

Some important features of (39) are briefly inspected before explicitly carrying out the integrations. The weak field $\mathcal{E}_1$ does not affect χ_2, consequently the inhomogeneously broadened 2-1 gain profile is unaltered by its presence. In contrast, $\mathcal{E}_2$ greatly influences the 1-1 gain profile. The resonant characteristics of the latter are determined by the L_{ij}, which exhibit two distince types of tunability: the usual two-level behavior, in which one applied field resonances with a pair of energy levels, enters through L_{10} and L_{20}; the Raman resonance[22], which enters through L_{21}, involves both fields and manifests itself when their frequency separation approaches the J=2, J=1 fine structure splitting. The former type of tunable behavior leads to "population saturation effects" and the latter type leads to "Raman effects". Raman effects are multiple-quantum processes which proceed from initial state to final state "coherently", that is, without loss of phase memory.[23] Population saturation effects, in contrast, proceed in a stepwise fashion, with complete phase disruption after each emission or absorption. Population saturation and Raman processes are intimately related in (39), a point to be elaborated on later. However, in understanding X_1 it may be helpful to first deal with these processes separately. To exclude the Raman terms, suppose $L_{21} \gg \gamma_{21}$ with L_{10} and L_{20} arbitrary (an impossibility!): then (36) reduces to

$$\chi_1 \to \frac{|\mu_{10}|^2}{\hbar L_{10}^*} \left\{ r_{10}^0 - 2 \frac{\gamma_{20}}{\gamma_0} \frac{|\beta|^2 r_{20}^0}{\Delta} \right\} \tag{40}$$

Equation 40 illustrates the aspects of (36) involving only population saturation effects and represents the "semiclassical" approximation, in which the radiation fields are considered independently.[21] In that limit χ_1 reduces to the 1-1 linear susceptibility, except that r_{10}^0 is replaced by r_{10}^u. The latter quantity, defined in (32), is determined by the extent of saturation of the 2-1 transition. Expression 40 is, of course, velocity dependent through the parameters

$$L_{10} = l_{10} - \delta k v \tag{41a}$$

and
$$L_{20} = l_{20} - k v , \tag{41b}$$

in which $l_{ij} = L_{ij}(v = 0)$ and the approximation $k_1 \cong k_2 = k$ has been made since $(k_2 - k_1) v = \Omega_{21} v/c \ll \gamma_{21}$. Inspection of (40), using (33) and (41), reveals that the principle contribution comes from atoms in the narrow range of velocities for which (41a) is resonant. If, in addition, Ω_2 is such that (41b) is also resonant then (40) may be substantially reduced. The latter condition is satisfied when

$$(\Omega_1 - \omega_{10}) \delta = (\Omega_2 - \omega_{20}) , \tag{42}$$

which leads to symmetrical effects about the 1-1 center frequency.
(See Figure 20.) Thus by building up the population of $|0\rangle$ the strong
field at Ω_2 tends to suppress laser action equally at both of the 1-1 gain
peaks. In actual practice the range over which this suppression is
effective may considerably exceed the homogeneous widths involved,
since closely spaced laser oscillations at the 2-1 high-frequency peak
may extend over hundreds of Mhz.

In passing it is noted that similar effects tend to suppress laser action
at the low-frequency side of the 2-1 gain profile, as well. In fact, the
retardation is "doubly" effective there, since both upper and lower levels
are being saturated by $\mathcal{E}_2^T$. This explains why the onset of laser action
at a particular point on the Doppler profile can inhibit laser action at the
region opposite line center, a tendency previously referred to.

Of course, (40) exhibits only the population saturation aspects of (36),
actually inseparable from the Raman effects. The latter enter χ_1 through

$$L_{21} = l_{21} + kv \, (\delta - 1) \tag{43}$$

which is subject to the same qualifications as (41). The asymmetrical
structure of (43) is the source of the asymmetrical 1-1 gain profile.
At the low-frequency peak $\delta = -1$, consequently as Ω_1 is tuned across
the line individual atomic velocity bands undergo Raman transitions one
by one. Thus the strength of the Raman effects is diluted over the
entire inhomogeneous linewidth, a fact which suggests that the resulting

influence is small. On the other hand, at the high-frequency peak $\delta = +1$, consequently (43) becomes independent of velocity, implying that as Ω_{21} approaches ω_{21} all the atoms can simultaneously undergo Raman transitions. The Raman frequency condition is also the one for which population saturation effects are maximum. (cf. (42), $\delta = +1$) This is so because when $\Omega_{21} = \omega_{21}$ the _same_ atoms strongly interacting with $\mathcal{E}_2^\tau$ also become resonant with $\mathcal{E}_1^\delta$, a situation in which $|2\rangle$ and $|1\rangle$ become closely coupled by strong multiple-quantum processes consisting of population saturation and Raman effects. In the following we shall refer to Raman-type coupling to emphasize the essential inseparability of the constituent processes.

B. Integration

In carrying out the velocity averages (39) it is convenient to introduce $W_j(v)$, the velocity distribution of atoms $|j\rangle$, normalized such that

$$\int_{-\infty}^{\infty} W_j (v) \, dv = n_j \, , \tag{44}$$

with n_j as the number of atoms per unit volume in $|j\rangle$. To an incident light beam of propagation constant k the frequency breadth of W_j may be characterized by ku_j, with u_j as the most probable speed of W_j. Needless to say, in the case at hand the W_j are non-Maxwellian. The ^3P levels are populated by dissociation, consequently the broad distributions of velocities tend to be rather flat.[24] Furthermore, the ^3S level is subject to heavy

reabsorption at low velocities which leads to an additional narrow bump at the center of its distribution. In general the integrals in (39) depend upon the specific form of the W_j. Nevertheless, because in the present case the $ku_j \gg \gamma_i$, the resonant behavior of $P(z,t)$ becomes largely independent of the W_j and it is possible to perform the averages (39) without recourse to their specific form.

To perform the averages, (36) and (37) are decomposed into their partial fractions. The integrals reduce to quantities of the form

$$\int_{-\infty}^{\infty} \frac{W_j(v)\,dv}{\omega - i\gamma + kv} \equiv \; < (\omega - i\gamma + kv)^{-1} >_j \tag{45}$$

in which ω and γ are real and $\gamma > 0$. In the limit $\gamma/ku_j \ll 1$,

$$(\omega - i\gamma + kv)^{-1} \rightarrow P\,(\omega + kv)^{-1} + i\pi\,\delta(\omega + kv), \tag{46}$$

where P denotes principle value, and (45) may be written

$$< (\omega - i\gamma + kv)^{-1} >_j = P \int_{-\infty}^{\infty} \frac{W_j(v)\,dv}{\omega + kv} + i\pi\,W_j\left(\frac{\omega}{k}\right) + O\left(\frac{\gamma}{ku_j}\right). \tag{47}$$

To make the notation of (47) more compact a complex dispersion function, $Z_j(\omega) = Z_j'(\omega) + iZ_j''(\omega)$, is introduced:

$$Z'_j (\omega) = P \int_{-\infty}^{\infty} \frac{W_j(v) \, dv}{\omega + kv} ,$$

$$Z''_j (\omega) = \pi \, W_j (\omega/k) .$$

(48)

The decomposition of (36) and (37) involves expressions of the type

$$H^{\pm} = [(\omega - i\gamma + kv)(\omega' - i\gamma' \pm kv)]^{-1} .$$

(49)

Using the above results, the averaged quantities corresponding to (49) may be written

$$<H^{\pm}>_j = \frac{1}{(\omega' \mp \omega) - i(\gamma' \mp \gamma)} \; [Z_j(\omega) \mp Z_j(\omega')] .$$

(50)

The only significant contribution to (50) arises from the immediate vicinity of $(\omega' \mp \omega) = 0$. Under the stated assumptions the Z_j vary slowly over this small region, consequently it is permissible to make the substitutions $Z_j(\omega') = Z_j(\pm \omega)$, thus simplifying (50) to

$$<H^+>_j = 0$$

$$<H^->_j = 2iZ''_j (\omega) .$$

(51)

In the latter expressions use has been made of the fact that Z' and Z'' are odd and even functions, respectively.

The partial fraction decompositions of $\chi_2(+,\underline{+})$ and $\chi_1(+,+)$ are straightforward. Utilizing (47) and (51) the corresponding inhomogeneously broadened susceptibilities are obtained:

$$\chi_2 = \frac{|\mu_{20}|^2}{\hbar} \left\{ Z'_{20} \{\Omega_2 - \omega_{20}\} + \frac{Z''_{20} \{\Omega_2 - \omega_{20}\}}{Q} \right\} , \qquad (52)$$

$$\chi_1^p = \frac{|\mu_{10}|^2}{\hbar} Z_{10} \{\Omega_1 - \omega_{10}\}$$

$$+ \Theta Z''_{20} \{\Omega_1 - \omega_{10}\} \; \frac{1_{21} + i \frac{\gamma_0}{2} (Q + 1)}{1_{21}[1_{21} + i \frac{\gamma_0}{2} (Q+1) + i\frac{\gamma_2}{2} (Q-1)] - |\beta|^2} , \qquad (53)$$

in which $Z_{ij} (\omega) = Z_i (\omega) - Z_j (\omega)$,

$$\Theta = \frac{|\mu_{20}|^2}{\hbar} \left| \frac{\mu_{10} \alpha_2}{2\hbar} \right|^2 \frac{2}{\gamma_0 Q} , \qquad (54)$$

and Q is the factor by which the saturated levels are broadened (cf. (36)):

$$Q = \left[1 + \frac{4|\beta|^2}{\gamma_0 \gamma_2} \right]^{1/2} \qquad (55)$$

Also, in evaluating Z_j in (52) and (53) the very reasonable approximation that $|\beta| \ll ku_j$ has been made.

To expedite the decomposition of χ_1 $(-,+)$, note that

$$\frac{1}{\Gamma(\delta=-)} \equiv \frac{1}{g} \left[\frac{1}{kv + b_-} - \frac{1}{kv - b_+} \right] , \tag{56}$$

in which

$$g = \left[(2\, \overset{*}{l}_{10} + l_{21})^2 + 8\, |\beta|^2 \right]^{1/2} \tag{57a}$$

and

$$b_{\pm} = \frac{1}{4} \left[g \pm (2\, \overset{*}{l}_{10} - l_{21}) \right] . \tag{57b}$$

Using (56) and proceeding as before, the corresponding inhomogeneously broadened susceptibility may be obtained:

$$\chi_1^a = \frac{|\mu_{10}|^2}{\hbar} \, Z_{10} \, \{\Omega_1 - \omega_{10}\} \tag{58}$$

$$- \frac{\Theta Z_{20}''\{\Omega_1 - \omega_{10}\}}{2g} \left\{ \frac{(2\, \overset{*}{l}_{10} + l_{21}) - d - i\gamma_0(Q-1)}{w + b_-} - \frac{(2\, \overset{*}{l}_{10} + l_{21}) + d - i\gamma_0(Q-1)}{w - b_+} \right\} ,$$

in which $w = i\gamma_{20}Q - (\Omega_2 - \omega_{20})$. The first term in (58) is the usual linear susceptibility and also appears in (53). To simplify the second term the identity (56) may be used, with w replacing kv. After some rearrangement, (58) may be cast in the following form:

$$X_1^a = X_1^{linear} - \Theta Z_{20}'' \{\Omega_1 - \omega_{10}\} \left[\frac{\xi_{21} + i\frac{\gamma_2}{2}(Q+1)}{\xi_{21}[\xi_{21} + i\frac{\gamma_2}{2}(Q+1) + i\frac{\gamma_0}{2}(Q-1)] - |\beta|^2} \right]^* \quad (59)$$

in which X_1^{linear} denotes the linear portion of the 1-1 susceptibility and ξ_{21} is the anti-parallel analog of l_{21}:

$$\xi_{21} = (\Omega_2 + \Omega_1) - (\omega_{20} + \omega_{10}) + i(\gamma_{10} + \gamma_{20}Q). \quad (60)$$

In this form the strong similarity between (59) and (53) is evident.

The linear term, the second term of (53), and the second term of (59) constitute the complete 1-1 susceptibility. The two latter contributions can be simplified by noting that in each case the numerator is a factor of the denominator. Slight rearrangement yields

$$X_1 = X_1^{linear}$$

$$- i \Theta Z_{20}'' \{\Omega_1 - \omega_{10}\} \left\{ \frac{1}{\frac{\gamma_1 + Q\gamma_2}{2} - i(\Omega_{21} - \omega_{21})} \right.$$

$$\left. + \frac{1}{\frac{\gamma_1 + Q\gamma_2}{2} + Q\gamma_0 + i[(\Omega_2 + \Omega_1) - (\omega_{20} + \omega_{10})]} \right\} \quad (61)$$

a remarkably simple result! In the limit of weak saturation $(Q \to 1)$ X_1 reduces to an expression consistent with reference 16, obtained by the method of Lamb.

7. Discussion of Lineshape

The 1-1 gain coefficient is

$$G_1 = 4\pi \frac{\omega_{10}}{c} \operatorname{Im} (X_1) \quad , \tag{62}$$

and the linear gain profile follows from (61). Thus the presence of a laser field at Ω_2 leads to depletions of the 1-1 gain curve over narrow regions on opposite sides of line center, at frequencies given by (42). The depleted regions are Lorentzians of equal area, but the parallel contribution (first term in brackets) is deeper and narrower than its anti-parallel counterpart (second term in brackets) because of an extra factor $\gamma_0 Q$ in the denominator of the latter. As previously mentioned a number of modes are observed oscillating simultaneously at the 2-1 high-frequency peak. Each of these leads to a pair of depleted regions on the 1-1 profile, resulting in a series of "holes", separated by the cavity mode spacing, burnt into both peaks of the 1-1 gain curve. The situation is depicted in Figure 21 for various values of the saturation parameter Q, using the accepted values [13] of $\gamma_1 = \gamma_2 = 0.5$ Mhz. and $\gamma_0 = 20$ Mhz. , and taking a mode separation of 50 Mhz. At the high-frequency peak deep, narrow holes leave the wide regions between them more or less unaffected, whereas at the low-frequency peak the broad holes tend to run together, depleting the gain fairly uniformly over its entire extent. Thus conditions for oscillation are more favorable at the high-frequency peak, which explains why laser action occurs most

Note:

THE HIGH FREQUENCY
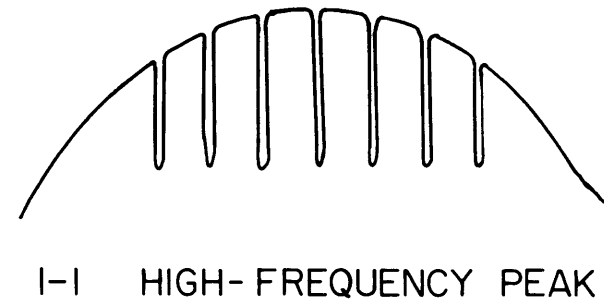RESONANCES ARE ACTUALLY
NARROWER THAN SHOWN HERE
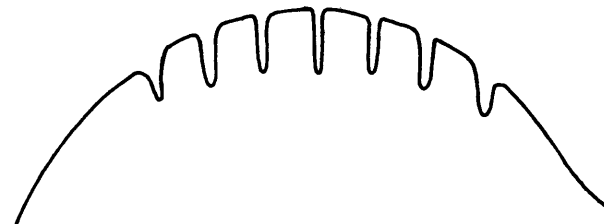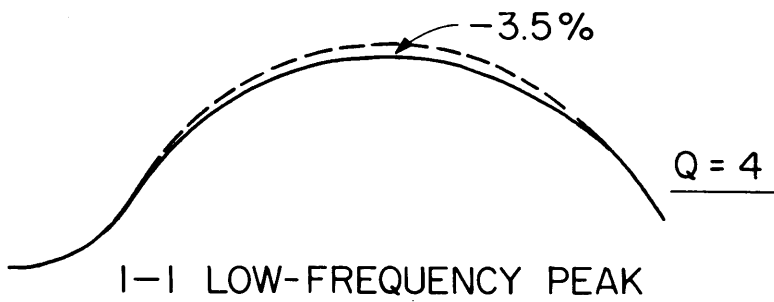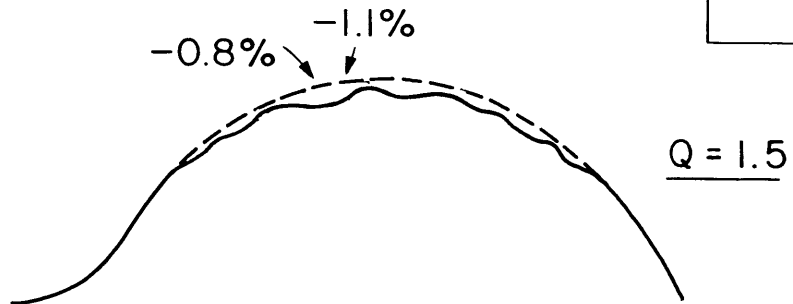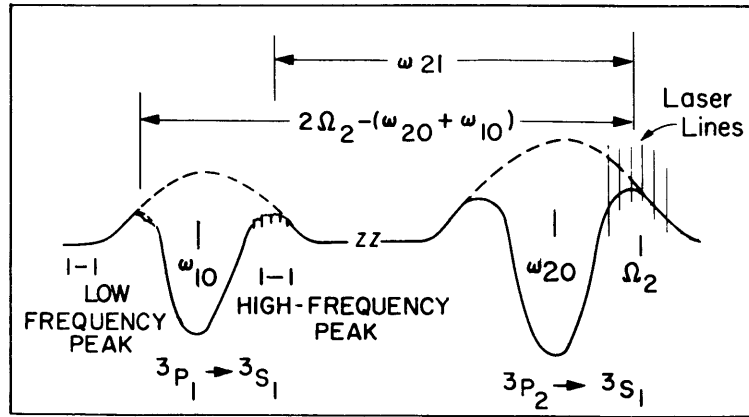
Figure 21. EFFECT OF LASER ACTION AT Ω_2 ON THE I−I GAIN PROFILE.

readily there. The exact positions of the laser lines depend upon the overall gain profile and the cavity frequencies, as well as the details of the 2-1 oscillations. It follows that the frequency separation between the two regions of laser action gives the $J = 2$, $J = 1$ fine-structure splitting with an error of possibly several cavity mode spacings, about 0.005 cm^{-1} in the present case. This accuracy is as good as that obtainable using the more advanced interferometric techniques,[1] and the possibility of photobeat experiments[25] offers a direct frequency measurement of the $J = 2$, $J = 1$ separation.

The simplicity of X_1 and the contrast between its parallel and anti-parallel contributions underscores several basic aspects of Raman-type processes. It is evident from (61) that the width of the parallel resonance is equal to the width of the transition $|1> \rightarrow |2>$, whereas that of the anti-parallel resonance is equal to the combined widths of $|1> \rightarrow |0>$ and $|2> \rightarrow |0>$. Note that in both cases the _saturated_ level widths $\gamma_0 Q$ and $\gamma_2 Q$ are involved, due to the presence of the strong field at Ω_2. (cf. (36).) In the discussion of Section 6A it was pointed out that in the anti-parallel case atoms of various velocities satisfied the Raman resonance condition at different values of Ω_1, effectively dissapating its influence over the entire gain profile. Thus X_1^a largely involves population saturation effects and proceeds through consecutive single-quantum processes in a stepwise fashion, accounting for the resulting width. This is shown diagramatically in Figure 22. (However, note that integration of the semi-classical

Matrix Elements are μ_{20} and μ_{10}

	Coherent process	Incoherent process
	$\Gamma = \gamma_1 + \gamma_2 Q$	$\Gamma = (\gamma_1 + \gamma_0 Q) + (\gamma_0 Q + \gamma_2 Q)$

Energy conservation involves   Complete phase disruption
initial and final states only.   occurs between single-quantum
                                       events.

a) Raman–Type Event   b) Population– Saturation Event
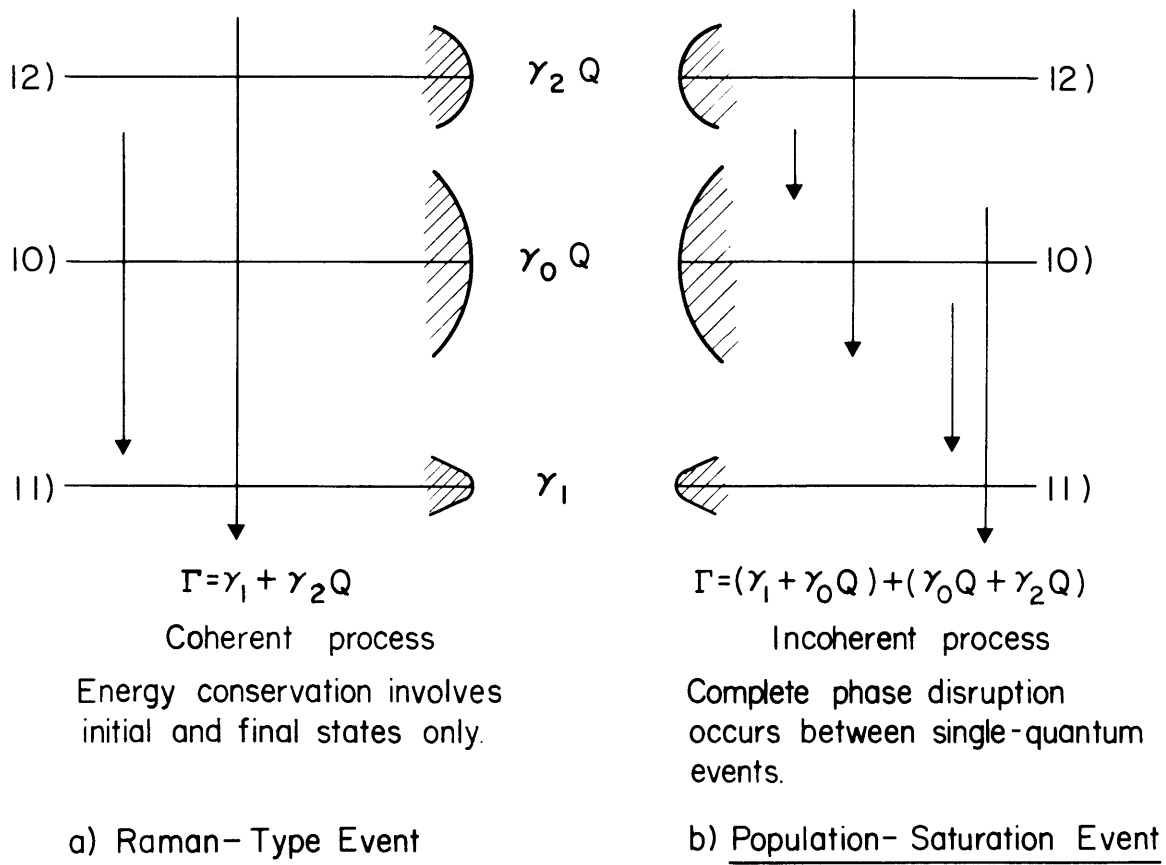
note: position of $|1\rangle$ has been changed to simplify diagram

Figure 22   Coherent and Incoherent Events

result (40) leads to a lineshape $\propto \xi_{21}^{-1}$, an incorrect result which does not take account of the fact that the weak field transition also involves the saturated value of γ_2.) On the other hand, in the parallel case the Raman condition becomes independent of velocity, and at resonance strong coherent multiple-quantum processes take place involving atoms of all velocities. The principle effect of inhomogeneous broadening here is to smear out the details of the lineshapes of individual velocity bands of atoms. The hallmark of these coherent processes remains, however, namely that energy conservation in individual events involves only the initial and final states. In this regard the situation is similar to the case of resonance fluorescence,[26] in which an exciting line narrow relative to the widths of the levels involved gives rise to an emitted line of the same width.[27] A novel feature in the present case is that the saturated width of γ_2 is involved, since it is broadened by $\mathcal{E}_2$. Note that the intermediate level enters implicitly into this width through Q. (See Figure 22).

PART IV. SPECTROSCOPIC APPLICATIONS OF RAMAN-TYPE
PROCESSES

1. General Remarks

Optical linewidths in gases are generally determined by Doppler
broadening which, at low pressures, is often many hundreds of times in
excess of the linewidths of individual molecules; in the microwave spec-
trum of inhomogeneously-broadened solids the coherent or "natural"
linewidths may be similarly obscured. Consequently in such systems
inhomogeneous widths usually limit the precision with which g-values,
fine and hyperfine structure and similar quantities can be measured.
In cases of very closely-spaced level structure the possibilities of such
measurements by conventional methods may be entirely precluded. On
the other hand the saturation properties of an inhomogeneously-broad-
ened system are primarily determined by its natural widths. Thus in
Part III it was shown that Raman-type processes in the 8446 $\overset{o}{A}$ oxygen
system lead to sharp changes in the 1-1 emission profile extending over
regions characterized by the natural widths of the levels involved. In
fact, the expressions developed there are directly applicable to a novel
class of non-linear spectroscopic techniques, first discussed by Feld,
Parks, Schlossberg and Javan, [28] which enables level structure in an
inhomogeneously-broadened system to be resolved with an accuracy
limited only by the natural response of the system.

The techniques are particularly well suited to the strong, mono-chromatic, multimode fields generated by lasers. Consider a multi-moding laser beam incident upon the inhomogeneously-broadened three-level system discussed in Part III. (See figure 19.) The laser should resonate with the absorption (or emission) lines of the sample. The mode separation, determined by the length of the laser inter-ferometer, is assumed large compared to the widths of the upper levels. Furthermore, assume that the separation of the upper levels may be tuned by applying a D. C. electric or magnetic field. (If this is not practicable the laser cavity itself may be tuned.) The attenuated laser beam is studied as a function of the separation of the upper levels. A simplified experimental arrangement is shown in figure 23.

In the absence of saturation, the absorption coefficient changes slowly as the levels are tuned, and appreciable changes in attenuation occur only when the frequency separation of the two upper levels varies by an amount comparable to the inhomogeneous broadening. In the presence of saturation, however, the situation is considerably different. As the splitting of the upper levels approaches the separation between two modes of the applied laser field, the attenuation changes sharply. These changes occur over a frequency range characterized by the upper level widths. This effect is referred to as mode crossing. [16] In addition, when the upper levels approach each other within their natural widths a
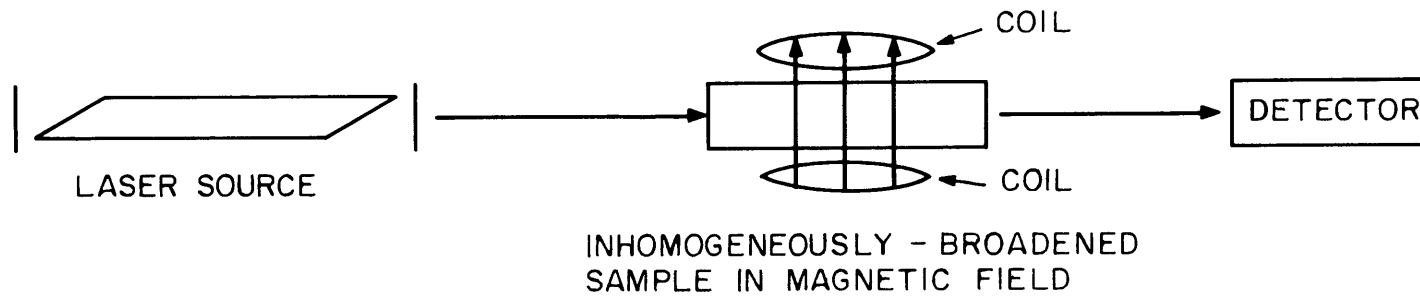
a) EXPERIMENTAL ARRANGEMENT

$\searrow \equiv$ LEVEL'S NATURAL BREADTH

NOTE THAT THIS MAY BE EXTREMELY NARROW COMPARED TO DOPPLER BREADTH
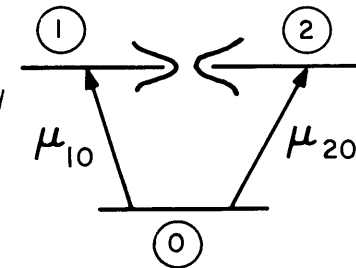
CASE I LEVELS I AND 2 ARE DEGENERATE
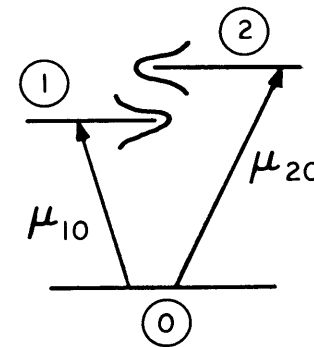
CASE 2 DEGENERACY BROKEN

b) LEVEL DIAGRAMS

FIGURE 23 NON-LINEAR CROSSING EXPERIMENTS

similar sharp change in attenuation occurs. We refer to this effect as non-linear level crossing.[29] It will be explained in section 3 how the mathematical formulation of the crossing effects is essentially given in the developments of Part III, a not unexpected result in view of the similarity of the physical processes involved: the sharp intensity changes observed in crossing experiments are due to the increased coupling between the quantum-mechanical system and the applied radiation field, leading to Raman-type processes. An attractive feature of crossing experiments is that one need not be concerned with the frequency stability of the laser source as long as the fluctuations are small compared with the inhomogeneous widths of the sample. (Note that the mode-crossing effect is only sensitive to the frequency separation between laser modes.)

By applying crossing techniques to the laser medium itself one may study the structure of the levels participating in laser action. An advantage of studying the laser directly is that saturation of the medium is insured. To see this one has only to note that the laser steady-state oscillation condition is reached when saturation losses build up to the point where they counterbalance the linear gain. When working inside the cavity additional standing-wave effects similar to the Lamb dip occur. These tend to average out under normal laser operating conditions because they are sensitive to the frequencies of individual laser modes.[16] The last term in equation 61 represents one such effect.

Working inside the laser cavity, we have measured some of the g-values and linewidth parameters in a new series of atomic oxygen laser lines, and also

Observation			Assignment	
line (microns)	vacuum wavenumbers (cm^{-1})	vacuum wavenumbers$^{(32)(33)}$ (cm^{-1})	transition	
			upper level	lower level
.8446	11836.20$\pm$.01^a	11836.15	$3p\,^3P_2$	$-\,3s\,^3S^o$
		11836.31	$3p\,^3P_2^o$	
	11835.64$\pm$.01	11835.61	$3p\,^3P_1^o$	$-\,3s\,^3S^o$
2.89	3456.9 $\pm$3.0	3454.90	$4p\,^3P_{2,1,0}$	$-\,4s\,^3S^o$
4.56	2192.4 $\pm$0.9	2192.26	$4p\,^3P_{2,1,0}$	$-\,3d\,^3D^o_{3,2,1}$
6.86	1458.4 $\pm$0.5	1457.75	$5p\,^3P_{2,1,0}$	$-\,5s\,^3S^o$
10.40	961.4 $\pm$0.2	961.26	$5p\,^3P_{2,1,0}$	$-\,4d\,^3D^o_{3,2,1}$
5.97	1674.9 $\pm$0.2^b	1671.40	$7d\,^3D^o_{3,2,1}$	$-\,6p\,^3P_{2,1,0}$

TABLE 1: ATOMIC OXYGEN LASER TRANSITIONS

a) Previously reported. [2]
b) This 0.2% discrepancy may be due to inaccuracy of Edlen's measurement. [33]

in the 8446 Å line.[30] The new laser lines are briefly described in the next section and the experimental measurements are discussed in section 4.

2. New C. W. Atomic Oxygen Laser Transitions

Five new C.W. laser lines have been observed and identified in neutral atomic oxygen.[30][31] They occur at wavelengths 2.89μ, 4.56μ, 5.98μ, 6.86μ and 10.40μ and have all been assigned[32][33] to the triplet system of the $2p^3(^4S^o)$ nx configuration. (See table 1 and Figure 24.) In four of the new lines the term from which laser action originates is of the same parity as the ground state ($2p^4 \, ^3P_2$). However, in the 5.98μ oscillation the parity of the upper laser levels is opposite that of the ground state. (This is also the case in the 3.39μ and 1.15μ He-Ne laser transitions.)

It is interesting to note that the 8446 Å oscillations also originate from this system. It is clear, however, from the observation of laser action in a pure oxygen discharge that the modes of production discussed by Bennett et al.[2] cannot fully account for oscillation in these cases.

All of these new lines[34] oscillate weakly in a pure oxygen discharge at a pressure of about 80 microns, using a 3 meter long, near-confocal resonator with one internal gold-coated mirror and one Brewster-angle window. The laser tube is quartz with an 11 mm i.d. Power is coupled out either via a gold coated mirror with a 2 mm hole or with a dielectric-coated BaF_2 mirror of 98% reflectance. The oscillations are detected with a CuGe (4°K) detector in the case of the 10.4μ line and either a PbSe (77°K) or a AuGe (77°K) detector for the shorter wavelengths. The laser has been operated successfully
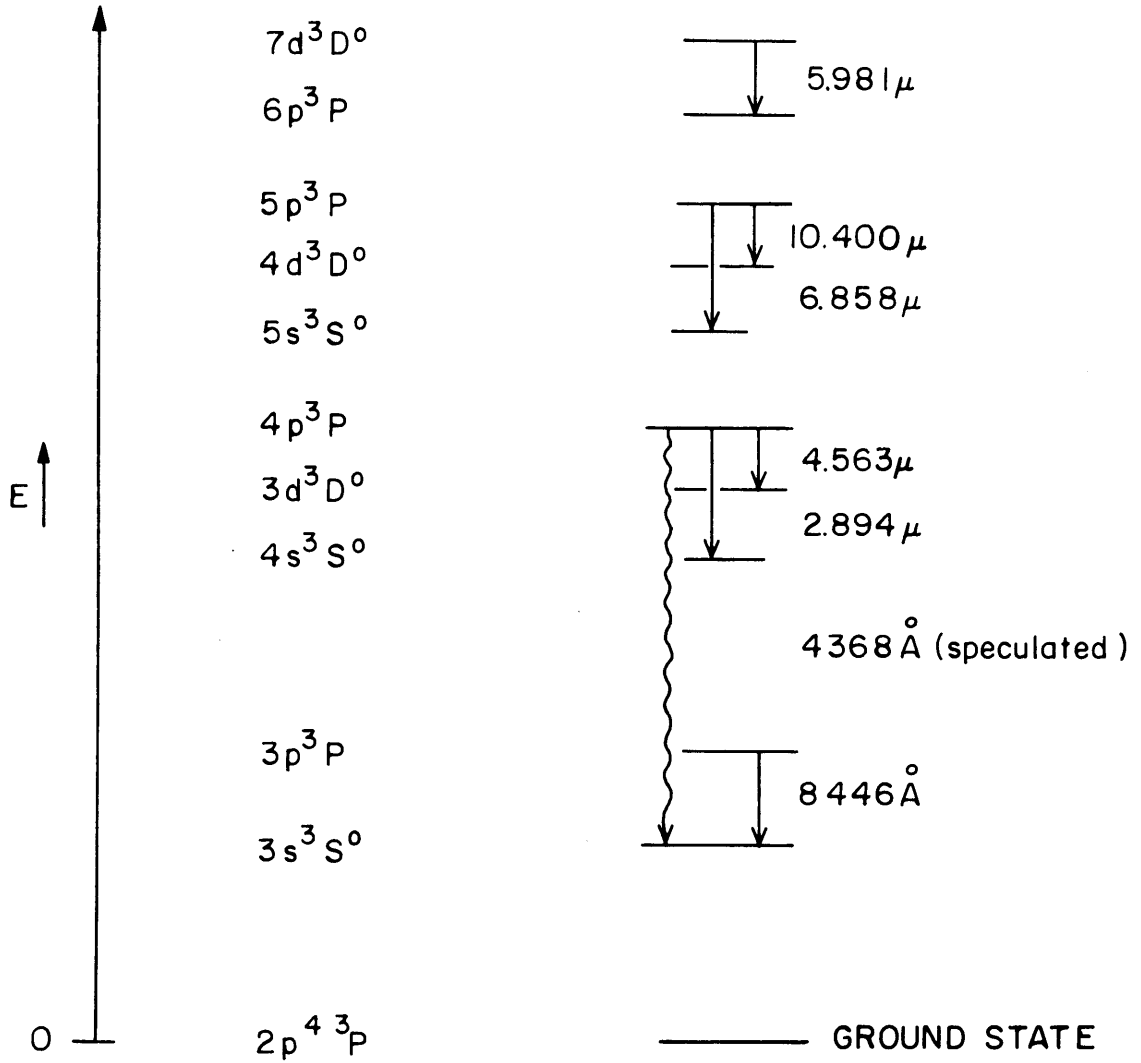
FIGURE 24: OXYGEN I –ENERGY LEVEL SCHEME,
AND OBSERVED LASER LINES

under both static and continuous flow conditions using either a DC or an RF discharge. Considerable enhancement is achieved by the addition of approximately 0.5-1.0 mm of either Ne or He, and output powers in the 1 milliwatt range are obtained under these conditions.

We expect that other laser lines arising from this system are oscillating farther in the infrared, beyond the sensitivity of our present detectors. In addition, one might expect laser action on the 4368 Å multiplet, which is formed by the upper levels of the 2.89μ line and the lower level of the 8446 Å line. (See Figure 24.) So far, all attempts to obtain oscillation there have failed. Note that one would observe this line only if the upper level, $4p^3P$, were sufficiently broadened by dissociative processes so that sizeable densities could occur beyond the trapping of the lower level, $3s^3S$. (See Part II.)

There is a further possibility that a high-resolution spectroscopic study of the new laser lines might reveal their hitherto unobserved fine structure.

3. Crossing Techniques: Theoretical Aspects

The non-linear crossing techniques are special applications of the Raman-type processes developed in Part III, and expressions for the mode-crossing and level-crossing polarizations follow directly from that formulation. Consider first the case of mode-crossing: the inhomogeneously-broadened three-level system of Figure 19 is subject to two colinear optical travelling waves propagating along the same direction; the splitting of the upper levels

can be tuned to equal the frequency separation of the applied fields. This is precisely the situation treated as the "parallel contribution" of Part III. The corresponding susceptibilities are therefore immediately given by (52) and the first two terms of (61).

Next, consider the level-crossing case: a single travelling-wave field interacts with the inhomogeneously-broadened three-level system of Figure 19, in which the upper levels can be tuned to cross. The ensemble-averaged equations of motion are given by (26), but now the applied field is simply $\mathcal{E}(\delta, \tau) = \mathcal{E}_1^\delta(z, t)$. (See equation 19.) Referring to the discussion following equation 27, one finds that a nearly complete solution of (26) may be obtained by choosing (28) as the off-diagonal density matrix elements, but with $\Omega_1 = \Omega_2$. This immediately leads to a set of coupled equations identical to (29), except that now $\beta = (\mu_{02} \mathcal{E}_1^\delta / 2\hbar)$ and $\Omega_{21} = 0$. The subsequent steps are unchanged, again leading to susceptibilities given by (52) and the first two terms of (61). In this case, of course, X_1 and X_2 are both driven at Ω_1.

One concludes, therefore, that both the mode-crossing and level crossing polarizations follow directly from the formulation of Part III. (In both cases, of course, these expressions are subject to the same approximation made in Part III, $|\alpha| \ll 1$.) These expressions extend the previously obtained third order level-crossing[29] and mode-crossing[16] polarizations to the case in which one of the transition probabilities is fully saturated.[35] The resulting power-broadening effects have already been

discussed in section III 7. Some experimental consequences will be noted in the next section.

The saturation aspects of the present crossing techniques distinguish them from those previous techniques, utilizing conventional light sources, which they superficially resemble.[36] For example, non-linear level crossing experiments differ considerably from linear level-crossing experiments.[37] In the latter, the observed effects are linearly proportional to the intensity of the excitation source. Furthermore, in the linear case one usually observes changes in the angular distribution and/or polarization of the emitted light as the levels cross. The total intensity, integrated over a sphere, is unchanged. In contrast, non-linear level crossing involves a net change in intensity, as the levels cross, proportional to the second and higher powers of the incident power. It is mentioned in passing that the use of a source capable of saturating the transitions involved in a "linear" level crossing experiment would lead to additional changes in the emitted light.

4. Crossing Techniques: Experimental Aspects

The crossing techniques have been used to study g-values and linewidth parameters of the 8446 Å, 2.89μ and 4.56μ atomic oxygen laser transitions.[30] In these experiments the laser intensity was studied as a function of an applied D. C. magnetic field. To enhance the signal-to-noise ratio a small audio-frequency component was superimposed on

this field. The detected signal was fed into a phase-sensitive amplifier tuned to the modulation frequency, and the output was recorded as a function of magnetic field. Accordingly, the curves obtained were derivatives of the laser signal.

Level tuning was achieved by means of retangular coils[38] which provided a magnetic field transverse to the axis of the laser tube. The laser system has been described in section 2. Adjacent modes were spaced $c/2L$ = 49.2 Mhz apart. The Brewster-angle end window was oriented so that the laser polarization was perpendicular to the magnetic field. Fields as large as 180 gauss could be applied to the entire length of the laser tube. The field inhomogeneity was approximately 10%. To reduce the gain of off-axis modes, an aperture several mm in diameter was inserted in the laser cavity, close to one mirror. In situations in which off-axis modes still proved troublesome it was found helpful to remove the reflective coating from all but a small central portion of the opposite mirror.

Typical traces for the various laser transitions are shown in Figures 25 through 28. The resonances at 0 gauss are due to the uncrossing of initially degenerate sublevels. At higher fields resonances are observed each time the splitting between a pair of upper levels connected to a common lower level approaches the separation between any two axial modes. (For $\mathcal{E} \perp B$ the selection rule is $\Delta M = \pm 2$.)

The g-values can be obtained from the mode-crossing signals using the relationship $2\mu_o g \Delta B = c/2L$, in which ΔB is the separation between

FIGURE 25 LEVEL SPLITTING SIGNAL IN ATOMIC OXYGEN, $3p^3P \rightarrow 3s^3S$
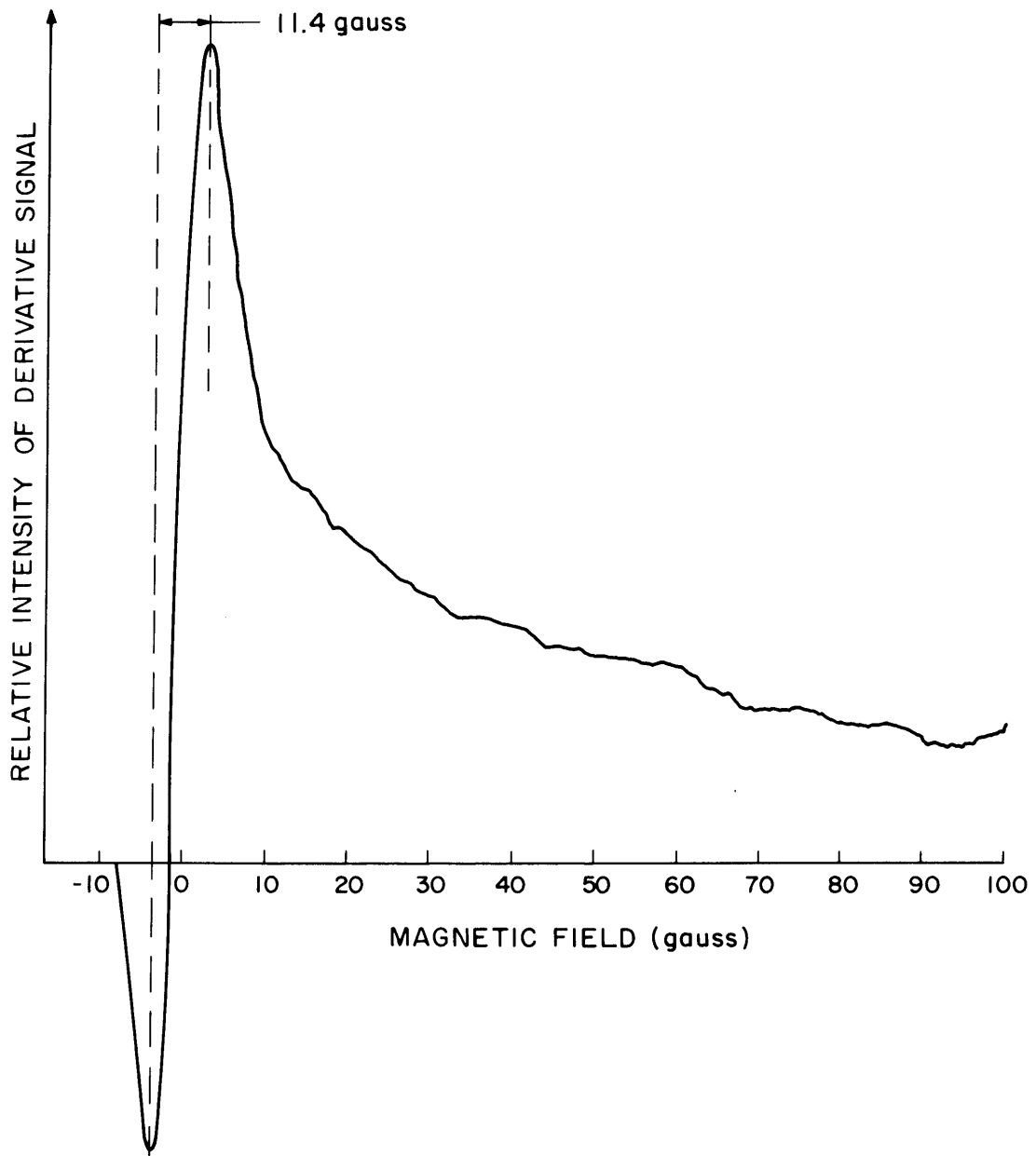
FIGURE 26 MODE CROSSING SIGNAL IN ATOMIC
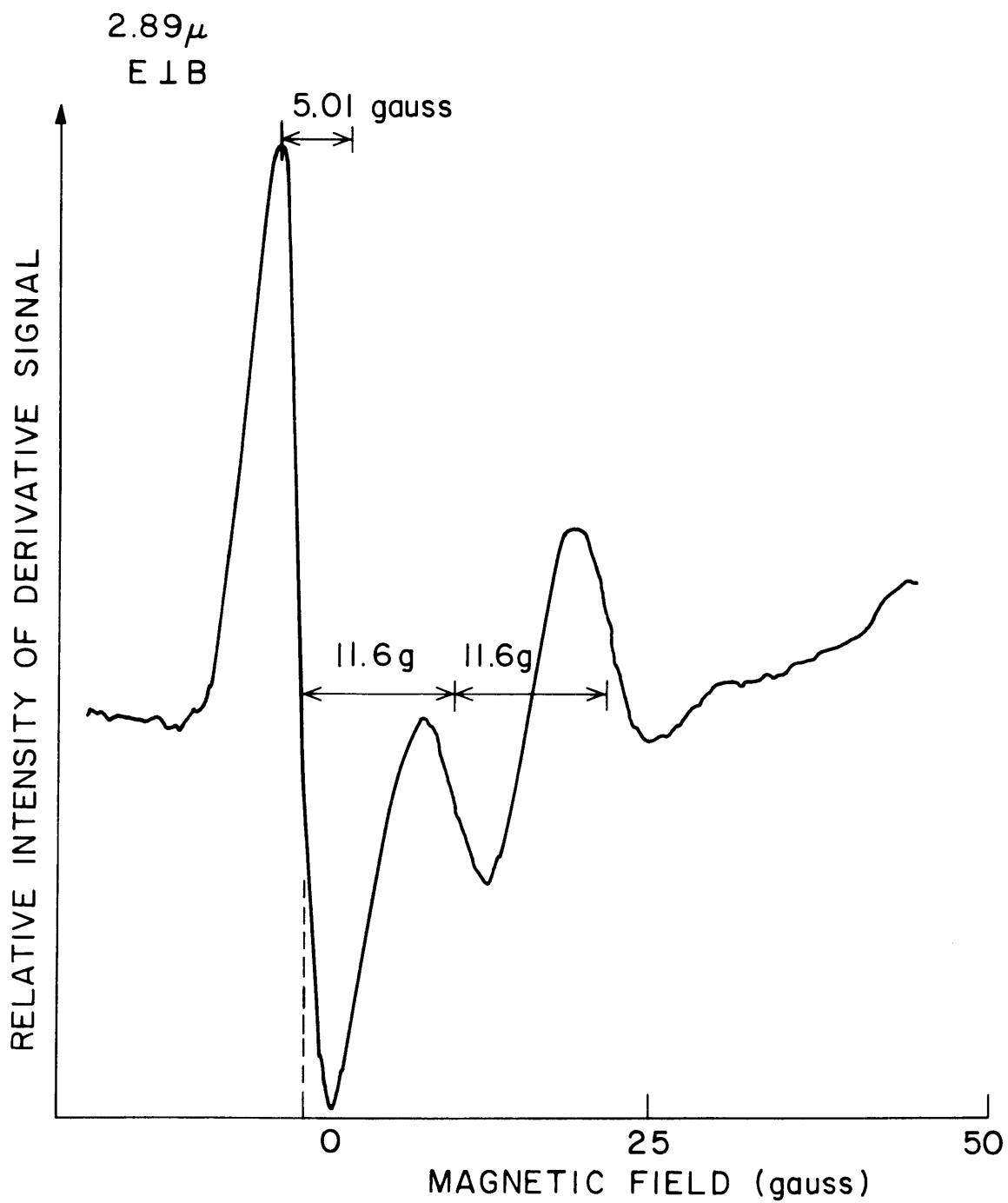OXYGEN, $3p^3P \longrightarrow 3s^3S$

FIGURE 27 CROSSING SIGNALS IN ATOMIC OXYGEN, $4p^3P - 4s^3S^o$
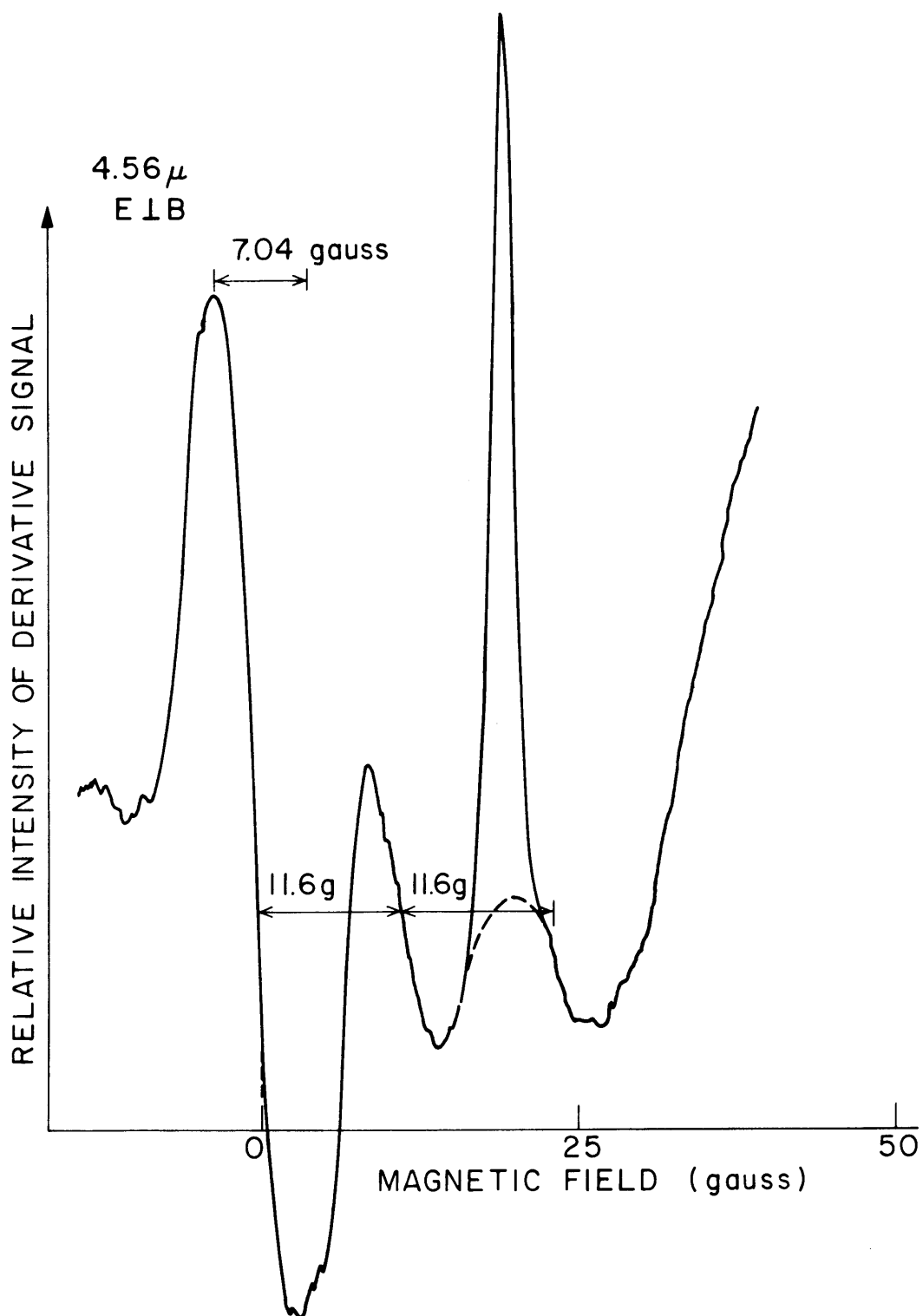
FIGURE 28 CROSSING SIGNALS IN ATOMIC OXYGEN ,
$4p\,^3P - 3d\,^3D^o$

resonances in units of magnetic field and μ_0 is the Bohr magneton. The observed g-values are listed in Table 2. These are in excellent agreement with the values predicted by L-S coupling for the <u>upper</u> levels. (In the three cases studied the upper multiplets are ^{3}P, for which L-S coupling predicts g-values of 3/2 for both J = 2 and J = 1 levels. In each case more than one fine-structure level may have participated in laser action. The present experiments did not resolve possible small variations between g[J = 1] and g[J = 2].) The mode-crossing of the <u>lower</u> levels was not observed because the linewidths were so broad that the signals overlapped and flattened out. Discussion of the linewidths is given below.

Once the g-values are known the level-crossing signals may be used to obtain the widths of the levels involved. The relationship is $\mu_0 \, g \, \delta B \approx \Delta \nu_{1/2}$,

$$(47)$$

in which δB is the full half-width of the observed signal (in units of magnetic field) and $\Delta \nu_{1/2}$ is the full half-width of a crossing level. The observed widths, listed in Table 2, are much wider than the estimated radiative widths of the upper levels. Except for the $3p\,^3$P multiplet, these widths are not known. The $3p\,^3$P width is about 1/2 Mhz, forty times narrower than the width observed. Field inhomogeneities cannot account for such large broadening, particularly near 0 gauss. Furthermore, at the laser operating pressures, a few hundred microns or less, collision broadening is not an important factor. This statement is supported by the observation that variations in laser pressure did not significantly change the widths of the crossing signals. In fact, the dominant broadening mechanism is

Mode Crossing

$$2\mu_o \, g\Delta B = \Delta \nu_{mode} = \frac{c}{2L} \approx 49.2 \text{ Mhz.}$$

Line	g_{exp}	g_{LS}
8446 $\overset{o}{A}$	1.51 $\pm$ 2%	3/2
2.89μ	1.51 $\pm$ 2%	3/2
4.56μ	1.51 $\pm$ 2%	3/2

Level Crossing

$$\Delta \nu_{1/2} = \mu_o g \, \delta B$$

Line	$\delta B_{(gauss)}$	$\Delta \nu_{1/2}$ (taking g = 1.5)
8446 $\overset{o}{A}$	11.4 $\pm$ 2%	24 Mhz
2.89μ	5.01$\pm$ 10%	11 Mhz
4.56μ	7.04$\pm$ 3%	15 Mhz

TABLE 2: OBSERVED g-VALUES AND LINEWIDTH PARAMETERS

saturation as discussed immediately below for the $8446 \overset{\text{o}}{\text{A}}$ case, the only one in which all the radiative parameters are known. Similar comments, or course, pertain to the other cases studied.

Raman-type coupling leads to resonances (crossing signals) of widths equal to the widths of the crossing levels. If one of the transitions is size-ably saturated, then the width of the resonance broadens, as discussed in section III 7. (See Figure 22). In the case at hand, both of the transitions involved are fully saturated, and the approximations made in Part III are no longer satisfied. To estimate the extent of saturation broadening in this case it is reasonable to assume that the width of the level-crossing signal is still given by the widths of the crossing levels, using their saturated values. From equations 55 and 61 the saturated width of a crossing level is $Q\Delta\nu_u$, with $Q \cong (\mu\, \mathcal{E}/\hbar\sqrt{\Delta\nu_u\, \Delta\nu_1})$; $\Delta\nu_1$ and $\Delta\nu_u$ are the unsaturated widths of the lower and upper (crossing) levels respectively, μ is the connecting matrix element (See Figure 18), and $\mathcal{E}$ is the field strength of a single mode in the laser cavity. From reference 13 the radiative parameters are found to be $\Delta\nu_u = 1/2$ Mhz, $\Delta\nu_1 = 20$ Mhz, and $\mu \approx 2 \times 10^{-18}$ e. s. u. Assuming a power of 0. 4 mw/mode outside the cavity and a 100-fold intensification within, and a beam area of 0. 1 cm^2, one obtains $\mathcal{E} \approx 6 \times 10^{-2}$ e. s. u. leading to $Q \approx 40$ and an estimated saturated width of 20 Mhz. This value is in good agreement with the observed width of 24 Mhz, emphasizing the importance of saturation effects in the laser medium.

An interesting phenomenon (and experimental difficulty) was encountered when working with the 2.89μ and 4.56μ laser lines. Spiking in the output signals, often close to the positions of expected resonances, sometimes completely masked them. An example of this behavior is shown in Figure 28. (Compare solid and dashed lines.) To investigate this effect the laser beatnotes were monitored on a spectrum analyzer as traces were taken. Ordinarily, strong beatnotes at multiples of the cavity mode-spacing were observed. However, at values of magnetic field corresponding to observed spikes these would completely break up, indicating an "unlocking" of the laser modes. This effect was rather sensitive to the size and position of the aperture, and by careful alignment spiking could be controlled, if not eliminated. Further consequences of this phenomenon are beyond the scope of the present discussion.

CONCLUDING REMARKS: FURTHER APPLICATIONS

In the foregoing study the processes of selective reabsorption and Raman-type coupling have been developed to explain the unusual spectral behavior of the 8446 $\overset{o}{A}$ laser, and the theory of Raman-type processes has been extended to a new class of high-resolution spectroscopic techniques. Our conclusions may be of interest in other applications outside the scope of the present study. Here, then, some examples of their further applicability are outlined.

It is expected that selective reabsorption will have wide applicability as an effect for obtaining laser action. The case of the neon afterglow, studied in detail by Connor and Biondi,[39] is a particularly attractive possibility. For example, at a pressure of about 2mm Hg dissociative re-combination of Ne_2^+ molecules leads to a sharp increase in the fluorescence of the $2p_1 - 1s_2$ (5852 $\overset{o}{A}$) Ne line several hundred μsec into the afterglow. The dissociation process is

$$Ne_2^+ + e \rightarrow (Ne_2^u)^* \text{ unstable} \rightarrow Ne^* + Ne + k. e. , \tag{63}$$
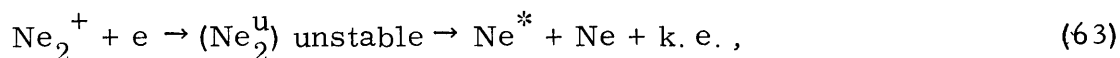
and creates a $2p_1$ velocity distribution with an observed width more than 3 times that of room temperature.[39] The $1s_2$ level is known to be heavily trapped. The breadth of the upper levels suggests, however, that the reabsorption may occur selectively over low velocities. The spontaneous lifetimes of 1.4×10^{-8} sec ($2p_1$) and 5×10^{-9} sec ($1s_2$) are obviously favorable for laser action. This possibility is currently being investigated at our laboratories.[40]

A further application of Raman-type processes suggests an interesting way of achieving laser action in gases (as well as inhomogeneously broadened solids).[41] Consider a strong laser field incident upon an inhomogeneously-broadened system in which two lower levels a few cm^{-1} apart are optically connected to a common upper level. The level scheme and one possible experimental arrangement are shown in Figure 29. If the laser resonates with the higher energy absorption line then, because of the unequal populations of the lower levels (due to the Boltzmann factors), there is a possibility of obtaining sizeable gain on the lower energy line at the frequency satisfying the Raman resonance condition. (See (42), $\delta = +1$.) The linear gain follows directly from (62) and the first two terms of (61), bearing in mind that its sign is reversed since the energy level scheme is now inverted.[42] Note that the frequency separation between the pump laser field and the induced Raman field precisely equals the separation between the lower levels, independent of the exact pump frequency. In the case of fully saturating pump field $(Q \gg 1)$ the Raman gain coefficient at resonance is given by

$$G_1 = (n_2 - n_1) \left\{ \frac{\alpha_{10}}{n_1 - n_0} \right\} \cong |\alpha_{10}| \frac{E_1 - E_2}{kT} , \tag{64}$$

in which α_{10} is the two-level linear absorption coefficient at the Raman frequency. Thus G_1 may be a few per cent of $|\alpha_{10}|$, and in favorable cases the gain can become sizeable over pathlengths of convenient dimension. In contrast, the semi-classical result leads to the erroneous

ABSORBING SAMPLE

RAMAN BEAM

PUMP BEAM

LASER SOURCE

a) EXPERIMENTAL ARRANGEMENT

γ_0 (———— |0)

PUMP FIELD

RAMAN FIELD

γ_2 (———— |2)

γ_1 (———— |1)
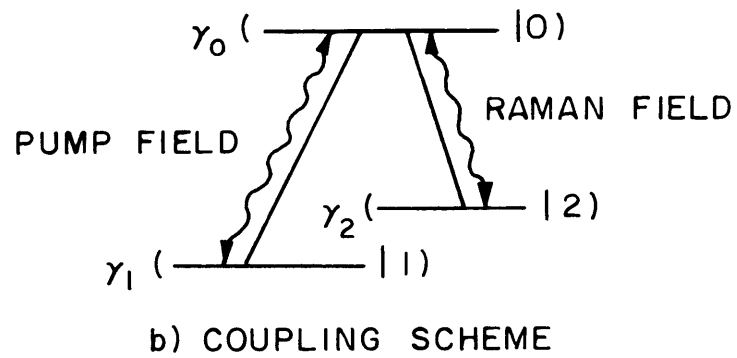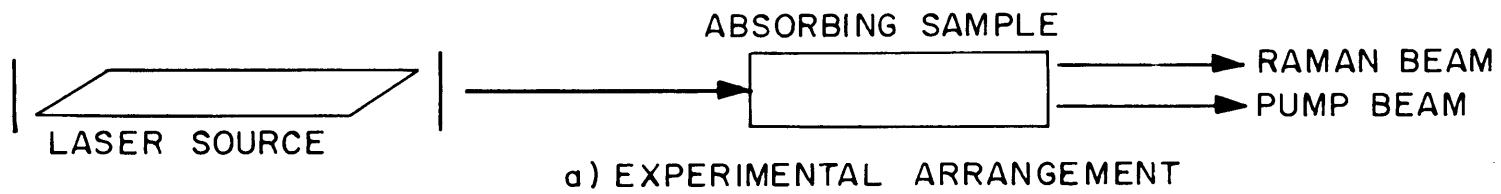
b) COUPLING SCHEME

FIGURE 29 RESONANT RAMAN LASER SCHEME

conclusion that it is virtually impossible to achieve gain under these conditions.[43]

As a specific example, the above coupling scheme is applicable to the rotational-vibrational transitions of a molecular gas. Estimates based upon a preliminary study of ammonia[44] indicate that the $\nu_2^s-0^a$ and $2\nu_2^a-\nu_2^s$ bands are likely candidates, using the 10.6μ CO_2 laser as a pump. Further details will be given elsewhere.

APPENDIX A: HOMOGENEOUSLY-BROADENED POLARIZATION OF A THREE-LEVEL SYSTEM, USING WAVE-FUNCTIONS

A 1. Equations of Motion

Consider the interaction of an N-level quantum-mechanical system with the classical field $\vec{\mathcal{E}}$ $(\vec{r}, t)$. The wave-function of the system can be expanded in the normalized eigenfunctions $|j>$ of the isolated system,

$$\Psi(\vec{R}, t) = \sum_{j}^{N} c_j(t) e^{-i\omega_j t} |j> \quad , \tag{A 1}$$

and in the interaction representation the Schrödinger equation may be written as

$$\dot{\vec{c}} = \underline{a} \, \vec{c} \tag{A 2}$$

where the c_j are components of the N-dimensional vector $\vec{c}$, and the matrix elements of the operator $\underline{a}$ are

$$a_{ij} = - \frac{\vec{\mu}_{ij} \cdot \vec{\mathcal{E}}(\vec{r}, t)}{i\hbar} e^{i\omega_{ij} t} \tag{A 3}$$

In the above equations $\vec{R}$ indicates the electron coordinates in the atomic reference frame, $\vec{r}$ is the position vector of the atomic center of mass, [45] and the other symbols have been defined in sections II.2 and II.5 of the text.

Equation A 2 describes the evolution of an undamped system. The effects of damping may be included by noting that over a wide range of

times$^{(46)}$ the incoherent decay of an ensemble of atoms is exponential:

$$\left| c_j \left(t - t_o\right) \right|^2 = \left| c_j \left(t_o\right) \right|^2 e^{-\gamma_j \left(t - t_o\right)} , \tag{A 4}$$

with γ_j the decay rate of $|j\rangle$. Accordingly, in the absence of applied fields $\underline{a} = \underline{0}$ and the probability amplitudes c_j should obey equations of motion of the type

$$\dot{c}_j = -\frac{1}{2} \gamma_j c_j . \tag{A 5}$$

Assuming that the presence of applied fields does not influence the mechanism of damping, and visa versa, (A 2) and (A 5) may be combined to yield

$$\dot{c}_i = \sum_i \left(a_{ij} - \frac{1}{2} \gamma_j \delta_{ij}\right) c_j . \tag{A 6}$$

The latter assumption, the independence of the Hamiltonian on t_o, and the random phase condition

$$\overline{c_i \left(t_o\right)^* c_j \left(t_o\right)} = \left| c_j \left(t_o\right) \right|^2 \delta_{ij} \tag{A 7}$$

(the bar denotes ensemble average) are equivalent to the approximations used in obtaining equation 24 of the text. Equation A 6 may be simplified by the substitution

$$d_j \left(t\right) = c_j \left(t\right) e^{+\frac{1}{2} \gamma_j t} , \tag{A 8}$$

which leads to a series of coupled equations strikingly similar to the undamped Schrodinger equation (A 2):

$$\dot{\vec{d}} = \underline{b} \, \vec{d} \tag{A 9}$$

where $\underline{b}$ is an operator with matrix elements

$$b_{ij} = a_{ij} \, e^{\frac{1}{2} (\gamma_i - \gamma_j) t} \quad . \tag{A 10}$$

Equation A 9 is a form particularly well suited for handling problems involving numerous decay rates. It is mentioned in passing that by forming the product $d_i d_j^*$, (A 9) leads directly to the density matrix equations of motion.

A 2. Ensemble-Averaged Polarization

The assumption of random phases, equation A 7, enables one to consider atoms to be produced in definite states with arbitrary phases, i. e., at $t = t_o$ $c_j(t_o) = \delta_{jk} e^{i\phi k}$. This boundary condition leads to an induced dipole moment for atoms at $\{\vec{r}, t\}$ and created in $|k>$ at t_o,

$$\vec{P}_k(\vec{r}, t, t_o) = \int d^3 R \, \Psi^* \, e\vec{R} \, \Psi$$

$$= \sum_{m, n} \vec{\mu}_{nm} \, d_n^* \, d_m \, e^{-i\omega_{mn} t} \, e^{-\gamma_{mn} t} \quad . \tag{A 11}$$

In considering the polarization due to atoms produced in a particular state it is necessary to include contributions from all possible past

times t_o. Thus the complete ensemble-averaged polarization is given by

$$\vec{P}(\vec{r}, t) = \sum_{k=1}^{N} \int_{-\infty}^{t} \rho_{kk}^{o} \; \gamma_k \; \vec{P}_k \; (\vec{r}, t, t_o) \; dt_o \tag{A 12}$$

(Compare (13). Extension of (A 12) to the moving frame is trivial; cf. (14) and related discussion.)

A 3. Perturbation Solution

For the three-level system shown in figure 19 and the applied fields given in equation 19, (A 9) reduces to the system of equations

$$\dot{d}_0 = i\alpha \, e^{i\delta_1 t} \, d_1 + i\beta \, e^{i\delta_2 t} \, d_2 \;,$$
$$\dot{d}_1 = i\alpha^* e^{-i\delta_1 t} \, d_0 \;, \tag{A 13}$$
$$\dot{d}_2 = i\beta^* e^{-i\delta_2 t} \, d_0 \;,$$

in which $i\delta_k = i\,(\Omega_k - \omega_{ko}) + \frac{1}{2}\,(\gamma_o - \gamma_k)$, and the other symbols are defined in section II 5 . In (A 13) only the resonant terms have been retained. From (A 11) the induced dipole moment for a particular set of initial conditions is

$$P_k(\vec{r}, t, t_o) = 2 \, \mathrm{Re} \left\{ \mu_{10} \; d_1^* \; d_0 \; e^{(i\omega_{10} - \gamma_{10})t} + \mu_{20} \; d_2^* \; d_0 \; e^{(i\omega_{20} + \gamma_{20})t} \right\}. \tag{A 1}$$

A solution of (A 13) for arbitrary β and for $|\alpha| << 1$ may be obtained using a perturbation theory[19] analogous to the one employed in section II 5.

The d_j are expanded in powers of α,

$$d_j(t) = d_j{}^u(t) + \alpha\, d_j'(t) + \alpha^2 d_j''(t) + \ldots \quad , \tag{A 15}$$

where, as before, the superscript u designates the uncoupled system $(\alpha = 0)$. We require the polarization complete to $O(\alpha)$, consequently only the two leading terms of (A 15) need be retained. Inserting these into (A 13) and equating coefficients of the powers of α, one obtains the following set of equations:

$$\dot{d}_0^u = i\beta\, e^{i\delta_2 t}\, d_2^u \quad ,$$

$$\dot{d}_2^u = i\beta^* e^{-i\delta_2 t}\, d_0^u \quad , \tag{A 16a}$$

$$\dot{d}_1^u = 0 \qquad \qquad ;$$

$$\dot{d}_0' = ie^{i\delta_1 t}\, d_1^u + i\beta\, e^{i\delta_2 t}\, d_2' \quad ,$$

$$\dot{d}_2' = i\beta^* e^{-i\delta_2 t}\, d_0' \qquad \qquad , \tag{A 16b}$$

$$\dot{d}_1' = i\frac{\alpha^*}{\alpha}\, e^{-i\delta_1 t}\, d_0^u \qquad \qquad .$$

For the system initially in $|1\rangle$ (A 16) leads to $d_1^u(t) = d_1^u(t_o)$ and $d_0^u(t) = d_2^u(t) = 0$, and for the system initially in $|0\rangle$ or $|2\rangle$ (A 16) implies $d_0'(t) = d_2'(t) = 0$. Bearing this in mind, (A 14) and (A 15) lead to the

following contributions to the induced dipole moment:

$$k = 1: \quad P_k(\vec{r}, t, t_o) = 2\,\mathrm{Re}\left[\alpha\,\mu_{10}\,e^{(i\omega_{10} - \gamma_{10})t}\,d_1^{u\,*}\,d_0'\right] + 0\,(\alpha^2), \quad (A\,17a)$$

$$k = 0, 2: \quad P_k(\vec{r}, t, t_o) = 2\,\mathrm{Re}\left[\mu_{20}\,d^{(i\omega_{20} - \gamma_{20})t}\,d_2^{u\,*}\,d_0^u\right.$$

$$\left. + \alpha^*\,\mu_{10}\,e^{(i\omega_{10} - \gamma_{10})t}\,d_0^u\,d_1'^{\,*}\right] + 0\,(\alpha^2). \quad (A\,17b)$$

It is evident from (A 16a) that d_0^u and d_2^u are the probability amplitudes for a damped two-level system. The solutions are straightforward: for the system initially in $|0\rangle$

$$d_0^u(t) = \frac{d_o(t_o)}{s}\,(q_+ e^{iq_- T} - q_- e^{iq_+ T})\,, \qquad (A\,18a)$$

$$d_2^u(t) = \frac{\beta^*\,d_o(t_o)\,e^{-i\delta_2 t}}{s}\,(e^{iq_+ T} - e^{iq_- T})\,; \qquad (A\,18b)$$

for the system initially in $|2\rangle$

$$d_0^u(t) = \frac{\beta\,d_2(t_o)\,e^{i\delta_2 t_o}}{s}\,(e^{iq_+ T} - e^{iq_- T})\,, \qquad (A\,19a)$$

$$d_2^u(t) = \frac{d_2(t_o)\,e^{-i\delta_2 T}}{s}\,(q_+ e^{iq_+ T} - q_- e^{iq_- T})\,. \qquad (A\,19b)$$

In these equations $T = t - t_o$, $s = \sqrt{\delta_2^2 + 4\,|\beta|^2}$, $q_\pm = \frac{1}{2}\,(\delta_2 \pm s)$, and

$$d_j(t_o) = e^{\frac{1}{2}\gamma_j t_o + i\phi_j}\,.$$

Equations A 16b include coupling effects to lowest order in α.

The first two equations can be combined to yield

$$\ddot{d}_0^{\mathfrak{f}} - i\delta_2 \dot{d}_0^{\mathfrak{f}} + |\beta|^2 d_0^{\mathfrak{f}} = (\delta_2 - \delta_1) d_1^{u}(t_o) e^{i\delta_1 t} \quad . \tag{A 20}$$

The boundary conditions for the system initially in $|1>$ are $d_1^{u}(t_o) = d_1(t_o)$
and $d_0^{\mathfrak{f}}(t_o) = \dot{d}_2^{\mathfrak{f}}(t_o) = 0$, leading to the complete solution (homogeneous plus inhomogeneous) of (A 20),

$$d_0^{\mathfrak{f}}(t) = \frac{d_1(t_o)(\delta_2 - \delta_1) e^{i\delta_1 t_o}}{s\left[\delta_1(\delta_2 - \delta_1) + |\beta|^2\right]} \left\{ s\, e^{i\delta_1 T} + \frac{|\beta|^2}{\delta_2 - \delta_1} (e^{iq_+ T} - e^{iq_- T}) \right.$$
$$\left. + (q_- e^{iq_+ T} - q_+ e^{-iq_- T}) \right\} . \tag{A 21}$$

The last equation of (A 16b) may be integrated directly:

$$d_1^{\mathfrak{f}} = i\, \frac{\alpha^*}{\alpha} \int_{t_o}^{t} dt\, e^{-i\delta_1 t}\, d_0^{u}(t) \quad . \tag{A 22}$$

For the system initially in $|2>$ (A 19a) and (A 22) yield

$$d_1^{\mathfrak{f}}(t) = \frac{\alpha^*\beta}{\alpha s}\, d_2(t_o)\, e^{i(\delta_2 - \delta_1)t_o} \left\{ \frac{e^{i(q_+ - \delta_1)T} - 1}{q_+ - \delta_1} \right.$$
$$\left. - \frac{e^{i(q_- - \delta_1)T} - 1}{q_- - \delta_1} \right\} ; \tag{A 23}$$

for the system initially in $|0>$ (A 18a) and (A 22) yield

$$d_1'(t) = -\frac{\alpha^*}{\alpha s} \, d_0(t_o) \, e^{-i\delta_1 t_o} \left\{ \frac{q_-[e^{i(q_+ - \delta_1)T} - 1]}{q_+ - \delta_1} \right.$$

$$\left. - \frac{q_+[e^{i(q_- - \delta_1)T} - 1]}{q_- - \delta_1} \right\}$$

(A 24)

The complete ensemble-averaged polarization (A 12) may be obtained directly from (A 17), (A 18), (A 19), (A 21), (A 23), and (A 24). Considerable algebra is involved. The final result is in full agreement with equations 36 and 37 of the text, as stated in section II5.

APPENDIX B: LINEAR GAIN FOR FIELDS POLARIZED AT RIGHT ANGLES

B1. Rotation of the Schrodinger Equation

In sections II. 3 - II. 7 the 1 - 1 linear gain was calculated for the case of mutually parallel fields. The case of mutually perpendicular fields is considered here. As before, the axis of quantization[18] is chosen along $\mathcal{E}_2$, and now for the sake of definiteness $\mathcal{E}_1$ is taken to be in the y-direction. The situation may be simplified by noting that $\mathcal{E}_1$ resonates only with the 1-1 transition and $\mathcal{E}_2$ only with the 0-1 and 2-1 transitions; the non-resonant coupling may be neglected, leading to the coupling scheme shown in figure 30 a with indicated matrix elements. The two five-level systems (1) and (2) are effectively decoupled from each other.

System (1) is considered first. In the presence of $\mathcal{E}_1^\delta$ and $\mathcal{E}_2^\tau$ the Schrödinger equation (A2) may be written as the following set of equations:

$$- i\hbar \dot{c}_{2,1} = V_2 e^{i\omega_{20}t} c_{1,1} \quad , \tag{B1a}$$

$$- i\hbar \dot{c}_{1,1} = V_2 e^{-i\omega_{20}t} c_{2,1} + i V_1 e^{-i\omega_{10}t} c_{1,0} \quad , \tag{B1b}$$

$$- i\hbar \dot{c}_{1,0} = -i V_1 e^{i\omega_{10}t} c_{1,1} + i V_1 e^{i\omega_{10}t} c_{1,-1} \quad , \tag{B1c}$$
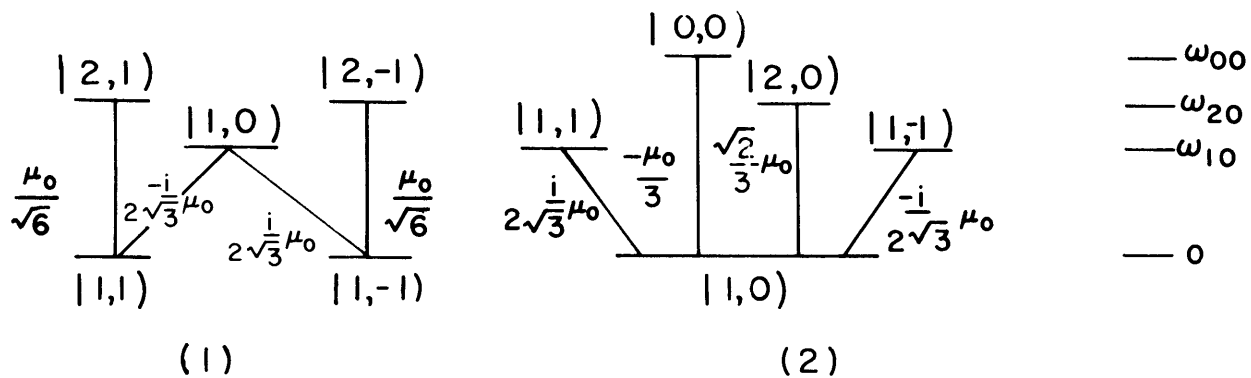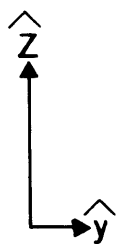
a) Energy levels, showing resonant coupling
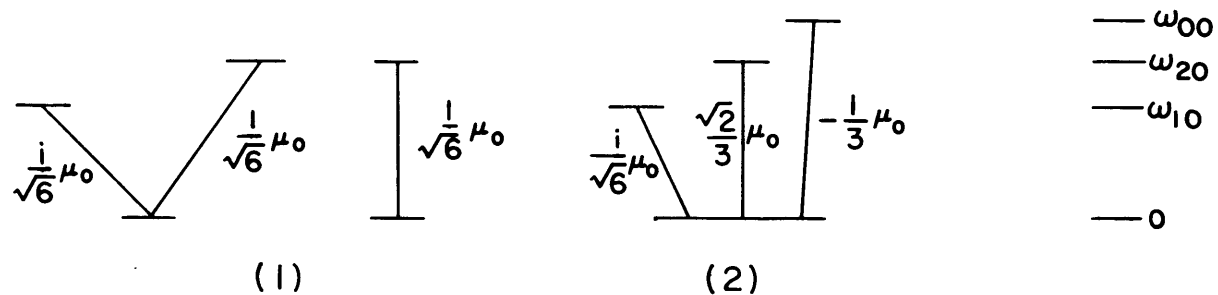
b) Coupling scheme after transforming equations of motion

Figure 30   8446 Å   Energy Levels and Matrix Elements, $\vec{\epsilon}_1 \perp \vec{\epsilon}_2 \parallel \hat{z}$

$$- i\hbar\, \dot{c}_{1,-1} = - iV_1 e^{-i\omega_{10}t}\, c_{1,0} + V_2 e^{-i\omega_{20}t}\, c_{2,-1} \quad , \qquad (B1d)$$

$$- i\hbar\, \dot{c}_{2,-1} = V_2 e^{i\omega_{20}t}\, c_{1,-1} \quad . \qquad (B1e)$$

Here $c_{J,M}$ is the probability amplitude corresponding to level $|J, M>$ and $V_1 = (\mu_0/2\sqrt{3})\, \mathcal{E}_1^\delta (z, t)$, $V_2 = (\mu_0/\sqrt{6})\, \mathcal{E}_2^\tau (z, t)$. The system B1 may be greatly simplified by means of the linear transformation

$$e_1 = \frac{1}{\sqrt{2}}\{c_{2,1} - c_{2,-1}\} \quad ,$$

$$e_2 = \frac{1}{\sqrt{2}}\{c_{1,1} - c_{1,-1}\} \quad ,$$

$$e_3 = - c_{1,0} \quad , \qquad (B2)$$

$$e_4 = \frac{1}{\sqrt{2}}\{c_{1,1} + c_{1,-1}\} \quad ,$$

$$e_5 = \frac{1}{\sqrt{2}}\{c_{2,1} + c_{2,-1}\} \quad ;$$

one obtains

$$- i\hbar\, \dot{e}_1 = V_2 e^{i\omega_{20}t}\, e_2 \quad ,$$

$$- i\hbar\, \dot{e}_2 = V_2 e^{-i\omega_{20}t}\, e_1 - i V_3 e^{-i\omega_{10}t}\, e_3 \quad , \qquad (B3a)$$

$$- i\hbar\, \dot{e}_3 = i V_3 e^{i\omega_{10}t}\, e_2 \quad ;$$

$$- i\hbar \dot{e}_4 = V_2 e^{-i\omega_{20}t} e_5 \quad ,$$

(B 3b)

$$- i\hbar \dot{e}_5 = V_2 e^{i\omega_{20}t} e_4 \quad ,$$

where $V_3 = \sqrt{2} V_1$. The normalization of (B2) is determined by the conservation of probability,

$$\sum_{j=1}^{5} |e_j|^2 = \sum_{j=1}^{5} |c_j|^2 \quad ,$$

(B4)

and insures that the polarization in the rotated system is equivalent to that of the original system. Equations B3 better reflect the symmetry of the coupling scheme. Evidently (B3a) is a three-level system completely decoupled from the two-level system (B3b). (Compare B1, neglecting the coupling between $|1,0>$ and $|1,1>$.) Thus the level scheme of figure 30b, (1), with indicated matrix elements, is entirely equivalent to that of figure 30a, (1).

System (2) may be handled similiarly. (See Figure 30a, (2).) In the presence of $\mathcal{E}_1^\delta$ and $\mathcal{E}_2^\tau$ the Schrodinger equation may be written as

$$- i\hbar \dot{c}_{1,1} = i V_1 e^{i\omega_{10}t} c_{1,0} \quad ,$$

$$- i\hbar \dot{c}_{1,0} = -i V_1 e^{-i\omega_{10}t} c_{1,1} + i V_1 e^{-i\omega_{10}t} c_{1,-1} - V_4 e^{-i\omega_{00}t} c_{0,0} + V_5 e^{-i\omega_{20}t} c_{2,0} \quad ,$$

$$- i\hbar \dot{c}_{1,-1} = -i V_1 e^{i\omega_{10}t} c_{1,0} \quad ,$$

(B5)

$$- i\hbar \dot{c}_{0,0} = - V_4 e^{i\omega_{00}t} c_{1,0} \quad ,$$

$$- i\hbar \dot{c}_{2,0} = V_5 e^{i\omega_{20}t} c_{1,0} \quad ,$$

in which $V_4 = (\mu_0/3) \mathcal{E}_2^{\tau} (z, t)$ and $V_5 = (\sqrt{2} \mu_0/3) \mathcal{E}_2^{\tau} (z, t)$. Using the transformation

$$f_1 = \frac{1}{\sqrt{2}} (c_{1,1} - c_{1,-1}) \quad ,$$

$$f_2 = c_{1,0} \quad ,$$

$$f_3 = \frac{1}{\sqrt{2}} (c_{1,1} + c_{1,-1}) \quad , \tag{B6}$$

$$f_4 = c_{0,0} \quad ,$$

$$f_5 = c_{2,0} \quad ,$$

(B5) is converted into four coupled levels and an isolated level:

$$- i\hbar \dot{f}_2 = - i V_3 e^{-i\omega_{10}t} f_3 - V_4 e^{-i\omega_{00}t} f_4 + V_5 e^{-i\omega_{20}t} f_5 \quad ,$$

$$- i\hbar \dot{f}_3 = i V_3 e^{i\omega_{10}t} f_2 \quad ,$$

$$\tag{B7a}$$

$$- i\hbar \dot{f}_4 = - V_4 e^{i\omega_{00}t} f_2 \quad ,$$

$$- i\hbar \dot{f}_5 = V_5 e^{i\omega_{20}t} f_2 \quad ;$$

$$- i \hbar \dot{f}_1 = 0 \quad . \tag{B7b}$$

The transformed four-level system is shown in figure 30b, (2) with indicated matrix elements.

B2. Calculation of Polarization

The foregoing discussion has shown that the coupling scheme for the case of mutually perpendicular fields may be simplified to the one shown in figure 30b. The latter should be compared to that of figure 18, which holds for the case of mutually parallel fields. Note the one to one correspondence between the absolute values of the individual matrix elements in the two schemes. This leads to the expected result that when both fields are weak the transmission properties are independent of the relative field orientation. However, strong coupling with $\mathcal{E}_2$ aligns the levels, leading to polarization-dependent effects.

The polarization for the case of mutually perpendicular fields is easily calculated from figure 30b, and consists of a two-level, a three-level and a four-level contribution. The two and three-level cases have already been dealt with. The four level polarization may be obtained by noting that since levels J=0 and J=2 are considerably separated with respect to the homogeneous widths involved, the non-linear effects coupling them to the J=1 level are independent and

additive. Thus using the previous results (52) and (61) the inhomo-
geneously-broadened standing-wave polarization may be written
down by inspection. For ease of comparison the final results for
mutually perpendicular fields, and also for mutually parallel fields,
are summarized below:

$$P(z,t) = Re\left\{ X_1 \mathcal{E}_1^o \cos k_1 z\ e^{i(\Omega_1 t + \phi_1)} + X_2 \mathcal{E}_2^o \cos k_2 z\ e^{i(\Omega_2 t + \phi_2)} \right\} \ ; \quad (B8)$$

$\vec{\mathcal{E}}_1 \parallel \vec{\mathcal{E}}_2 :$
_____

$$X_1 = 2X_a^{linear} - 2iZ_{PS}''\ \{\Omega_1 - \omega_{10}\}\ \Theta_a R_a\ (J=2); \qquad (B9a)$$

$\vec{\mathcal{E}}_1 \perp \vec{\mathcal{E}}_2 :$
_____

$$X_1 = 2X_a^{linear} - iZ_{PS}''\ \{\Omega_1 - \omega_{10}\}\ \Big[\Theta_a R_a\ (J=2) + \Theta_b R_b\ (J=2)$$

$$+ \Theta_c R_c\ (J=0) \Big] \ ; \qquad (B9b)$$

$\vec{\mathcal{E}}_1 \parallel \vec{\mathcal{E}}_2$ and $\vec{\mathcal{E}}_1 \perp \vec{\mathcal{E}}_2 :$
_____

$$X_2 = \frac{|\mu_o|^2}{9\hbar} \left\{ 5Z_{PS}'\ \{\Omega_2 - \omega_{20}\} + \left[\frac{3}{Q_a} + \frac{2}{Q_b} \right] Z_{PS}''\ \{\Omega_2 - \omega_{20}\} \right.$$

$$\left. + Z_{PS}'\ \{\Omega_2 - \omega_{00}\} + \frac{1}{Q_c} Z_{PS}''\ \{\Omega_2 - \omega_{00}\} \right\} \ . \qquad (B10)$$

Equation B8 is just (17) for M=2, and

$$X_a^{linear} = \frac{|\mu_a|^2}{\hbar}\ Z_{PS}\ \{\Omega_1 - \omega_{10}\} \ , \qquad (B11)$$

with $Z_{PS} \{\omega\} = Z_P \{\omega\} - Z_S \{\omega\}$, where the subscripts P and S refer
to ^{3}P and ^{3}S magnetic sublevels, respectively. Also,

$$\Theta_j = \frac{|\mu_j|^2}{3\hbar\gamma_S Q_j} \left|\frac{\mu_0 \mathcal{E}_2^o}{4\hbar}\right|^2 \tag{B12}$$

and

$$R_j (J) = \left[\frac{\gamma_P}{2} (1+Q_j) - i(\Omega_{21} - \omega_{J1})\right]^{-1}$$

$$\tag{B13}$$

$$+ \left[\frac{\gamma_P}{2} (1+Q_j) + \gamma_S Q_j + i\{(\Omega_2 + \Omega_1) - (\omega_{J0} + \omega_{10})\}\right]^{-1},$$

with

$$Q_j = \left[1 + \frac{1}{\gamma_P \gamma_S} \left|\frac{\mu_j \mathcal{E}_2^o}{2\hbar}\right|^2\right]^{1/2} ,$$

$$\tag{B14}$$

$$\mu_j = \begin{array}{ll} i\mu_0/\sqrt{6} & j = a \\ \sqrt{2}\mu_0/3 & j = b \\ -\mu_0/3 & j = c \end{array} \quad ;$$

γ_j is the decay rate of a particular sublevel of $|j\rangle$, and $\hbar\, \omega_{J0}$ =
$E(^3P_J) - E(^3S_1)$.

Comparison of (B9a) and (B9b) shows that the non-linear coupling
effects are slightly more pronounced in the case of fields oriented at
right angles. This suggests the possibility of the polarization-dependence
of the 1-1 laser line. These effects have not yet been studied experimentally.

Finally, it is interesting to note that in the case of mutually per-
pendicular fields an extra pair of depletions occurs in the 1-1 gain
profile, somewhat removed from the gain peaks. These enter via the
R_c term in (B9b) and are due to the additional coupling with the J=0
level.

REFERENCES

1. D. O. Davis and K. W. Meissner, "The Fine Structure of the $(^4S^o)\ 3p\ ^3P$ Term of Oxygen OI." J. Opt. Soc. Am. 43, 510 (1953).

2. W. R. Bennett, Jr., W. L. Faust, R. A. McFarlane and C. K. N. Patel, "Dissociative Excitation Transfer and Optical Maser Oscillation in $Ne-O_2$ and $Ar-O_2$ rf Discharges." Phys. Rev. Letters 8, 470 (1962).

3. W. R. Bennett, Jr., "Relaxation Mechanisms, Dissociative Excitation Transfer and Mode Pulling Effects in Gas Lasers." Proceedings of the Third International Conference on Quantum Electronics (Dunod Cie., Paris, and Columbia University Press, New York, 1963).

4. C. K. N. Patel, R. A. McFarlane and W. L. Faust, "Optical Maser Action in C, N, O, S, and Br on Dissociation of Diatomic and Polyatomic Molecules." Phys. Rev. 133, A1244 (1964).

5. In references 2 and 3 these anomalies were attributed to an unidentified ozone absorption band. This explanation seems to have been disproved in reference 4.

6. M. S. Feld, B. J. Feldman and A. Javan, "Frequency Shifts of the Fine Structure Oscillations of the 8446 Å Atomic Oxygen Laser." Bull Am. Phys. Soc. 12, 669 (1967).

7. L. N. Tunitsky and E. M. Cherkasov, "Interpretation of Oscillation Lines in $Ar-Br_2$ Laser." J. Opt Soc. Am. 56, 1783 (1966).

8. I am grateful to Leo Zschau of the D. W. Mann Company for the expert manner in which he took the microdensitometer tracings.

9. Gaussian profiles are not in accord with the expression for dissociative-broadened Doppler lines given by Rogers and Biondi in section IIIC of reference 24. The descrepancy may be due in part to the low finesse ($\sim$15) of our Fabry-Perot.

10. See, for example, W. R. Bennett, Jr., "Gaseous Optical Masers." Applied Optics, Supplement 2: Chemical Lasers, p.3 (1965).

11. T. Holstein, "Imprisionment of Resonance Radiation in Gases. I." Phys. Rev. 72, 1212 (1947).

12. T. Holstein, "Imprisionment of Resonance Radiation in Gases. II." Phys. Rev. 83, 1159 (1951).

13. The Einstein A coefficients have been taken from: W. L. Wiese, M. W. Smith and B. M. Glennon, Atomic Transition Probabilities, Vol. I. U. S. Department of Commerce, National Bureau of Standards, Wash. D. C.

14. Traces of O^{18} present in ordinary oxygen samples could, in principle, lead to asymmetrical behavior. The atomic spectrum of O^{18} is not known. However, the ratio $O^{18} : O^{16} \approx 1/500$ is sufficiently small so that its possible effects are negligible compared to the influence of Raman-type processes.

15. W. E. Lamb, Jr., "Theory of an Optical Maser." Phys. Rev. 134, A1429 (1964), and also reference 17.

16. H. R. Schlossberg and A. Javan, "Saturation Behavior of a Doppler-Broadened Transition Involving Levels with Closely Spaced Structure." Phys. Rev. 150, 267 (1966).

17. W. E. Lamb, Jr., "Theory of Optical Maser Oscillators", in Quantum Electronics and Coherent Light (Proceedings of the Internation School of Physics "Enrico Fermi", Varenna, Italy) edited by C. H. Townes and P. A. Miles, New York: Academic Press, p. 78 (1964); note especially the discussion beginning on p. 96.

18. The wave-function coordinate $\vec{R}$, referred to here, measures the position of the electron from the atomic center of mass. It should not be confused with the atomic position vector $\vec{r}$, previously referred to, which locates atoms in the Fabry-Perot cavity.

19. See reference 45.

20. A. Javan, "Theory of a Three-Level Maser." Phys. Rev. 107, 1579 (1957).

21. T. Yajima, "Three-Level Maser Action in Gas. I. Theory of Multiple Quantum Transition and Doppler Effect in Three-Level Gas Maser." J. Phys. Soc. Jap. 16, 1594 (1961).

22. A. Javan, "Stimulated Raman Effect", in Quantum Electronics and Coherent Light (Proceedings of the International School of Physics "Enrico Fermi," Varenna, Italy) edited by C. H. Townes and P. A. Miles, New York: Academic Press, p. 284 (1964).

23. These details are fully discussed in references 20 and 22.

24. W. A. Rogers and M. A. Biondi, "Studies of the Mechanism of Electron Ion Recombination: II." Phys. Rev. 134, A1215 (1964).

25. This attractive possibility is the result of newly developed diodes which combine optical detection and microwave heterodyning functions in a single element. See J. L. Hall and W. W. Morey, "Optical Heterodyne Measurement of Neon Laser's Millimeter Wave Difference Frequency." Appl. Phys. Letters 10, 152 (1967).

26. See, for example, W. Heitler, The Quantum Theory of Radiation (Clarendon Press, Oxford, Third Edition, 1954); Section 20.

27. I am indebted to Prof. C. H. Townes for pointing out this similarity.

28. M. S. Feld, J. H. Parks, H. R. Schlossberg and A. Javan, "Spectroscopy with Gas Lasers", in Physics of Quantum Electronics edited by P. L. Kelley, B. Lax, and P. E. Tannenwald, New York: McGraw-Hill, p. 567 (1966).

29. M. S. Feld, "Interaction of a Saturating Optical Field with Crossing Levels." NASA Research Grant NsG-330, December 30, 1966.

30. G. W. Flynn, M. S. Feld and B. J. Feldman, "New Infrared Laser Transitions and g-Values in Atomic Oxygen." Bull. Am. Phys. Soc. 12, 669 (1967).

31. Mark Kovacs and Prof. George Flynn discovered the first new oxygen laser lines.

32. C. E. Moore, Atomic Energy Levels, Vol. I, National Bureau of Standards Circular No. 467 (U. S. Government Printing Office, Washington, D. C., 1949).

33. B. Edlén, "Das Bogenspektrum des Sauerstoffs, OI." Kgl. Svenska Vetenskapsakad. Handl. (3) 20, 10 (1943).

34. A possible exception is the 10.4µ line, which has not been tried under these conditions.

35. When α and β are both weak the polarization up to third order may be recovered from the present expressions. This may be achieved by expanding the second term of (61) to lowest order in $|\beta|^2$ and noting that there must be symmetry between α and β. For X_1 the result is just the first two terms of (61), but with $Q = 1$; an analagous expression holds for X_2. The result is in agreement with reference 16 (except for several misprints appearing there.)

36. See, for example, J. Brossel, "Pompage Optique", in Quantum Optics and Electronics, edited by C. DeWitt, A. Blandin, and C. Cohen-Tannoudji, Gordon and Breach, New York, 1964.

37. P.A. Franken, "Interference Effects in the Resonance Fluorescence of 'Crossed' Excited Atomic States". Phys. Rev. 121, 508 (1961).

38. F.K. Harris, "Coil Arrangements for Producing a Uniform Magnetic Field." Nat. Bur. Stand. J. Research 13, 391 (1934).

39. T.R. Connor and M.A. Biondi, "Dissociative Recombination in Neon: Spectral Line-Shape Studies." Phys. Rev. 140, A779 (1965).

40. B.J. Feldman and A. Javan (private communication).

41. The present mechanism differs from the one utilized in conventional Raman lasers in that it involves resonant pumping, leading to "population effects" intimately connected with the "Raman effects". A complete discussion of previous Raman lasers can be found in, "An Investigation of Stimulated Raman Emission" by E. M. Garmire, Ph. D. Thesis, M. I. T, 1965. (Unpublished.)

42. A formal proof of this statement begins by noting that in the inverted system ω_{01}, ω_{02} and ω_{21} are all positive quantities, so that the off-diagonal density matrix elements of (28) are no longer the resonant components of the equations of motion (26). Taking the complex conjugate of each of the equations of motion followed by the substitutions $\rho_{ij}^{*} \to \rho_{ij}'$ and $-\mu_{ij}^{*} \to \mu_{ij}'$ restores (26) to its original form. The polarization

$$P' = 2Re \{\mu_{10}' \rho_{01}' + \mu_{20}' \rho_{02}'\} = -2Re \{\mu_{10}\rho_{01} + \mu_{20}\rho_{02}\}; \quad Q. E. D.$$

43. The semi-classical result is given by the first two terms in equation 61, except that the denominator of the second term is replaced by

$$[(\gamma_{10} + Q\gamma_{20}) -i (\Omega_{21} - \omega_{21})]^{-1}.$$

44. L. A. Aronberg, "Measurement of Absorption Parameters in Ammonia Gas Using the 10.6μ CO_2 Laser." S. B. Thesis, M. I. T. , 1967. (Unpublished).

45. Strictly speaking, $\vec{r}$ is the position vector of the atomic <u>electron</u>. However, the atom is much smaller than the wavelength of the optical field, hence the applied field strength at the electron is very nearly the same at the center of mass. Thus the statement in the text implies an approximation very similar to the electric dipole approximation, effectively decoupling the Fabry-Perot coordinates ($\vec{r}$) and the wave-function coordinates ($\vec{R}$). (See equations 20 and A11.)

46. V. F. Weisskopf and E. P. Wigner, "Berechnung der natürlichen Linienbreite auf Grund der Diracschen Lichttheorie." Z. Physik <u>63</u>, 54 (1930). The Weisskopf-Wigner treatment is discussed by Heitler: reference 26, Section 18.

47. Strictly speaking, $\mu_o g \delta B$ is the full half-width of the non-linear decrease in laser <u>polarization</u>, which is only approximately equal to the half-width of the laser power-output dip. The latter quantity, proportional to the square of the field-strength within the laser cavity, is obtained by equating the gain coefficient of the laser modes to the average cavity loss per unit length. In more accurate linewidth determinations the exact expression should, of course, be used.

BIOGRAPHICAL NOTE

The author was born in New York City on November 11, 1940. He attended the Lynbrook, Long Island public schools. In June, 1963 he received the S. B. degree in Humanities and Science and the S. M. degree in Physics at M. I. T. He studied at University College, London University, England, in the academic year 1961-1962. He was married in 1963 to the former Mary Haskell and is the father of three year old twin boys, David and Jonathan. Since June, 1963 he has been a research assistant in the Optical and Infrared Laser Group at M. I. T.

Publications of the author include: "Observation of the Stark Effect in Infrared Molecular Transitions, Using Helium-Neon Masers", Bull. Am. Phys. Soc. 10, 87 (1965); "Spectroscopy with Gas Lasers", in Physics of Quantum Electronics edited by Kelley, Lax and Tannenwald, New York: McGraw-Hill, p. 567 (1966); "Laser Spectroscopy of Gases with Special Reference to Analytical Applications" (invited talk at 1966 Gordon Conference on Analytical Chemistry), Science 151, 1254 (1966); "Frequency Shifts of the Fine-Structure Oscillations of the 8446 $\overset{o}{A}$ Atomic Oxygen Laser", Bull. Am. Phys. Soc. 12, 669 (1967); "New C. W. Infrared-Laser Transitions and g-Values in Atomic Oxygen", Bull. Am. Phys. Soc. 12, 669 (1967); "Frequency Shifts of the Fine-Structure Oscillations of the 8446 $\overset{o}{A}$ Atomic Oxygen Laser" Phys. Rev. , to be published.

The author is a member of the Society of Sigma Xi.